Tissues as active materials: spontaneous flows and topological defects in active cellular nematics

Louis Brézin

THÈSE DE DOCTORAT
de Sorbonne Université

Spécialité : Physique

École doctorale n°564: Physique en Île-de-France

réalisée

au Laboratoire Physico-Chimie de l'Institut Curie &
au Collège de France

sous la direction de Jean-François Joanny & Thomas Risler

présentée par

Louis Brézin

Sujet de la thèse :

Tissues as active materials: spontaneous flows and topological defects in active cellular nematics

soutenue le 18 décembre 2020

devant le jury composé de :

M^me^	Hawkins Rhoda,	University of Sheffield,	Rapporteuse
M.	Giomi Luca,	Leiden University,	Rapporteur
M.	Sagués Francesc,	Universitat de Barcelona,	Examinateur
M.	Voituriez Raphaël,	Sorbonne Université,	Examinateur
M.	Silberzan Pascal,	Institut Curie,	Membre Invité
M.	Joanny Jean-Francois,	Collège de France,	Directeur de Thèse
M.	Risler Thomas,	Institut Curie,	Directeur de Thèse

Contents

Acknowledgments

This PhD would have not been possible without the support of many people whom I want to thank. Let me first thank the jury members, I feel very honored that you have accepted to review my work. I want to thank my two PhD advisors, Jean-François and Thomas. I tried to absorb as much as possible of the incredible intuition for physics that Jean-François possesses, and it was a privilege to work along side him. His optimism about science was a great relief in my moments of doubt. It was such a pleasure to work with Thomas, whom I want to thank for his rigor, precision and honesty that I appreciated greatly.

I want to thank Thibault and Trinish for our collaboration, for accepting to deal with a theoretician that always ask why we cannot have more stuff. Now I have learned that answering some seemingly simple questions takes weeks of experiments. Thank you for you patience and dedication! I also want to thank Pascal Silberzan for being so open about the projects and always willing to discuss. I also want to thank Carles for his support throughout my whole PhD and for precious insights on how to deal with experimental data, and for useful tips about numerical solving of non-linear PDEs.

I want to thank Mathieu Coppey and Vincent Hakim for their support and insights as advising committee during my PhD. I also want to thank Aleksandra Walczak and Thierry Mora for their precious guidance.

I want to thank the many people at Curie that made life so much more enjoyable, in particular the whole theory group which is really an amazing environment. Thanks to the people that shared my office, Efe, Amit, Mathieu, Rémi and Gert-jan, this was a great place to be thanks to you! Curie in general is a great place, and a special mention goes to Elie, John and Alicia for being there. Thanks to Doron, Ram, Tridib and Ohad for making the third floor of the Collège de France annex a fun and interesting place.

I also want to thank the people that where at ENS when I first started my PhD, in particular Marco, Lorenzo and Diego with whom I shared great moments, in particular the Cargèse summer school and our bike trip around Corsica.

I have many dear friends that counted so much during these years that I want to thank. I want to thank my high-school friends Jean, Sam and Diego for being there, with a special mention to Sam, I was so happy that we shared the PhD experience roughly at the same time, and our extended lunches around Jussieu were very precious.

I want to thank my friends from ENSTA, in particular Samar and Aldo. Aldo, thank you for inviting me to the Philharmonie for the first time and opening my ears to wonderful music. Wednesdays were often the best day of the week thanks to you.

During these three years, climbing kept me mostly sane, and not only because of how refreshing going to Fontainebleau is, but because I made great friends through it, and I want to thank Faustine, Joachim, Marion, Quentin, Tim, Christophe, and in general the climbing club of Jussieu. A special mention goes to Quentin for introducing me to the sport, and for all that came afterwards. I hope we have years of climbing and science together ahead of us.

I want to thank my family, in particular my parents for giving me all the tools to succeed in life, and for giving me the freedom to decide what that means. A warm thanks goes to my grandfather Édouard, who showed me from a young age how fascinating the laws of nature are. Since then, you have accompanied me greatly, and I am so grateful to have a grandfather I can go to when I have questions about the BKT-transition, and with whom I can share my experiences in science.

Finally, I want to thank my partner Laura, for being who she is, and for accepting me for who I am.

Introduction

In this manuscript, I present the research I conducted during the three years of my PhD at Institut Curie and at Collège de France. During this time, I worked in close collaboration with two experimentalists, Thibault Aryaksama and Trinish Sarkar, who were doing their PhD at the same period in the group of Pascal Silberzan at Institut Curie. At the beginning of my PhD, I started working on new experiments T. Aryaksama was conducting. T. Aryaksama was plating C2C12 mouse myoblast cells on stripes with abrasions perpendicular to the stripe direction. Adding abrasions was a continuation of previous work by Duclos, Blanch-Mercader *et al.* [1]. Abrasions were modeled by an external field in chapter 2, and the purpose is to make an analogy, for live cells, with the Freedericksz transition in liquid crystals.

In between experimental results, I started discussing with Trinish Sarkar about his project on topological defects and got very excited. T. Sarkar was looking at topological defects in monolayers of C2C12 myoblasts and their role in multilayering. Studying topological defects peaked my interest as a theoretician, notably for their universal properties and their existence in many areas of physics. Our collaboration focused on the onset of multilayering, and we looked at the flow created by activity in the vicinity of positive half-integer topological defects. Surprisingly, we discovered a class of non-motile positive half-integer defects. To account for this class of non-motile defects, we computed the stall force necessary to stop the motion of a defect.

This collaboration was a rich experience for me, and I particularly appreciated the cross talk between theory and experiments. It is a challenging endeavor because nothing really goes as planned, but it provided theoretical questions that would not necessarily have been asked otherwise, such as the pinning of defects or the rotation of the external field in stripes. I like to believe that the theoretical work in this thesis was also beneficial for the experiments. In stripes, theory provides insight on the contact-guidance mechanism, suggesting that there is an intrinsic length-scale below which contact-guidance has no effect over confinement. For defects, the theoretical conditions to obtain non-motile defects lead to the observation of elongated focal adhesions at the core of defects, suggesting a stronger anchoring of the cells on the substrate.

This manuscript is organized as follows. Chapter 1 introduces tissues from a physics

perspective, and the theory used to describe them. I give a brief description of cell and tissue mechanics in section 1.1.1. Then, I focus of the continuum description of tissues as active materials in section 1.1.2, and give a brief overview of the definition and issues related to the field of active matter in section 1.1.3. In section 1.2, I give a derivation of the hydrodynamic theory for active nematics, from minimal assumptions based on symmetries. This construction shows how the activity of elongated cells generates an active stress in tissues, which is at the basis of the phenomena described in this thesis.

Chapter 2 is about the experiments of T. Aryaksama on active nematic cells that are confined in stripes of varying widths and quasi-infinite lengths. In section 2.1, I present the main experimental observations that serve as a basis for the theoretical description. A comparison is made between stripes with abrasions in the perpendicular direction and stripes without. The effect of the abrasions is noticeable for stripes wider than $2-300\mu$m. In large stripes, cells align with abrasions perpendicular to the stripe. When the angle of the abrasions with respect to the direction of the stripes is varied, a competition between the effect of activity and the effect of abrasions is measured. I recall in section 2.2.1 and 2.2.2 results about the passive Freedericksz transition for passive nematics and its analog for active nematics. Modifications of this active transition when taking into account cell division and extrusion, as well as interactions with the substrate through viscous drag, have been studied in ref. [1] and are reminded in section 2.3. The effects of perpendicular abrasions are modeled using an external orientation field in section 2.4. The effect of a change of the direction of the field with respect to the direction of the stripes is studied in section 2.5, and provides a method to measure the flow-alignment parameter ν. Finally, I compare quantitatively the experiments with the theory in section 2.6. The results of this chapter are discussed in section 2.7.

Chapter 3 focuses on topological defects and the experiments of T. Sarkar. A general introduction to topological defects and their mathematical description is the object of section 3.1. The main experimental observations of T. Sarkar are summarized in section 3.2, notably the contractile nature of these defects and the existence of non-motile defects. Later sections are devoted to the flow created by topological defects in different approximations. Section 3.3 is devoted to the computation of the flow created by an isolated positive half-integer defect on a substrate when the orientation dynamics of the nematic are neglected. The stall force for such a defect is computed in section 3.4. A coupling between orientation and flow via the torques created by the antisymmetric stress is considered in perturbation in section 3.5. The effects of cell division and extrusion around defects are considered in section 3.6: a pressure-dependent net division rate contributes to the active motion of positive half-integer defects. Finally, section 3.7 provides a limit size for an isolated defect, since the orientation of the defect is perturbed by the active flow it generates. A discussion about the results of chapter 3 in relation with experimental observation is given in section 3.9.

At the end of this manuscript, the main results are summarized. Perspectives are

given that bridge the two different studies of active nematics given in chapters 2 and 3.

Chapter 1

Describing the collective behavior of cells

1.1 Cellular organization and physics

1.1.1 From cells to tissues

Animals and plants are large pluricellular organisms of various shapes and sizes, and understanding their development from one or two cells to their fully developed forms is a long-standing problem in biology, but also in chemistry, mathematics, and physics. At the heart of developmental biology is the collective organization of cells into larger cohesive structures called tissues, which in turn can make larger structures of complex shape such as organs or muscles. Collective cellular organization is key for embryogenetic processes [2] like gastrulation [3], tissue renewal [4], and morphogenesis [5]. It is also key for invasive processes that require the migration of cells, notably for cancer metastasis [6] or wound healing [7].

Cells are extremely complex biochemical structures, and giving a description of the collective behavior of cells is a difficult task. In order to deal with this complexity, one can try to rely as much as possible on logical assertions using mathematics, starting from as few assumptions as possible using basic physical principles like conservation laws. This way of approaching biology is not new and D'Arcy Thompson in 1917 wrote a book called "On Growth and Form" [8] where, in the last chapter *The comparison of related forms*, he famously compares the shapes of different animals using mathematical transformations. Although motivated by a mathematical description of forms rather than an explanation of them, D'Arcy Thompson suggests that the existence of mathematical transformations between different species is a motivation to look for physical principles controlling forms.

In order to apply physical principles to biological problems, one has to look for physical observables in biology. For the collective behavior of cells, with an emphasis on

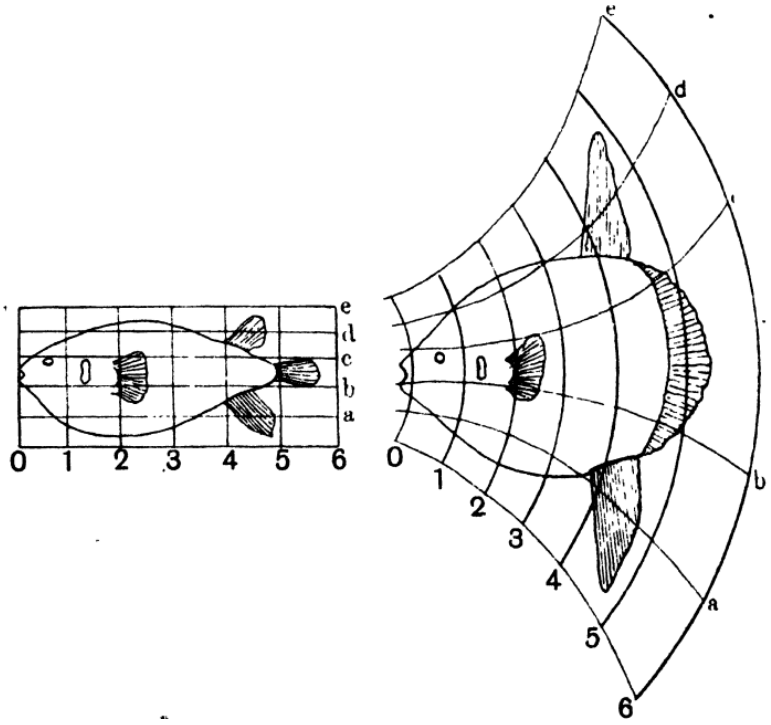

Figure 1.1: On the left is a drawing of a porcupine fish. On the right is the same drawing with a change of coordinates. The horizontal axis is transformed using hyperbolas and the vertical one using concentric circles. The result on the right is very similar to a sun fish. Figure taken from [8].

migration and shape that involve displacements of cells, the main physical observables are mechanical. Growth, motion and shape changes all require the application of forces. The study of forces in biology is a field called mechanobiology, and a great challenge of the mechanobiology of tissues is the existence of different mechanisms to generate forces at different scales [9, 10]. Making a complete introduction to mechanobiology is outside the scope of this work, and I will present examples relevant to the object of this thesis. For a deeper introduction on the subject aimed at physicists, see refs. [9–15].

At the level of a single cell, the cytoskeleton inside the cell is the main complex that exert forces on the plasma membrane and can therefore deform the cell [14]. The forces to deform the cell are of the order of pN [16, 17]. There are different mechanisms for the motility of animal cells [15], and I present as an example the mechanism of crawling [18]. The cell first makes a protrusion by polymerizing filaments of the cytoskeleton. At the end of the protrusion, the cell adheres to the surface by using proteins. By exerting contraction forces along the cytoskeleton, the cell body is dragged back and a forward motion is possible. A schematic representation is given in fig. 1.2.a.

This motion requires mechanical work, which is provided by proteins called molec-

ular motors. Molecular motors are capable of producing mechanical work through conformation changes. These conformational changes are the result of a chemical reaction that produces energy, the hydrolysis of ATP into ADP. Other chemical reactions can be transformed into mechanical work, but for the purposes of this work, we only retain that cells have the capacity to transform chemical energy into mechanical work.

For cells to make up a tissue and not an assembly of individual cells without cohesion, interactions between cells are needed. Cell-cell adhesion is achieved by proteins called cadherins that make a link between the cytoskeleton filaments of neighboring cells, as seen on fig. 1.2.b. Cells can therefore transmit forces to neighboring cells, of the order of one to hundreds of nN [16].

I gave a very simplified picture of different mechanisms to generate forces involved in collective cell organization and migration, to give context at the scales studied in this manuscript. It is a difficult task to describe the mechanics of a large number of cells such as in a tissue by considering forces created by individual cells or inter-cellular forces. Such models however exist and usually require computer simulations. Individual cells can be modeled using molecular dynamics' simulation, with interaction potentials depending on cell-cell adhesion [19]. Tissues have been described using vertex models, models where tissues are represented by a network of polygon shapes that represent cells [20–22]. However, if we are interested in the collective behavior of cells and not in their individual motion, we can apply the principles of non-equilibrium statistical mechanics. Instead of dealing with the dynamics of a large number of individual particles, we look at the average behavior of coarse-grained variables. In the limit of a large number of particles, details of the system vanish and the system is described by a low number of macroscopic thermodynamic variables such as pressure, temperature and volume. The same can be applied to tissues: we can build a continuum description of tissues and treat them as materials such as fluids or solids. We no longer consider individual cells, their motion and forces, but construct coarse-grained physical variables such as density, velocity and stress fields. From a theory perspective, a continuum description of tissues can be made using a hydrodynamic approach [23] that considers only averaged values of physical quantities, over large length and time scales. This is the approach used in this manuscript to describe two problems that are both related to spontaneous motions in tissues. The systematic construction of the relevant hydrodynamic theory is presented in section 1.2. The advantages of a hydrodynamic theory of tissues from a modeling perspective is that is does not require a precise description of cell mechanics, but only a small number of key properties such as symmetries and the ability to perform mechanical work. This is similar to the fact that in order to describe the behavior of liquid water, precise value of the interaction potential between water molecules is irrelevant for any macroscopic properties, in particular all properties associated to water flow.

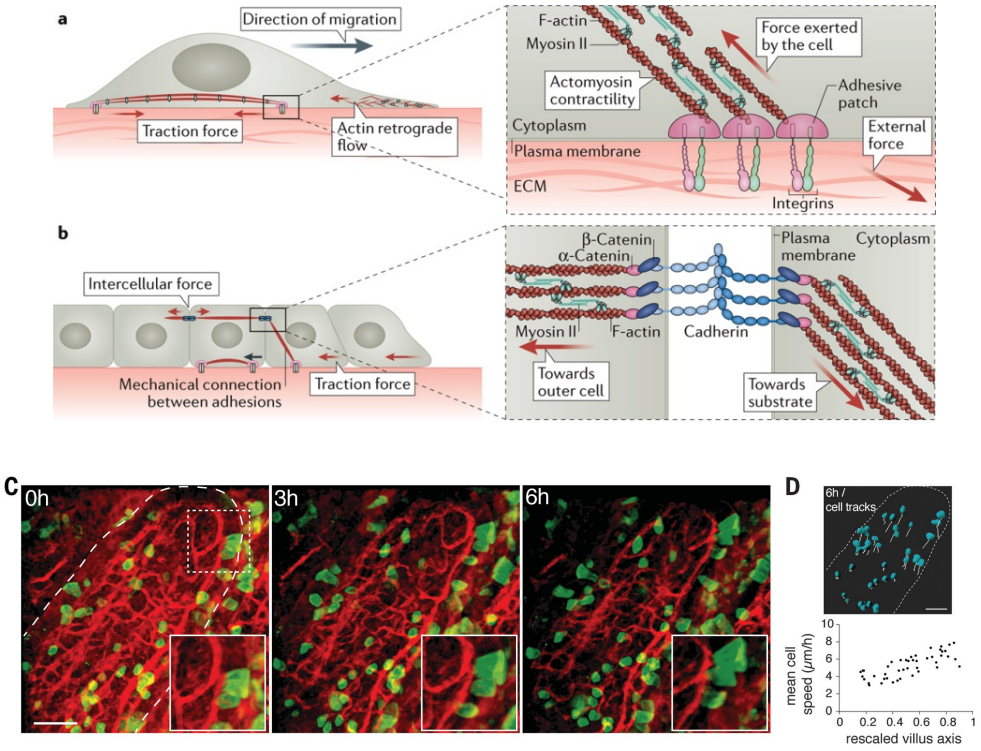

Figure 1.2: **Different scales of cellular organization.** **a** Mechanisms of locomotion at the single-cell level and the different proteins involved. **b**, Mechanisms for cell-cell interactions using cadherins. a,b, Adapted from [9]. **c**, Example of the continuum description of tissues, here for cell migration in a villus of the gut. Some cells are marked in green and the tracking of these cells is shown in **d**. c,d adapted from [4].

1.1.2 Tissues as active materials

From now on, we shall consider tissues as continuum materials, and use hydrodynamic variables to describe them. From an experimental point of view, fields like density, velocity, and orientation can be determined by optical measurements (see fig. 1.4 for example). This provides a natural coarse-graining through the optical resolution. Measurements of stress fields require more elaborate processes, such as the plating of cells on deformable substrates of known mechanical properties [16, 24].

Tissues can have different mechanical behaviors depending on the time-scales and external conditions. However, at large length scales compared to the cell size (10 to 50 μm) and at long time scales compared to the typical cell-division time (from an hour

to several days in cancerous tissues), tissues have a liquid-like behavior [25], meaning that they flow. Even in tissues were cells are not motile, cells move notably because of rearrangements after division or extrusion (a process where cells are removed from a layer of tissue) [25].

The mechanical forces in cells are generated by the cytoskeleton, which has a preferential direction due to the polarity of long filaments [14, 24, 26], giving a preferential direction for mechanical forces on average. Moreover, cells in tissues are sometimes elongated, creating a preferential direction. It has been shown that elongated cells align over long distances compared to the cell size [27, 28]. These features are characteristic of liquid crystals, materials that do not have positional order (hence the name liquid) but have long-range orientational order (as in a crystal).

Under confinement, when the density increases because of cell divisions, tissues can become jammed, a state where cells do not flow, without positional order [27, 29].

As a material, tissues are particularly interesting because they are made of living cells that consume energy. From the brief description given previously, the relevant feature is that cells have the ability to perform mechanical work (through the hydrolysis of ATP for example). This local mechanical work performed in the tissue maintains the tissue out of equilibrium and can lead to rich physical behaviors [23, 30–32].

From a modeling point of view, due to the liquid-like behavior, the long-range orientational order, and the production of local mechanical work, tissues can be considered as active liquid crystals. Tissues show another feature of liquid-crystal behavior: the existence of topological defects, points or lines in space where the orientation is singular. In layers of cells, topological defects appear at the boundary of patches of aligned cells of different directions [28, 33]. The observation of topological defects is useful to obtain information on the underlying symmetries of the cells and their interaction [28, 33–35]. There has been observation of half-integer defects in tissues [28, 33, 36, 37], defined precisely in section 3.1.2. A positive and a negative half-integer defect in a cell monolayer are shown in fig. 1.3. Half-integer defects only exist if the cells have nematic interactions within the tissue, which means that cells align along a preferred orientation but not a preferred direction (which would be polar interactions). This fact can seem surprising since individual cells are polar (although what constitutes the polarity axis is a debated topic). The nematic symmetry observed in tissue is still an open question and is either due to rapid switching of polarity compared to the timescale we are interested in (several hours) or to a nematic interaction of cells, meaning that the direction of polarity does not matter in the cell alignment. This rapid switching of polarity could be due to a process called Contact Inhibition of Locomotion (CIL) [9, 38], where upon contact two cells repel each other like in an elastic collision. At high densities, CIL could lead to a sufficiently rapid switching of polarity of the cells and give on average a nematic symmetry for our observation times of several hours.

Let us now go over some features of active nematics that are observed in tissues. A

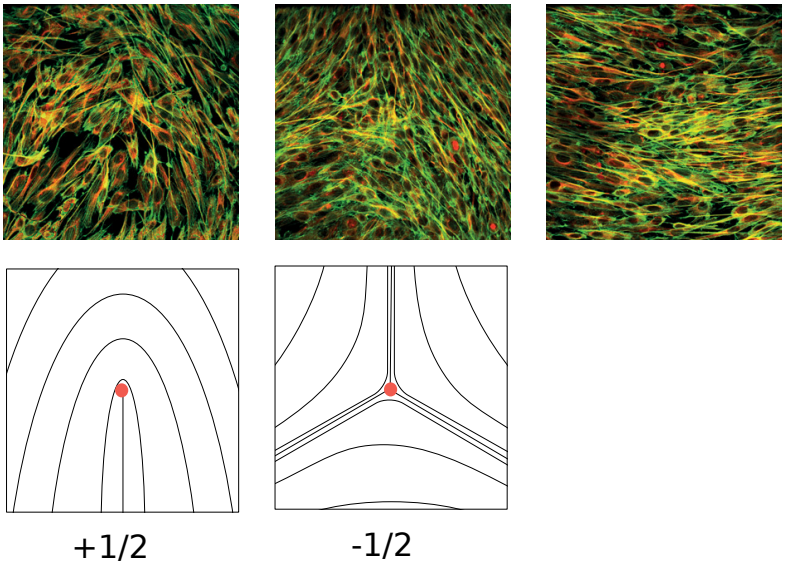

Figure 1.3: Actin fluorescent images of topological defects. Actin is in red and tubulin in green. On the left a $+1/2$ cellular topological defect, in the middle a $-1/2$ defect. On the right an aligned state. Adapted from [33].

key feature of active systems at the core of this work is the existence of spontaneous flows due to activity: the fact that there is local consumption of energy can result in spontaneous collective motions of cells without any external forcing. For an active nematic, the important feature is that gradients of orientation create active forces that induce motion. With this in mind, topological defects create gradients of orientation, which in turn create active forces. These active forces lead to the spontaneous motion of $+1/2$ topological defects [39, 40], which has been observed in cellular systems [33, 36, 37].

Perfect nematic order in tissues can be obtained by confining tissues [27]. However, the theory predicts that a motionless uniform alignment state becomes unstable when the activity of the system increases [41]. This instability is referred to as the active Freedericksz transition by analogy with a transition in passive nematics [35, 42]. This instability has been observed in different types of epithelial and muscle cells [1], where a gradient of orientation develops in a monolayer of cells and a spontaneous anti-parallel flow arises without any external drive (see fig. 1.4). There has been *in vivo* observation of anti-parallel flows of cancer cells in confining channels moving away from the tumor from which it originated but also towards it [43].

When the activity of the system becomes large, active nematics can become turbulent [44]. This active turbulence is possible at low Reynolds numbers because the activity induces the proliferation of defects that in turn create flows. This feature has been observed in tissues, even though they are at very low Reynolds numbers [45], as

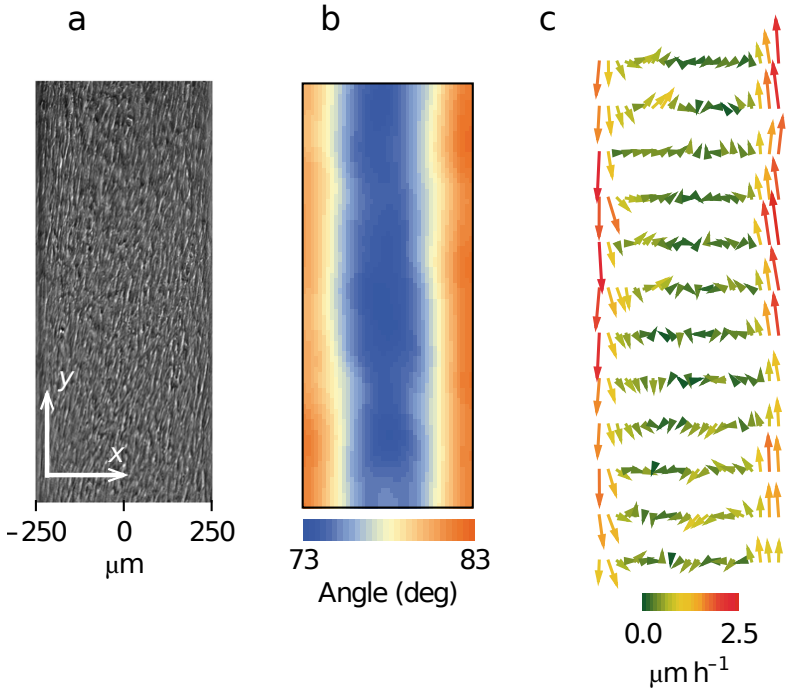

Figure 1.4: **Epithelial cells in confinement.** **a** Optical image of cells confined to a 500μm wide stripe. **b** Continuum representation of the orientation field of the cells on the left panel. There is a gradient of orientation formed by a tilt in the middle of the stripe. **c** Velocity field of the cells on the left panel. We can see an anti-parallel shear flow close to the edges. Adapted from [1].

seen in fig. 1.5.

Another important feature of active systems, outside of the scope of hydrodynamics, is the existence of giant number fluctuations [46]. For a passive system, the local number of particles fluctuates as the square-root of the number of particles, a general consequence of the central limit theorem. However, for active systems, the theory predicts larger fluctuations. For an active nematic in two dimensions, the fluctuation of the local number of particles ΔN scales linearly with the local number of particles N. Experimental measurements of cells platted on a substrate show a scaling law $\Delta N = N^{\alpha}$ with $1/2 < \alpha < 1$ [27, 47, 48], showing a non-equilibrium behavior.

1.1.3 Active matter: local driving out of equilibrium

Until now, I focused on the collective behavior of cells in tissues and presented its description as an active liquid nematic. I defined loosely active matter as local consumption of energy and I want to add precision and dive a bit more into the rich physics of active systems. The field of active matter is extremely vast and encompasses all

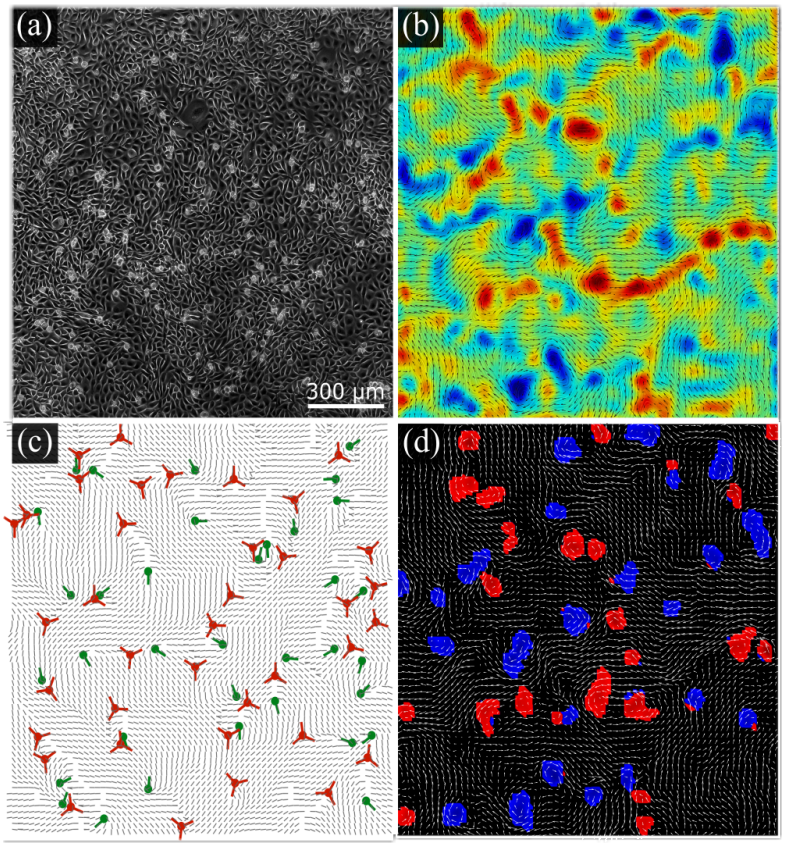

Figure 1.5: **Turbulent regime of human bronchial epithelial cells (HBEC). a** Phase contrast image of cells. **b** shows the vorticity map, **c** shows the position of topological defects responsible for low reynolds turbulence. **d** is a representation of vortices using the Okubo-Weiss parameter. Adapted from [45].

branches of non-equilibrium statistical mechanics, from stochastic dynamics of molecular systems to hydrodynamic theories. I will therefore not go into too much details, but I refer to [23, 30, 32, 49] for a broader description.

A precise thermodynamic definition of an active system is a subtle task. What makes an active system special compared to a system driven out of equilibrium by maintaining an external gradient such as imposing a shear on a fluid [50]? Local consumption of energy can be reformulated by saying that active systems break microscopic time-reversibility by injecting energy into the system. This breaking of detailed balance can give rise to phenomena that cannot be describe by thermal equilibrium physics. However, let us take for example Active Brownian Particles (ABP) – particles that are self-propelled at constant velocity v but have rotational diffusion, or Run-And-Tumble (RTP) particles – model particles for bacteria motion where particles are self-propelled,

but instead of rotational diffusion, they have rapid reorientation processes (tumbles) at a finite rate. These two models are simple toy models to study active matter dynamics. Their particles are active because they need local energy to maintain a self-propulsion velocity. However, it is easy to imagine that over large times compared to the rotational diffusion or tumble timescale, the behavior of a single particle is not different from regular passive brownian dynamics with a higher effective temperature that reflects the self-propulsion velocity [51]. In other words, this seemingly active system does not display active behavior in the sense that it can be described using equilibrium physics. However, when looking at the dynamics of multiple particles, even simple systems like ABP show non-equilibrium features such as clustering in the absence of attractive forces [52]. This was just to give an example of the subtleties that can exist when talking about active systems. The general rule is that active systems give rise to non-equilibrium phenomena and a possible thermal-equilibrium description is the exception. When there are broken symmetries in the system like polar or nematic order, this leads to specific active behaviors. A striking example is for flocks of polar active particles, which can develop long-range order in two dimensions, an apparent violation of the Mermin-Wagner-Berezinskii theorem [53]. Active nematic systems also develop active stresses which result in spontaneous motion due to gradients of orientation [23], and can give rise to novel thermodynamic phases associated to active topological defects [54].

There is no uniform class of active systems, what is meant by active must be carefully specified when constructing a theory for a system. In this work, when presenting a hydrodynamic description of active nematics in section 1.2, I define activity as local work production. By doing so, we see that the orientational order that breaks rotational symmetry is key for an active out-of-equilibrium behavior. Without this symmetry breaking, in the hydrodynamic limit, activity would just renormalize pressure and the system would behave as in thermodynamic equilibrium with an effective pressure.

I find that active matter is a beautiful example of the exchange between physics and biology. Active matter comes from the will to describe living systems, that are precisely out-of-equilibrium (death being the equilibrium state) because of local energy consumption (nutrients for a self propelled bacterium, ATP for a cell and so on). This way of going out of equilibrium motivated by living systems is now a standalone sub-field of non-equilibrium statistical mechanics with fundamental questions to be solved, fueled by biological questions. Experimentally, active-matter theories are tested on synthetic systems like vibrated rods [55] or synthetic polar particles [56]. Inversely, the study of biological system can learn from the study of active matter. Indeed, by developing a unifying framework using core physical principles, it provides a paradigm to understand multiple biological phenomena. Under this paradigm, we can understand using the same core principles the collective motion of bacteria, flocks of birds, the motion of tissues, or the cytoskeleton dynamics inside cells [23], as depicted on fig. 1.6.

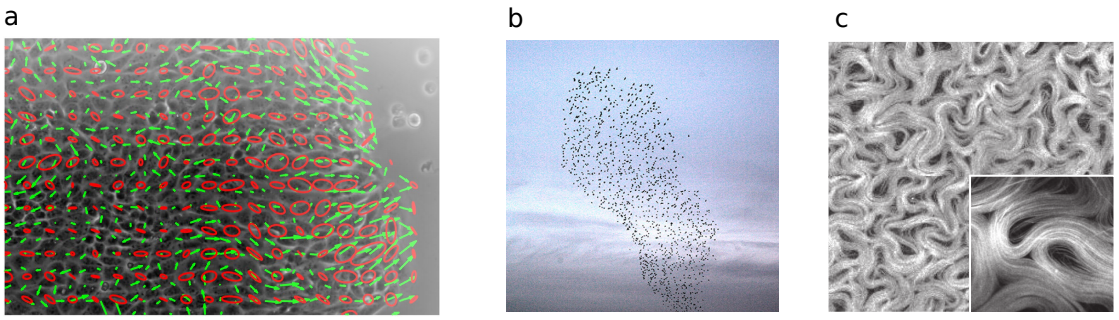

Figure 1.6: **Different systems of active matter. a** Collective migration of cells with the velocity field (green arrows) and local stress tensor indicated by red ellipses. Adapted from [57]. **b** Flock of birds, that can be modeled by polar active particles. Adapted from [58]. **c** Synthetic active nematic made of microtubules and molecular motors in a turbulent regime. Adapted from [59]. a,b,c are three very distinct systems from a biological perspective, but they can all be described using models of active matter.

1.2 Hydrodynamics of active nematics

1.2.1 Introduction: constructing a hydrodynamic theory

In this work, we are interested in a continuum description of tissues as active materials, introduced in sections 1.1.1 and 1.1.2. We study two dimensional tissues made of elongated active cells that organize in a nematic phase, similar to the experimental studies of refs. [1, 27, 33]. We are specifically interested in the spontaneous flow that appears in monolayers of cells in confinement (see chapter 2) and because of topological defects (see chapter 3). From a theoretical perspective, we use a hydrodynamic theory to study tissues that have two fundamental properties: cells organize into an ordered nematic phase and can convert chemical energy into work [1, 27, 33, 36, 37]. If we are only interested in the collective behavior of the cells and seek to describe a tissue over long distances compared to a cell size and over long times compared to the relaxation time of the tissue (typically the time for several cell divisions), only few key variables are relevant. This is possible because over large scales and given sufficient time, if the system is perturbed most of the variations owing to microscopic details relax to their steady-state value in finite time. The few key variables relevant in the large-scale and long-time limit are called the hydrodynamic or slow variables. These are the variables for which their relaxation time diverges with the system size [60]. Such variables belong to three potential categories:

- Conserved variables: consider a quantity f that follows a conservation law

$$\partial_t f = -\nabla \cdot (j_f) \tag{1.1}$$

where j_f is the current density for the quantity f. Writing $f = f_0 e^{\omega t - i\mathbf{q}\mathbf{x}}$, the conservation law given by eq. (1.1) implies that for a long wave-length perturbation that diverges in $1/|q|$, the characteristic relaxation time $1/\omega$ diverges also. Therefore, in the large-scale long-time the variable f is relevant.

- Variables associated to a continuously broken symmetry that give rise to Goldstone modes. Take for example the nematic director in the ordered phase. Since a uniform rotation of the director does not cost energy, the relaxation time of a uniform deformation diverges with the size of the deformation. The orientation of the nematic director is therefore a hydrodynamic variable [61].

- Variables corresponding to an order parameter in a system close to a second order transition point, for which the relaxation time diverges [62]. We will not deal with those in this manuscript.

One of the power of hydrodynamic theories is the systematic procedure to derive them, proposer by Martin, Perodi and Pershan [60]. The identification of the hydrodynamic variables is the most critical part in the construction of the theory [42, 60]. Indeed, once the variables are identified one can follow a set of principles based on entropy production to derive the evolution of the system close to thermal equilibrium. The signature for a system to be out of equilibrium is the existence of a finite entropy production. Therefore, close to equilibrium, one can perform a linear expansion of the entropy production as a function of the previously identified hydrodynamic variables. Then, the Onsager reciprocal relations [63] provide a systematic coupling between the different hydrodynamical variables that only depends on symmetries, called constitutive equations. We therefore obtain a linear hydrodynamic theory. Other equivalent approaches exist to determine the out-of-equilibrium dynamics based on the minimization of a dissipation functional called the Rayleighian [64].

Let us now construct this linear hydrodynamic theory for an active nematic fluid. In what sense the system is active is specified when considering the entropy production. A simpler case of constructing a hydrodynamic theory for passive isotropic fluids can be found in [42,65]. For passive liquid crystals,a pedagogical derivation is given in [35,42].

1.2.2 Conservation laws and hydrodynamic variables

Let us now consider a tissue made of a large number of cells that make a two dimensional monolayer, at constant temperature T. We assume that through coarse-graining we can construct local continuous quantities, such as the mass density $\rho(\mathbf{x})$ defined as the average mass density of cells in a coarse-graining volume centered at point $\mathbf{x}$. Similarly, the velocity field $\mathbf{v}(\mathbf{x})$ is the average velocity of cells contained in the same coarse-grained volume. The size of a coarse-grained volume should be large compared to the cell size, but in practice it is of the same order of magnitude. A discussion on

the validity of the hydrodynamic description is given in section 2.7. The slow variables are determined using core physical principles. The first one is mass conservation which gives for the mass density ρ:

$$\partial_t \rho + \partial_\alpha(\rho v_\alpha) = 0 \tag{1.2}$$

Energy is conserved, and the coarse-grained energy density e satisfies

$$\partial_t e + \partial_\alpha J^e_\alpha = 0, \tag{1.3}$$

where J^e_α is a density flux of energy, i.e a local conserved exchange of energy.
The equation of motion is a conservation equation for the momentum density $\rho\mathbf{v}$:

$$\partial_t(\rho v_\alpha) - \partial_\beta(\sigma^t_{\beta\alpha} - \rho v_\alpha v_\beta) = 0 \tag{1.4}$$

Cases where the momentum is not conserved due to interactions with the substrate will be discussed throughout chapters 2 and 3. In the context of active matter, systems where momentum is conserved are referred to as wet active matter, while systems where momentum is not conserved are referred to as dry active matter. Wet active matter is more suited to tissues where cell-cell adhesion induces flow of momentum through shear forces while dry active matter is used typically to describe fluids made of bacteria where friction with the substrate dominates [23]. In the context of cells that are at very low Reynolds number, the so-called Reynolds stress $\rho v_\alpha v_\beta$ is ignored in the following with respect to other contributions to the stress.

The tissues that we consider are deep in an ordered nematic phase [27]. Let us call $\mathbf{p}$ the polarization vector and in the nematic phase only the orientation of $\mathbf{p}$ matters. The orientation is given via the principal directions of the two dimensional nematic tensor $Q_{\alpha\beta} = p_\alpha p_\beta - \delta_{\alpha\beta}/2$. We construct the theory with the polarization vector $\mathbf{p}$ instead of a nematic tensor because the theory for wet active polar fluids is similar (except in the nematic phase we impose the $\mathbf{p} \to -\mathbf{p}$ symmetry). In the nematic phase, the rotational symmetry is continuously broken by the orientation of $\mathbf{p}$. However, only the orientation of $\mathbf{p}$ is a slow mode in two dimensions, the modulus of $\mathbf{p}$ relaxes rapidly to the steady-state value $\mathbf{p}^2 = 1$ in the ordered phase.

1.2.3 Entropy production rate

As it is common practice for non-equilibrium thermodynamics [65], in the coarse-graining we assume local equilibrium, meaning that for the coarse-grained volume one is capable of writing densities of state functions such as energy and entropy. The evolution of the entropy density s is given by the second law of thermodynamics:

$$\partial_t s + \partial_\alpha J^s_\alpha = \theta_s, \tag{1.5}$$

with $J^s_\alpha = v_\alpha s + j^s_\alpha$ the current of entropy. The current j^s_α is an "exchange" of entropy, i.e a local heat flux.

The entropy production rate $\theta_s > 0$ needs to be given as a function of the hydrodynamic variables, which is achieved by relating θ_s to the free energy production rate. The evolution of the free energy density $f = e - Ts$ is:

$$\partial_t f + \partial_\alpha J^f_\alpha = \theta_f, \tag{1.6}$$

with $J^f_\alpha = v_\alpha f + j^f_\alpha$ the free energy current and θ_f the free energy production rate. In what follows, we consider that the temperature is constant in the tissue and we drop any temperature derivatives. Let us now relate the free energy production to the entropy production. From the definition of the free energy,

$$\partial_t f = \partial_t e - T\partial_t s \tag{1.7}$$

Using the evolution of the energy (1.3) and of the entropy (1.5),

$$\partial_t f = -\partial_\alpha (J^e_\alpha - TJ^s_\alpha) - T\theta_s \tag{1.8}$$

The form of (1.8) defines the free energy flux J^f_α and the free energy production rate θ_f as

$$J^f_\alpha = J^e_\alpha - TJ^s_\alpha \tag{1.9}$$

$$\theta_f = -T\theta_s \tag{1.10}$$

We are now left with the task of computing the free energy production θ_f. For the hydrodynamic theory, only the evolution of the free energy density with respect to the hydrodynamic variables matter, and we consider $f(p_\alpha, \rho, \rho v_\alpha)$. Formally, the evolution of the free energy density in terms of the hydrodynamic variables is:

$$\partial_t f = \frac{\partial p_\alpha}{\partial t}\frac{\delta f}{\delta p_\alpha} + \frac{\partial \rho}{\partial t}\frac{\delta f}{\delta \rho} + \frac{\partial(\rho v_\alpha)}{\partial t}\frac{\delta f}{\delta(\rho v_\alpha)} \tag{1.11}$$

We introduce the following physical quantities:

- The molecular field $h_\alpha = -\frac{\delta f}{\delta p_\alpha}$. h_α gives the direction to minimize the free energy. Indeed, if $p_\alpha \sim h_\alpha$, then $\delta f = -h_\alpha \delta p_\alpha = 0$.
- The chemical potential $\mu_c = \frac{\delta f}{\delta \rho}$

We make the assumption that the free energy depends on momentum only through the kinetic energy, therefore $\delta f/\delta(\rho v_\alpha) = v_\alpha$. Using the conservation laws (1.2) and (1.4),

$$\partial_t f = -h_\alpha \partial_t p_\alpha - \mu_c \partial_\alpha(\rho v_\alpha) + v_\alpha \partial_\beta \sigma^t_{\beta\alpha} \tag{1.12}$$

which can be rewritten

$$\partial_t f + \partial_\alpha \left((\mu_c \rho - \sigma^t_{\alpha\beta}) v_\beta \right) = -h_\alpha \partial_t p_\alpha + \rho v_\alpha \partial_\alpha \mu_c - \sigma^t_{\beta\alpha} \partial_\beta v_\alpha \tag{1.13}$$

The expression (1.13) allows us to identify a free energy current $J^f_\alpha = (\mu_c\rho - \sigma^t_{\alpha\beta})v_\beta$ and a density of free energy production rate $\theta_f = -h_\alpha\partial_t p_\alpha + \rho v_\alpha\partial_\alpha\mu_c - \sigma^t_{\beta\alpha}\partial_\beta v_\alpha$. Therefore, the density of entropy production rate is:

$$T\theta_s = h_\alpha\partial_t p_\alpha - \rho v_\alpha\partial_\alpha\mu_c + \sigma^t_{\beta\alpha}\partial_\beta v_\alpha \tag{1.14}$$

Until this point we have been constructing a hydrodynamic theory for a passive nematic [35,42,65]. We are however interested in an active nematic tissue. The activity of the tissue comes from the ability of the cells to convert chemical energy into mechanical work, which contributes to the free energy density production. As presented in section 1.1.1, we take ATP hydrolysis to be the model chemical reaction providing mechanical work. ATP hydrolysis into ADP releases an energy $\Delta\mu$, and if there is a rate r of hydrolysis, there is an added mechanical power term in the entropy production rate $r\Delta\mu$. From a hydrodynamic perspective, the exact source of mechanical work is not important, what makes the system active and changes the hydrodynamic behavior compared to a passive system is the existence of local mechanical work. This active power source modifies the density of entropy production rate:

$$T\theta_s = h_\alpha\partial_t p_\alpha - \rho v_\alpha\partial_\alpha\mu_c + \sigma^t_{\alpha\beta}\partial_\alpha v_\beta + r\Delta\mu \tag{1.15}$$

Remarks

1. It is clear from the derivation that this procedure can be generalized to a broader context to include chemical reactions, multiple components or different thermodynamic conditions, but the steps of writing the production of the thermodynamic potential using the hydrodynamic variables to get the entropy production remains the same [66].

2. The entropy production given in (1.15) is not unique and depends on what is considered as a current or a production rate of free energy. However the rest of the derivation shows that the expression of the entropy production is set by the symmetries of the system.

3. The definition of active matter as local source of work can seem restrictive but considering also local sources of heat creates terms in $J^s_\alpha\partial_\alpha T$ and does not lead to a new class of behavior with respect to more classical out-of-equilibrium thermodynamics

A system is out of equilibrium when it develops local finite fluxes (microscopically when detailed balance breaks down) that must vanish when equilibrium is recovered. Therefore, close to equilibrium, each term on the right-hand side (RHS) of the entropy production (1.15) can be interpreted as the product between a flux and a conjugate thermodynamic force. The hydrodynamic evolution of the system is then given by writing

phenomenological equations that linearly couple the forces and the fluxes driving the system out of equilibrium [65]. This ensures that, when equilibrium is recovered, both fluxes and conjugated forces vanish. These phenomenological equations in the context of continuum mechanics are referred to as constitutive equations. To give a formal description of the Onsager procedure [63], let us call the fluxes X_i and the thermodynamic forces F_i. After explaining the criteria to derive the constitutive equations from a formal point of view, I will apply the procedure to this specific problem. The entropy production rate is of the form $T\theta_s = \sum_i X_i F_i$. The phenomenological equations state that $X_i = \sum_j L_{ij} F_j$. The L_{ij} are coupling coefficients that must satisfy certain properties to conserve the symmetries of the problem:

1. Time-reversal symmetry: Onsager proves in refs. [63, 67] that the hypothesis of microscopic reversibility on the underlying processes contributing to the entropy production imposes specific symmetries for the coefficients L_{ij}. The different thermodynamic forces F_i can have different signatures upon time-reversal. F_i can be odd with respect to time-reversal ($F_i \to -F_i$ when reversing time) or even ($F_i \to F_i$ when reversing time). Microscopic reversibility imposes that the coupling coefficients associated to two forces of the same signature with respect to time-reversal are symmetric: $L_{ij} = L_{ji}$ if F_i and F_j have the same signature. For forces of different time-signature, the coefficients must be anti-symmetric: $L_{ij} = -L_{ji}$ if F_i and F_j have different signatures. The fluxes with symmetric coupling coefficients are called dissipative fluxes, because they contribute to entropy production. The fluxes with antisymmetric coupling coefficients are called reactive fluxes, because they do not contribute to entropy production. Positivity of the entropy production imposes that the symmetric matrix of dissipative coefficient is positive, which imposes that all eigenvalues of the matrix are positive. One of the conditions for positivity is that diagonal coefficient must be positive $L_{ii} > 0$ (for example a negative viscosity is inadmissible).

2. "Space" symmetries: following the Curie principle, the forces and fluxes driving the system out of equilibrium must have the same underlying space symmetries of the system. In our case of nematic tissue, there is translational invariance but rotational invariance is broken because there is a particular orientation in the ordered phase given by the director $\mathbf{p}$. If we rotate the frame of a certain amount, the director $\mathbf{p}$ must be rotated by the same amount if we want the rotation to be invariant. Forces and fluxes can have different tensorial nature (for example a rank-two tensor flux coupled to a scalar force), therefore coupling coefficients are tensorial but must be constructed using tensors that respect the symmetries.

Let us now derive the phenomenological constitutive equations from the entropy production rate (1.15). In order to satisfy the symmetry requirements, it is convenient to re-write the RHS of eq. (1.15) with quantities that satisfy the translational and rotational

symmetries. To this extent, we split the velocity gradient into a symmetric part $u_{\alpha\beta}$ and an anti-symmetric part $\omega_{\alpha\beta}$ related to rotation: $\partial_\alpha v_\beta = u_{\alpha\beta} + \omega_{\alpha\beta}$ with $u_{\alpha\beta} = \left(\partial_\alpha v_\beta + \partial_\beta v_\alpha\right)/2$ and $\omega_{\alpha\beta} = \left(\partial_\alpha v_\beta - \partial_\beta v_\alpha\right)/2$. Similarly, we split the total stress $\sigma^t_{\alpha\beta}$ into a symmetric part $\sigma^S_{\alpha\beta} = (\sigma^t_{\alpha\beta} + \sigma^t_{\beta\alpha})/2$ and an anti-symmetric one $\sigma^A_{\alpha\beta} = (\sigma^t_{\alpha\beta} - \sigma^t_{\beta\alpha})/2$. The existence of an antisymmetric stress tensor is due to torques created by the free energy. If the system is not chiral, the antisymmetric stress is given by [35]:

$$\sigma^A_{\alpha\beta} = \frac{1}{2}(\mathbf{h}\times\mathbf{p}) = \frac{1}{2}\left(h_\alpha p_\beta - h_\beta p_\alpha\right) \tag{1.16}$$

For the non-equilibrium dynamics, one needs to differentiate, in the remaining symmetric part of the total stress tensor, the "hydrostatic" stress from the "out-of-equilibrium" stress. For isotropic system a change of volume changes the free energy and give rise to a hydrostatic pressure. For a system with nematic symmetry, a change of volume changes the free energy in an anisotropic manner and there is stress tensor associated to this free energy change (see appendix A) instead of a scalar. This stress tensor is called the Ericksen stress tensor and it satisfies a Gibbs-Duhem relation:

$$\partial_\beta \sigma^E_{\beta\alpha} = -\rho\partial_\alpha \mu_c - h_\gamma \partial_\alpha p_\gamma \tag{1.17}$$

The symmetric stress $\sigma^S_{\alpha\beta}$ is now decomposed into an out-of-equilibrium stress $\sigma_{\alpha\beta}$ and the Ericksen stress $\sigma^S_{\alpha\beta} = \sigma_{\alpha\beta} + \sigma^E_{\beta\alpha}$. In summary, the velocity gradient tensor and the stress tensor have the following decomposition:

$$\partial_\alpha v_\beta = u_{\alpha\beta} + \omega_{\alpha\beta} \tag{1.18}$$

$$\sigma^t_{\alpha\beta} = \sigma_{\alpha\beta} + \sigma^E_{\alpha\beta} + \sigma^A_{\alpha\beta} \tag{1.19}$$

This gives for the term $\sigma^t_{\alpha\beta}\partial_\alpha v_\beta$ in (1.15):

$$\sigma^t_{\alpha\beta}\partial_\alpha v_\beta = \sigma_{\alpha\beta}u_{\alpha\beta} + \sigma^A_{\alpha\beta}\omega_{\alpha\beta} + \sigma^E_{\alpha\beta}\partial_\alpha v_\beta \tag{1.20}$$

From eq. (1.16) $\sigma^A_{\alpha\beta}\omega_{\alpha\beta} = \omega_{\alpha\beta}p_\beta h_\alpha$. In the entropy production rate, one can perform a sort of "integration by part" because if there is a term of the form $u\,\mathrm{d}v$, it can be written $u\,\mathrm{d}v = \mathrm{d}(uv) - v\,\mathrm{d}u$ and the total derivative changes the entropy current, not the entropy production. From eq. (1.17), $-\partial_\beta\sigma^E_{\beta\alpha}v_\alpha = \rho v_\alpha\partial_\alpha\mu_c + h_\beta v_\alpha\partial_\alpha p_\beta$. The entropy production rate (1.15) now reads:

$$T\theta_s = \sigma_{\alpha\beta}u_{\alpha\beta} + h_\alpha\mathcal{P}_\alpha + r\Delta\mu \tag{1.21}$$

With $\mathcal{P}_\alpha = \frac{Dp_\alpha}{Dt} = \partial_t p_\alpha + v_\beta\partial_\beta p_\alpha + \omega_{\alpha\beta}p_\beta$ the covariant co-rotational time derivative of the director $\mathbf{p}$.

1.2.4 Constitutive equations

Now that the entropy production is given by eq. (1.21), we can write the phenomenological constitutive equations. There is no *a priori* rule to determine from the entropy production, for a term such as $\mathcal{P}_\alpha h_\alpha$, which is considered a flux and which a force between $\mathcal{P}_\alpha$ and h_α. There is a choice to make that do not impact the physics, only the physical meaning of the coupling coefficients. Once the choice of forces is made, we identify their signature under time-reversal: $+1$ if the force is even under time reversal symmetry, and -1 if is odd. The choice of fluxes and forces along with the time signature of the force is given in Table 1.1.

Flux	Force	signature of the force
$\sigma_{\alpha\beta}$	$u_{\alpha\beta}$	-1
$\mathcal{P}_\alpha$	h_α	$+1$
r	$\Delta\mu$	$+1$

Table 1.1: Choice of fluxes and forces, and time signatures of the forces that define the symmetry of the Onsager coefficients

We split the stress into a traceless part indicated by a upper tilde and an isotropic diagonal part that represents pressure. The fluxes are separated into a dissipative part (superscript ^{d}) and a reactive part (superscript ^{r}):

$$\sigma_{\alpha\beta} = \tilde{\sigma}^d_{\alpha\beta} + \tilde{\sigma}^r_{\alpha\beta} - (P^d + P^r)\delta_{\alpha\beta} \tag{1.22}$$

$$\mathcal{P}_\alpha = \mathcal{P}^d_\alpha + \mathcal{P}^r_\alpha \tag{1.23}$$

$$r = r^d + r^r \tag{1.24}$$

Furthermore, we consider an incompressible fluid such that the divergence of the velocity vanishes, $\partial_\gamma v_\gamma = 0$. Therefore, the symmetric velocity gradient tensor $u_{\alpha\beta}$ is traceless.

We now write the coupling between the fluxes and the forces respecting the symmetries. The only vector that respects the breaking of rotational invariance due to the ordered nematic phase is p_α, and the only traceless tensor is $q_{\alpha\beta} = p_\alpha p_\beta - \frac{\delta_{\alpha\beta}}{2}$. The dissipative fluxes are given by

$$\tilde{\sigma}^d_{\alpha\beta} = 2\eta u_{\alpha\beta} \tag{1.25}$$

$$P^d = \bar{\eta}\partial_\gamma v_\gamma = 0 \tag{1.26}$$

$$\mathcal{P}^d_\alpha = \frac{1}{\gamma} h_\alpha + \lambda\Delta\mu p_\alpha \tag{1.27}$$

$$r^d = \lambda p_\alpha h_\alpha + \Lambda\Delta\mu \tag{1.28}$$

whereas the reactive fluxes are

$$\tilde{\sigma}^r_{\alpha\beta} = -\zeta\Delta\mu q_{\alpha\beta} + \frac{\nu}{2}(p_\alpha h_\beta + p_\beta h_\alpha - \frac{2}{3}p_\gamma h_\gamma \delta_{\alpha\beta}) \tag{1.29}$$

$$P^r = -\bar{\zeta}\Delta\mu + \bar{\nu}p_\gamma h_\gamma \tag{1.30}$$

$$\mathcal{P}^r_\alpha = -\nu u_{\alpha\beta}p_\beta \tag{1.31}$$

$$r^r = \zeta q_{\alpha\beta}u_{\alpha\beta} \tag{1.32}$$

Physical meaning of coupling coefficients

Let us now comment on the coupling coefficients introduced in eqs. (1.25) to (1.32). The coefficient coupling the stress to the velocity gradient is the usual viscosity η. In this work we choose to keep a scalar viscosity instead of taking a different viscosity coefficient for the nematic direction and the perpendicular direction.

The coefficients γ and ν are standard liquid-crystal hydrodynamic coefficients. γ is a rotational viscosity and ν is the so-called flow-alignment parameter. In a nematic fluid, the orientation and the velocity field are coupled by ν. A perturbation of the director can create a velocity gradient and vice-versa.

There are two "active" coefficients, ζ and λ. In the ordered phase $\mathbf{p}^2 = 1$ the coefficient λ is not important since it acts on the modulus of $\mathbf{p}$ which is not a hydrodynamic variable. At the cost of redefining ζ by $\zeta + \lambda\gamma\nu$, there is no loss of generality in taking $\lambda = 0$ [41]. The important active coefficient is ζ, which determines the active stress $\sigma^{\text{act}}_{\alpha\beta} = -\zeta\Delta\mu q_{\alpha\beta}$. This active stress is at the origin of the non-equilibrium behavior of active nematic fluids. Because of this active stress, a gradient of orientation creates an active force that can generate a spontaneous flow. We distinguish two types of activity depending on the sign of ζ. If $\zeta < 0$, the active stress is contractile along $\mathbf{p}$. Coming back to cells in a tissue, a contractile tissue means that the internal forces of a cell are contracting. Inversely, the active stress is extensile along $\mathbf{p}$ if $\zeta > 0$. A representation of the internal forces is given on fig. 1.7. Although cells are contractile at the individual level, there is no clear and obvious reason for a tissue to be either contractile and extensile, it is determined experimentally. This is not so surprising since the active stress is a global hydrodynamic effect that encompasses a multitude of microscopic effects such as active cell contractility, active cell-cell adhesions and active interactions with the substrate [68]. For example, looking at the motion of topological defects, monolayers of MDCK (Madin Darby canine kidney) cells and neural progenitor cells were reported having an extensile behavior [36, 37]. NIH 3T3 mouse embryo fibroblasts and C2C12 mouse myoblasts were reported having a contractile behavior [33, 36]. The experiments that this manuscript is referring to were made with C2C12 myoblasts. When confined in a stripe, C2C12 cells display an extensile behavior (see [1] and chapter 2) while the motion of topological defects in a free monolayer is consistent with contractile active stresses (see chapter 3). This apparent contradiction can be understood by the

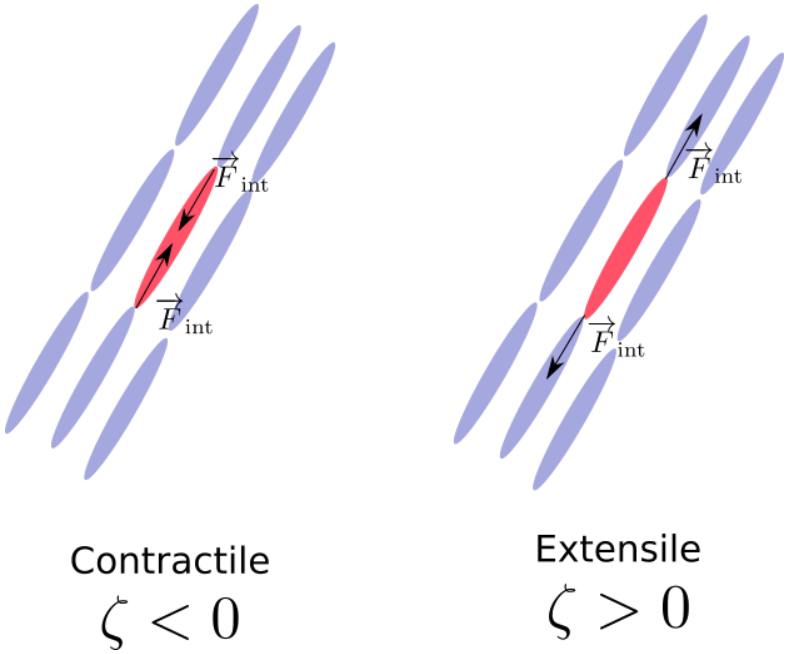

Figure 1.7: On the left is the effect of a contractile stress on a cell in a monolayer, while on the right is the effect of an extensile stress.

fact that the extensile or contractile nature of the tissue is not an intrinsic property but an emergent hydrodynamical property. As such, interactions with the substrate could generate different active contributions depending on the geometry, as suggested by Maitra *et al.* [68].

Equations of motion

At the end of this procedure, the goal is to solve the equations of motion for an active nematic tissue. The total stress is

$$\sigma^t_{\alpha\beta} = 2\eta u_{\alpha\beta} - \zeta \Delta\mu q_{\alpha\beta} + \frac{\nu}{2}(p_\alpha h_\beta + p_\beta h_\alpha - \frac{2}{3} p_\gamma h_\gamma \delta_{\alpha\beta}) + \frac{1}{2}\left(h_\alpha p_\beta - h_\beta p_\alpha\right) + \tilde{\sigma}^E_{\alpha\beta} - P\delta_{\alpha\beta}, \tag{1.33}$$

where the pressure P is the diagonal part of the total stress and contains the diagonal parts of all other contributions. The exact contributions of thermodynamic quantities in P are irrelevant: P is the mechanical pressure and is a Lagrange multiplier for the incompressibility condition that must be determined through force balance. We therefore introduced in eq. (1.33) the traceless part of the Ericksen stress $\tilde{\sigma}^E_{\alpha\beta}$. We have two vectorial "equations of motion": momentum conservation given by eq. (1.4) and the

evolution of the director obtained by summing eq. (1.27) and eq. (1.31):

$$\partial_\beta \sigma^t_{\beta\alpha} = 0 \tag{1.34}$$

$$\partial_t p_\alpha + v_\beta \partial_\beta p_\alpha + \omega_{\alpha\beta} p_\beta = \frac{1}{\gamma} h_\alpha - \nu u_{\alpha\beta} p_\beta \tag{1.35}$$

With $\sigma^t_{\beta\alpha}$ given by eq. (1.33).

We can verify that this problem is well posed given appropriate boundary conditions, because in two dimensions we have two scalar equations for the momentum, two scalar equations for the polarization and one equation for incompressibility, making a total of five equations. As unknowns, we have two components for the velocity, two components for the polarization and a component for the pressure, which makes five unknowns.

The main consequence of activity is that orientation gradients create active forces because of the active stress. Then the state where $\mathbf{p}$ is parallel to $\mathbf{h}$ and there is no gradient of velocity can become unstable. Among active hydrodynamic effects, a uniform band of active nematic at rest is no longer stable above a critical band width [41]. Indeed, gradients of orientation can arise spontaneously due to the activity and the coupling between orientation and velocity gradients. This effect is explored in depth in chapter 2. When a gradient of orientation is imposed such as for a topological defect, active forces are generated and can create a flow. Flows created by defects are detailed in chapter 2. This behavior is different from a passive nematic liquid, that can deform without developing velocity gradients, for example due to an external magnetic field [35].

Chapter 2

Spontaneous tilt and flows in stripes

In chapter 1 we introduced the properties of tissues that are studied in this manuscript and the hydrodynamic theory for active nematic fluids to describe such tissues. In this chapter we investigate the effect of the active stress for a confluent monolayer of elongated cells (most experiments by T. Aryaksama were done using C2C12 mouse embryo myoblasts) confined in a infinite stripe of varying widths (see fig. 2.4). This simple geometry allows us to make analytical treatment of eqs. (1.34) to (1.35) and to perform experiments. This chapter is organized as follows: a first section introduces the experimental setting and the general qualitative behavior of the studied cells. We then recall a classical problem of confined passive liquid crystals called the Freedericksz transition, and present its active analog where the active stress plays the role of an external field and creates spontaneous shear flows [41]. We then present the hydrodynamic effects of cell division, as well as the interactions with the substrate presented in [1]. Finally, we present the results of this PhD work where we have investigated the effect of orientational cues in the stripes that favor a specific orientation in the stripe (a sort of external field), and its potential competition with the active stress.

2.1 Experiments

I introduce in this section the experiments performed by Thibault Aryaksama in the group of Pascal Silberzan at Institut Curie that are at the core of the work in this chapter. In the experiments, elongated cells are plated on adhesive stripes of varying widths, from tens of micrometers to a millimeter. The length of the stripes can be considered as infinite compared to the size of the cells, since it is in centimeters. At initial time, there are several cells in the stripe that divide over time, until confluency is reached. After confluency, the monolayer of cells organize into a well ordered nematic phase, as shown on figure 2.1. For certain type of cells (RPE1 and C2C12 cells in the experiments of T. Aryaksama as well as in ref. [1]), cells after confluency acquire a gradient of orientation

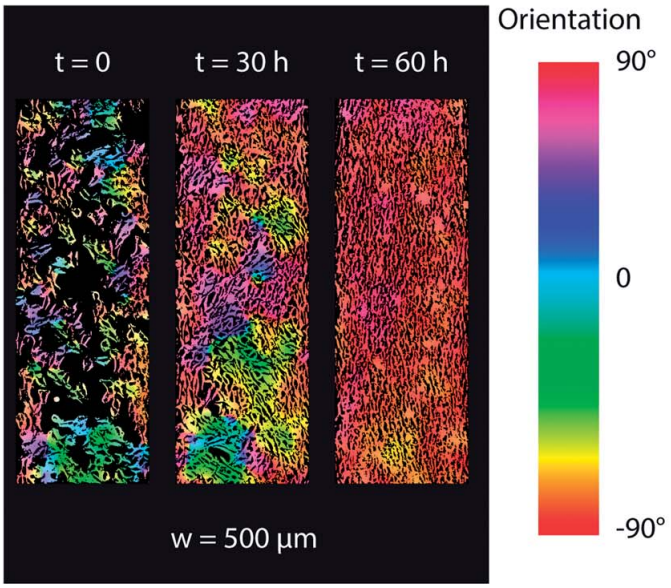

Figure 2.1: Picture of the different stages when platting NIH-3T3 fibroblast cells on a stripe of width $500\mu m$. Cells divide until reaching confluency (soon after 30h). Once confluency is reached, cells align almost perfectly in a nematic phase, as seen on the 60th hour. Adapted from [27].

along the width of the stripe, as shown on figs. 1.4 and 2.4. The cells at the center of the adhesive stripes are tilted with respect to the cells at the boundary, which align with the direction of the stripe. As it is expected by the hydrodynamic theory there is a shear flow associated to this gradient of orientation. The direction of the flow with respect to the gradient of orientation gives the extensile or contractile nature of the cells, as detailed in section 2.2.3. On top of the tilt and the shear flow predicted by Voituriez *et al.* [41], there are convergent flows in the perpendicular direction of the stripe due to division at the boundary of the stripe and extrusion at the center. Cells like NIH-3T3 do not show this active behavior, even for stripes that have a width of the order of a millimeter. This behavior can be attributed to an interaction with the substrate [1]. Effects of division are investigated in section 2.3.1 and the influence of the substrate in section 2.3.2.

In this thesis, following the work of Duclos, Blanch-Mercader *et al.* [1], we are interested in controlling the orientation of cells inside the stripe. This is an attempt at imposing a cell orientation in competition with the orientation imposed by the geometry of the stripe. An external field orienting a nematic between two plates perpendicular to the field is a classical liquid-crystal problem called the Freedericksz transition [35] that is detailed in section 2.2.1. Control over the orientation of cells can be achieved by micro-patterning grooves or by creating abrasions on the substrate, as shown on fig. 2.2. The fact that orientation of cells can be controlled by micro-patterning of the

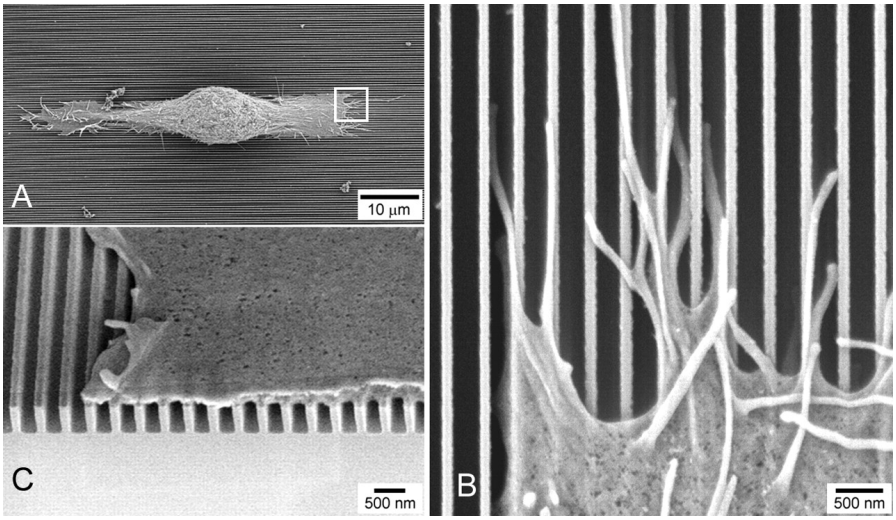

Figure 2.2: Scanning electron microscope image of coronal epithelial cell on a micro-patterned substrate. A. The cell aligns in the direction made by the grooves. B. Zoom on filopodia and their interaction with the grooves. C. Transverse view of the cell that do not go into the grooves. Adapted from [69].

substrate is called "contact guidance" [69–72]. Explaining the mechanisms producing contact-guidance is outside the scope of this work, and is a debated topic [70]. I simply specify that contact-guidance is not necessarily an universal feature of all cells. Different orientations can be obtained depending on the cell type and on the topography of the substrate. Varying width and frequencies of the groove pattern can lead to different behavior [71]. Cells can for example align perpendicularly to the direction of the grooves. For the experiments studied in this work, T. Aryaksama performed micro-abrasions by sliding sandpaper in the perpendicular direction of the stripe. Instead a producing a well defined pattern as shown in fig. 2.2, this method creates asperities of different depth and separated by different lengths, all in the same direction. A Fourier transform of the glass therefore has a broad spectrum. C2C12 cells were observed to align with the direction of the abrasions over long distances compared to the cell in a free monolayer of abraded substrate, as shown on fig. 2.3.

In the studied stripes, we see on fig. 2.4 that for width larger then around 400μm, cells orient perpendicular to the stripe and parallel to the direction of the abrasions. For smaller width between 30 – 200μm, cells show a moderate tilt, similar to the case when there are no abrasions. On fig. 2.4 is shown the central angle as a function of the width of the stripe.

From a theoretical perspective, the modeling of the abrasions as an external field creates a competition between "passive" effects due to the external field and "active" effects due to the active stress. A goal of the experiments that were performed is the

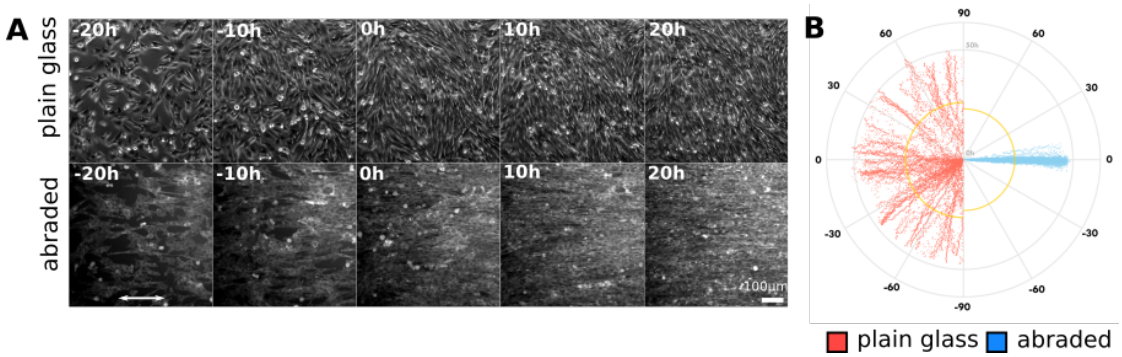

Figure 2.3: A. On top a free C2C12 monolayer without abrasions (plain glass) and on the bottom one with abrasions. The direction of abrasions is indicated by the white double arrow at time -20h and is perpendicular to the direction of the page. Confluency is determined by time 0h. We see that after confluency when there are abrasions there is almost perfect alignment everywhere in the field of view compared to plain glass. B. Representation of the distribution of angles on the plain glass (in red) and on the abraded surface (blue). We see that the plain glass has a broad distribution of angles, while with abrasions there is almost perfect alignment. Courtesy of Thibault Aryaksama.

identification of hydrodynamic parameters that can be extracted from the behavior of cells when varying the width [1]. The control over orientation by the abrasions is an added tool to probe hydrodynamic parameters. Experimentally varying the magnitude of the effect of the micro-patterning is not consistent but T. Aryaksama was able to change the orientation of the micro-abrasions with respect to the direction of the stripe. Competition between the active stress and the effect of the micro-abrasion allows for the measurement of the flow-alignment parameter ν. This result is presented in section 2.5.

2.2 Active Freedericksz transition

2.2.1 Competition between anchoring and energy: the passive Freedericksz Transition

Before going into active effects, let us start be presenting the Freedericksz transition, a classical problem which served as the basis for the creation of liquid crystal displays (LCD). Imagine that we confine a monolayer of ordered nematic between two plates and we make an hypothesis of strong anchoring, which means that the nematic is aligned with the direction of the plate at the boundary. We impose a uniform magnetic field $\mathbf{H}$ perpendicular to the direction of the stripe, as shown on fig. 2.5. Because of the breaking of symmetry in the nematic phase, the magnetization can be anisotropic and have different values in the direction of the polarization vector $\mathbf{p}$ and in the orthogonal

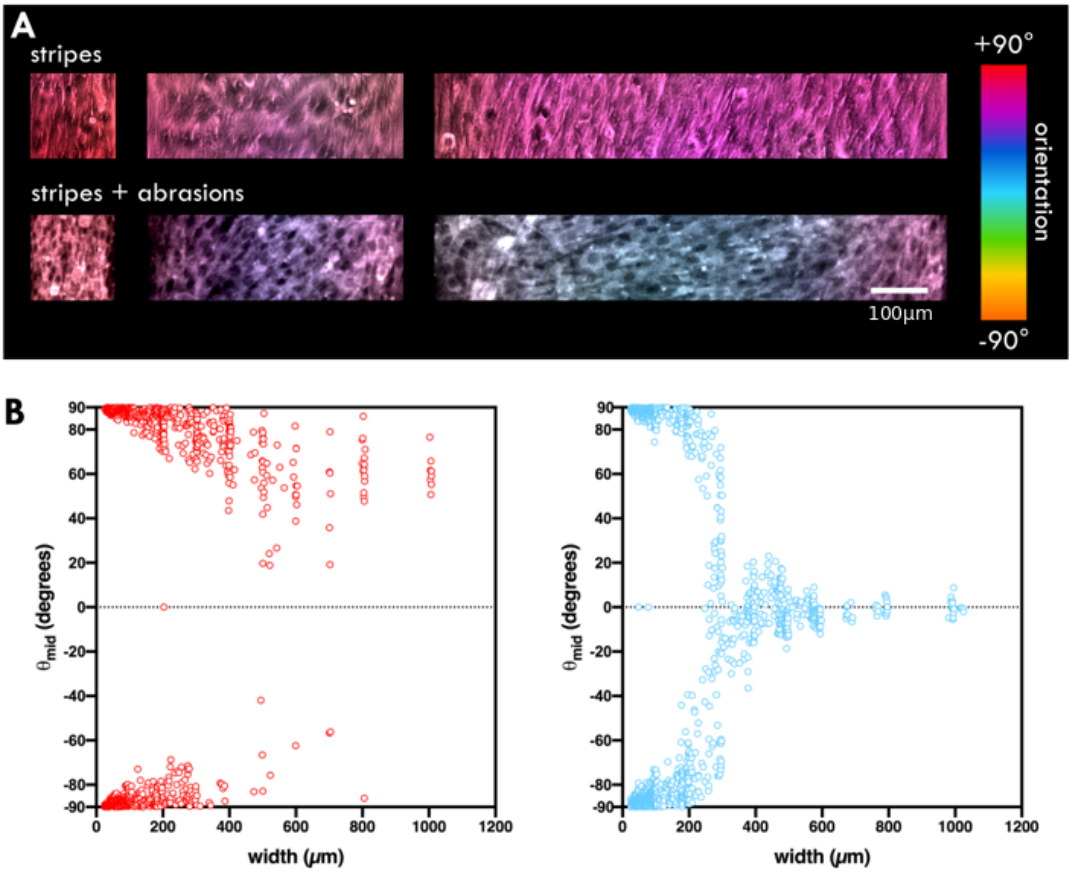

Figure 2.4: A. Picture of C2C12 cells in stripes of different widths, on plain glass (top) and on glass with abrasions perpendicular to the stripe (bottom). On the left for small stripes there is no tilt. On the middle there is a comparable tilt between abrasions and plain glass and on the right for large stripes the cells on the bottom align with the abrasions while the tilt is moderate for cells on plain glass. B. Angle in the middle of the stripe as a function of the width of the stripe, for plain glass (left, red) and for stripes with abrasions (right, blue). We see that when there are abrasions the cells align almost perfectly with the direction of the abrasions for stripes larger than around $400 - 500\mu m$. On plain glass, the middle angle does not reach a constant value. Preliminary figures, courtesy of Thibault Aryaksama.

direction $\mathbf{p}^{\perp}$. If $\mathbf{m}$ is the density of magnetization, then

$$\mathbf{m} = \chi_{||}(\mathbf{H} \cdot \mathbf{p})\mathbf{p} + \chi_{\perp}(\mathbf{H} \cdot \mathbf{p}^{\perp})\mathbf{p}^{\perp} \tag{2.1}$$

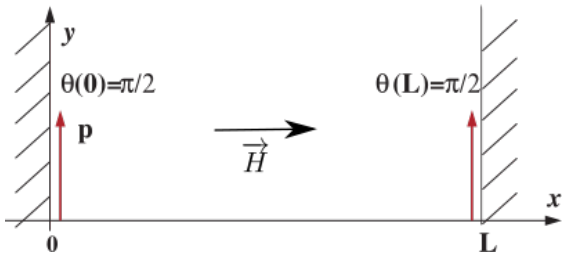

Figure 2.5: Schematic of the passive Freedericksz transition apparatus: a nematic is confined between two parallel plates and there is strong anchoring, the nematic at contact with the plates must be parallel to the plate. A magnetic field **H** perpendicular to the plates is applied.

where we introduced the parallel and perpendicular susceptibilities, respectively $\chi_{||}$ and $\chi_\perp$. This creates a density of magnetic energy f_m given by

$$f_m = -\frac{1}{2}\mathbf{m}\cdot\mathbf{H} \tag{2.2}$$

$$= -\frac{1}{2}(\chi_{||}-\chi_\perp)(\mathbf{p}\cdot\mathbf{H})^2 - \frac{1}{2}\chi_\perp\mathbf{H}^2 \tag{2.3}$$

$$= -\frac{\chi_a}{2}(\mathbf{p}\cdot\mathbf{H})^2 + C \tag{2.4}$$

with $\chi_a = \chi_{||} - \chi_\perp$ the difference between the parallel and orthogonal susceptibilities, and $C = -\chi_\perp\mathbf{H}^2/2$ is a constant that we can drop from the free energy density. Assuming that $\chi_a > 0$ (the case of interest for this work), the free energy is minimum when the polarization **p** is parallel to the magnetic field **H**.

Intuitively, there is a competition between the magnetic field that favors orientation perpendicular to the stripes, and the anchoring that favors an orientation parallel to the stripe. This competition is due to an distortion free energy that penalizes gradient of orientations. This distortion free energy is built as a gradient expansion of the director, that must respect the nematic symmetry $\mathbf{p} \to -\mathbf{p}$. The free energy is therefore constructed with terms of order $(\nabla\mathbf{p})^2$. Without going into the details of listing all possible terms (see ref. [35], section 3.2.1), there are two fundamental modes of deformation in two dimensions: splay corresponding to a pure divergence deformation, and bend corresponding to a pure curl deformation. The two types of deformation are represented on fig. 2.6. The distortion free energy also called the Frank free energy is given in two dimensions by an expansion in splay and bend:

$$F = \int dx\,dy\left[\frac{K_1}{2}(\nabla\cdot p)^2 + \frac{K_3}{2}(\nabla\times p)^2 - \frac{1}{2}h_{||}^0 p^2\right] \tag{2.5}$$

K_1 is the Frank constant associated with splay deformation and K_3 is the Frank constant associated with bend deformation. We are interested in effects deep in the nematic

Figure 2.6: The two fundamental modes of deformation in two dimensions. On the left a pure splay deformation, characterized by the Frank constant K_1. On the right a pure bend deformation, characterized by the Frank constant K_3. In three dimensions there is a third deformation out of the plane called twist (with a constant K_2).

phase, and to this extent we introduce a Lagrange multiplier $h_{\parallel}^0$ to ensure that we are in an ordered state where $\mathbf{p}^2 = 1$. For simplicity, we can consider the one-constant approximation $K = K_1 = K_3$. We do not deal with this case in this work, but the one-constant approximation can be relaxed depending on experimental observation, for example for topological defects [73]. In the one-constant approximation, the Frank free energy (2.5) is:

$$F = \int dx\, dy \left[\frac{K}{2} \partial_\alpha p_\beta \partial_\alpha p_\beta - \frac{1}{2} h_{\parallel}^0 p^2 \right] \tag{2.6}$$

In the presence of an external magnetic field $\mathbf{H}$ there is an added magnetic contribution to the free energy given by eq. (2.4), and the total free energy reads, up to a constant:

$$F = \int dx\, dy \left[\frac{K}{2} \partial_\alpha p_\beta \partial_\alpha p_\beta - \frac{\chi_a}{2} (\mathbf{p} \cdot \mathbf{H})^2 - \frac{1}{2} h_{\parallel}^0 \mathbf{p}^2 \right] \tag{2.7}$$

Critical field or length

With the free energy given by (2.7), we show that deep in the nematic phase the competition between the anchoring and the external field leads to a critical field of equivalently a critical width above which a gradient of orientation appears in the stripe.

Since we are in a well ordered nematic phase and we are not concerned with the dynamics of the modulus of $\mathbf{p}$, we consider that $\mathbf{p}^2 = 1$ and we use the angle θ with the $x-$axis such that $p = (\cos\theta, \sin\theta)$ in the (e_x, e_y) basis given on figure 2.5. In terms of the angle θ, up to a constant the free energy density is:

$$f = \frac{K}{2} (\nabla\theta)^2 - \frac{\chi_a}{2} H^2 \cos^2\theta \tag{2.8}$$

The anchoring condition imposes $\theta(x=0) = \theta(x=L) = \pi/2$, and in the ordered phase without external field the free energy is minimum at the only admissible uniform state $\theta(x) = \pi/2$. Looking at the free energy given in eq. (2.8), small angles are favored due to the magnetic field but are penalized by the distortion energy because of the anchoring condition that creates a gradient. There is a critical value for the magnetic field H_c, above which a gradient of orientation is favored and below which the uniform field is favored. Let us now calculate this critical field using free-energy arguments. Because of translation invariance in the $y-$direction, we will treat this problem as a one dimensional problem in the $x-$direction. We want to know what are the conditions for the uniform state $\theta = \pi/2$ to be stable. Let us make a small perturbation $\delta\theta$ to the ordered state: $\theta = \pi/2 + \delta\theta$ and Fourier expand this perturbation that must vanish in $x = 0$ and $x = L$: $\delta\theta(x) = \sum_n \delta\theta_n \sin q_n x$. Because of the anchoring condition $\theta(x=0) = \theta(x=L) = \pi/2$, $q_n = n\pi/L$, with n integer. With this Fourier expansion, the free energy density is given by

$$f = \sum_n \frac{1}{2}\delta\theta_n^2 \left(K q_n^2 - \chi H^2\right) \tag{2.9}$$

The condition for stability of the uniform state is that the free energy contribution of $\delta\theta$ is positive, therefore that $\chi H^2 < K q_n^2$. The smallest q_n is given for $n = 1$ and defines a critical field H_c given by

$$H_c = \frac{\pi}{L}\sqrt{\frac{K}{\chi}} \tag{2.10}$$

For $H > H_c$, at least the mode $q_1 = \pi/L$ becomes unstable. Above the critical field H_c, the uniform state $\theta(x) = \pi/2$ is no longer stable and a gradient of orientation determined by non-linear terms (see section 2.2.3) develops between the plates, as shown on fig. 2.7. Equivalently, we can think of a critical length L_c at fixed field, which is going to be the way we look at things in the following sections. L_c is given trivially from (2.10):

$$L_c = \frac{\pi}{H}\sqrt{\frac{K}{\chi}} \tag{2.11}$$

Above the critical length, the uniform state aligned with the direction of the stripe is no longer stable, there is a tilt at the center of the stripe and a gradient of orientation along the width.

In the following sections of this chapter, we study the active analog to this Freedericksz transition and describe the fields close and far from the transition length.

2.2.2 Critical length in the active Freedericksz transition

Let us now turn to an active system. A consequence of activity is the existence of an analog to the Freedericksz transition driven by activity instead of an external field [41].

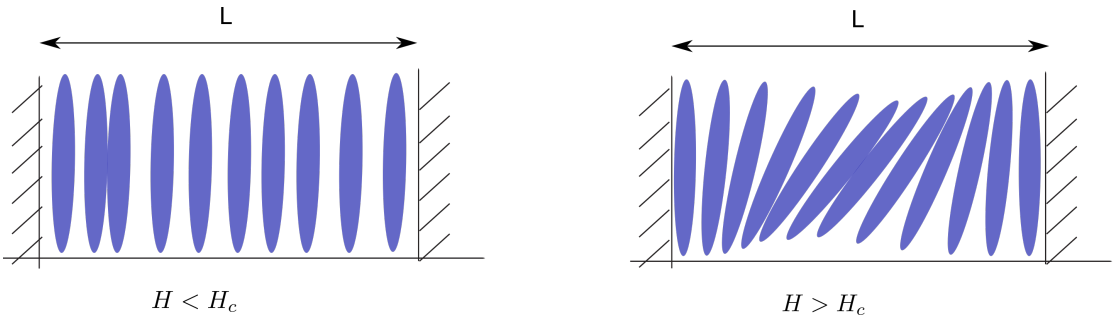

Figure 2.7: Schematic representation of the configuration for fields smaller (left) and greater (right) than the critical field. When $H < H_c$ the uniform configuration parallel to the plates is stable. When $H > H_c$ the uniform configuration is no longer stable and gradient of orientation (a tilt) develops between the plates.

The consequence is that a band of uniformly aligned nematics becomes unstable above a critical width L_c that depends on the activity of the system, which is represented hydrodynamically by the magnitude of the active stress $\zeta\Delta\mu$. A detailed calculation is given in this section but let me give first a hand-waving argument as to how this instability can develop: if we take a uniform alignment that is slightly perturbed, there is a gradient of orientation and therefore an active force. This active force in turn creates a flow. Because in nematics there is a coupling between flow and orientation through the flow-alignment parameter ν, this flow can further increase the perturbation. The existence of this positive feedback loop can give rise to an instability depending on values of the active stress coefficient ζ and of the flow-alignment parameter ν.

The set up for the active transition is similar to the one presented in the passive case, and is shown on fig. 2.8. We consider an active nematic liquid in a stripe of width L in

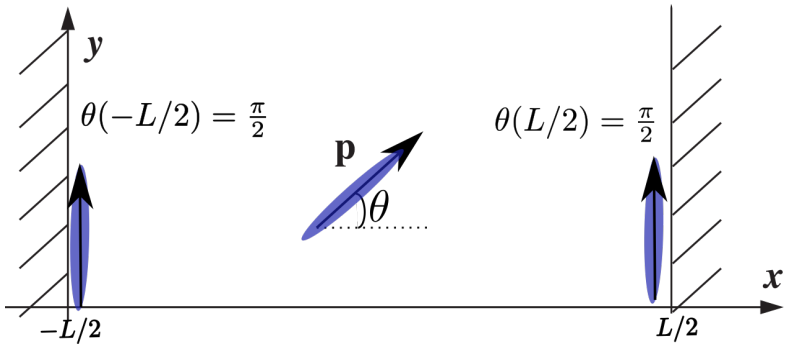

Figure 2.8: Configuration for the active Freedericksz transition: there is strong anchoring, i.e the orientation is parallel at the boundary. The angle θ is defined with respect to the $x-$axis.

the $x-$direction, and infinite in the $y-$direction. There is no external force acting on the system apart from the room pressure and strong anchoring is imposed. The following boundary conditions are imposed:

1. The cells have to be parallel to the walls at the boundary : $\theta(-L/2) = \theta(L/2) = \pi/2$
2. There is no transverse force at the walls: $\sigma^t_{xy}(-L/2) = \sigma^t_{xy}(L/2) = 0$
3. Cells cannot escape the stripe : $v_x(-L/2) = v_x(L/2) = 0$

The second boundary condition is a particular case and other boundary conditions lead to the same type of instability [41]. Given this geometry, there is an invariance in the $y-$direction. Therefore, force balance in the $y-$direction is given by

$$\partial_x \sigma^t_{xy} = 0 \tag{2.12}$$

Consequently, the stress is constant along the width of the stripe, and given the free boundary condition,

$$\sigma^t_{xy} = 0 \quad \text{in the entire stripe} \tag{2.13}$$

Let us now develop the equation (2.13) with the different contributions to the stress given in eq. (1.33). It is convenient to consider the molecular field $\mathbf{h}$ in the basis of the director $\mathbf{p}$. We define $\mathbf{h} = h_\parallel \mathbf{p} + h_\perp \mathbf{p}^\perp$. In the $xy-$basis, the molecular field is given by $h_x = h_\parallel \cos\theta - h_\perp \sin\theta$ and $h_y = h_\parallel \sin\theta + h_\perp \cos\theta$. The $xy-$component of the deviatoric part of the stress referred to as σ_{xy} in section 1.2.3 reads:

$$\sigma_{xy} = \eta \partial_x v_y - \frac{\zeta \Delta\mu}{2} \sin 2\theta + \frac{\nu}{2}(h_\parallel \sin 2\theta + h_\perp \cos 2\theta) \tag{2.14}$$

The $xy-$component of the anti-symmetric part of the stress given in eq. (1.16) reads:

$$\sigma^A_{xy} = -\frac{h_\perp}{2} \tag{2.15}$$

We are concerned with the stability of the uniformly aligned state, and the Ericksen stress is of second order in gradients of orientation and is usually neglected when interested in linear or weakly non-linear perturbations. In this specific geometry, it turns out that the Ericksen stress vanishes exactly. See appendix A for details on the Ericksen stress. Finally, the total stress reads:

$$\sigma^t_{xy} = 0 = \eta \partial_x v_y - \frac{\zeta \Delta\mu}{2} \sin 2\theta + \frac{\nu}{2}(h_\parallel \sin 2\theta + h_\perp \cos 2\theta) - \frac{h_\perp}{2} \tag{2.16}$$

We are now left with the incompressibility condition and the two equations for the evolution of the director. When the cell number is conserved, the incompressibility condition given the $y-$invariance is:

$$\partial_x v_x = 0 \tag{2.17}$$

Since cells cannot escape the stripe, $v_x = 0$ and we are only concerned with v_y. We project the equation for the director (1.35) onto $\mathbf{p}$ and on the perpendicular vector $\mathbf{p}^\perp$. On $\mathbf{p}$, eq. (1.35) reads:

$$0 = \frac{h_\parallel}{\gamma} - \frac{\nu}{2}\partial_x v_y \sin 2\theta \tag{2.18}$$

On the perpendicular direction $\mathbf{p}^\perp$, eq. (1.35) reads:

$$\partial_t \theta = \frac{h_\perp}{\gamma} - \frac{\partial_x v_y}{2}(\nu \cos 2\theta - 1) \tag{2.19}$$

The three equations of motions (2.16),(2.18) and (2.19) can be recast into a single non-linear equation for the angle θ by eliminating the parallel component of the molecular field $h_\parallel$ and the velocity gradient $\partial_x v_y$. The dynamics of the angle θ is given by:

$$\partial_t \theta = \frac{1}{4\eta + \gamma\nu^2 \sin^2 2\theta}\left[\frac{h_\perp}{\gamma}\Big(4\eta + \gamma(\nu^2 - 2\nu\cos 2\theta + 1)\Big) - \zeta\Delta\mu \sin 2\theta(\nu\cos 2\theta - 1)\right] \tag{2.20}$$

The perpendicular molecular field $h_\perp$ is given by the distortion free energy. The distortion free energy of an active nematic is exactly the same as in the passive case and, keeping the one Frank constant approximation, is given by eq. (2.6). We can rewrite the distortion energy using the angle θ:

$$F = \int \mathrm{d}x\, \mathrm{d}y\, \frac{K}{2}(\nabla\theta)^2 \tag{2.21}$$

Similarly, $h_\perp$ can be written in terms of the angle θ and is given by

$$h_\perp = -\frac{\delta F}{\delta\theta} \tag{2.22}$$

$$= K\nabla^2\theta = K\partial_x^2\theta \tag{2.23}$$

We therefore arrive at the final partial derivative equation (PDE) for the angle in the stripe:

$$\partial_t \theta = \frac{1}{4\eta + \gamma\nu^2 \sin^2 2\theta}\left[\frac{K\partial_x^2\theta}{\gamma}\Big(4\eta + \gamma(\nu^2 - 2\nu\cos 2\theta + 1)\Big) - \zeta\Delta\mu \sin 2\theta(\nu\cos 2\theta - 1)\right] \tag{2.24}$$

The question being asked is the stability of the uniform state $\theta = \pi/2$ as a function of the width of the stripe L. In order to do so, a linear stability analysis is performed. We perturb the angle near the uniform state $\theta(x,t) = \pi/2 + \delta\theta(x,t)$. We expand the perturbation in Fourier modes $\delta\theta(x,t) = \theta_0 e^{\omega t - iqx}$, and look what are the conditions for

the perturbation to grow with time. Re-injecting this linear expansion into eq. (2.24) gives the following mode equation:

$$\omega = -\frac{Kq^2}{\gamma}\left(1 + \frac{\gamma(\nu+1)^2}{4\eta}\right) - \frac{\zeta\Delta\mu(\nu+1)}{2\eta} \tag{2.25}$$

There is an instability if the perturbation grows with time, i.e if $\omega > 0$. From equation (2.25), this is possible only if $\zeta(\nu+1) < 0$. Assuming it is the case, there is is critical wavenumber q_c below which the uniform state is unstable given by

$$q_c^2 = \frac{-2\zeta\Delta\mu(\nu+1)}{K\left(4\eta/\gamma + (\nu+1)^2\right)} \tag{2.26}$$

The strong anchoring at the edge of the stripe $\theta(-L/2) = \theta(L/2) = \pi/2$ relates the wavenumber to the width of the stripe L such as $qL = \pi$. There is therefore a critical length above which the uniform state is no longer stable given by

$$L_c = \pi\sqrt{\frac{K\left(4\eta/\gamma + (\nu+1)^2\right)}{-2\zeta\Delta\mu(\nu+1)}} \tag{2.27}$$

Or equivalently at fixed length L there is a critical activity $\Delta\mu_c$ defined by:

$$\Delta\mu_c = \frac{K\pi^2\left(4\eta/\gamma + (\nu+1)^2\right)}{-2L^2\zeta(\nu+1)} \tag{2.28}$$

Physical meaning of $\zeta(\nu+1) < 0$ Both ζ and ν can either be positive or negative and only the two cases where they are of opposite sign lead to an instability. We consider the case of $|\nu| > 1$, the so-called flow-aligning regime. The case $|\nu| < 1$ corresponds to the so-called flow-tumbling regime, where the director continuously rotates under an imposed shear.

- $\zeta < 0$ and $\nu > 1$ which corresponds to a case of contractile nematic $\zeta < 0$ with disk-like behavior $\nu > 1$, meaning that the nematic have a tendency to orient perpendicular to a shear flow

- $\zeta > 0$ and $\nu < -1$ which corresponds to a case of an extensile nematic $\zeta > 0$ with rod-like behavior $\nu < -1$, meanin that the nematic have a tendency to orient parallel to a shear flow

- The cases of a disk-like extensile nematic $\zeta > 0, \nu > 1$ or a rod-like contractile nematic $\zeta < 0, \nu < -1$ do not show any instability.

If one were to constrain a monolayer of active nematic between two plates separated by a distance L, either $L < L_c$ and the nematic stays in a uniform state parallel to the plate, or $L > L_c$ and there is a gradient of orientation between the plates, resulting in a tilt of the nematic between the plates. The schematic representation is the same as in the passive Freedericksz transition on fig. 2.7 and can be seen on nematic cells on adhesive stripe on figs. 1.4 and 2.4. The critical difference with the passive case presented in section 2.2.1 is that the orientation instability is also a shear flow instability, as developed in the following section.

2.2.3 Spontaneous tilt angle and shear

In this section, we investigate at steady-state the relation between the shear flow and the tilt, as well as their respective amplitudes close to the transition length. We also investigate the value of the tilt angle for very large widths.

Tilt and shear close to the transition length

The shear $\partial_x v_y$ is given simply by (2.19):

$$\partial_x v_y = \frac{2h_\perp}{\gamma(\nu \cos 2\theta - 1)} \tag{2.29}$$

The presence of a finite shear flow is something one would not expect for a passive system. In a passive system, or more generally a system whose dynamics derives from a free energy, you expect at steady-state that $h_\perp = 0$ (recalling that the molecular field $\mathbf{h}$ gives the direction to minimize the free energy). However, for an active nematic, since the system is actively driven in a way that does not derive from a free energy but from a local active power $r\Delta\mu$ (see section 1.2), the perpendicular component of the molecular field does not vanish at steady state. From (2.20) we see that, at steady state, the molecular field (and thus the shear) is proportional to the active stress:

$$\partial_x v_y = \frac{2\zeta\Delta\mu \sin 2\theta}{4\eta + \gamma(\nu^2 - 2\nu\cos 2\theta + 1)} \tag{2.30}$$

Close to the transition, the amplitude of the tilt angle for a stripe of width L such that $L - L_c \ll L_c$ is given by non-linear terms eq. (2.24). We perform a weakly non-linear perturbation detailed in appendix B and obtain the tilt angle

$$\theta(x,t) = \frac{\pi}{2} + \tilde{\theta}_0\sqrt{\frac{L-L_c}{L_c}}\cos\left(\frac{\pi x}{L}\right) + O(\frac{L-L_c}{L_c}), \tag{2.31}$$

with

$$\tilde{\theta}_0 = \pm 2\sqrt{\frac{(\nu+1)\left(4\frac{\eta}{\gamma} + (\nu+1)^2\right)}{4\frac{\eta}{\gamma}(1+4\nu) + 1 + \nu^2(3+4\nu)}} \tag{2.32}$$

There is a symmetry between positive and negative angles. This symmetry is broken if we consider a chiral nematic [66,74] that has a preferred direction of rotation. Although this was investigated in the work by Duclos, Blanch-Mercader *et al.* [1], because of an apparent breaking of symmetry between positive and negative angles that can be seen on fig. 2.4. We do not consider chiral effects in this work, notably because chiral effects do not seem to matter when there are abrasions (see section 2.4). The tilt angle from eq. (2.31) determines the $y-$component of the velocity field:

$$v_y = -\frac{4L_c\tilde{\theta}_0\zeta\Delta\mu}{\pi\left(4\eta+\gamma(\nu+1)^2\right)}\sqrt{\frac{L-L_c}{L_c}}\sin\left(\frac{\pi x}{L_c}\right)+O(\frac{L-L_c}{L_c}) \tag{2.33}$$

$$= \frac{2\tilde{\theta}_0\pi K}{L_c(\nu+1)\gamma}\sqrt{\frac{L-L_c}{L_c}}\sin\left(\frac{\pi x}{L_c}\right)+O(\frac{L-L_c}{L_c}) \tag{2.34}$$

From eq. (2.33) we see that the direction of the shear at a given angle depends on the sign of the active stress coefficient ζ, and the direction is set by the extensile or contractile nature of the active nematic, as shown on fig. 2.9

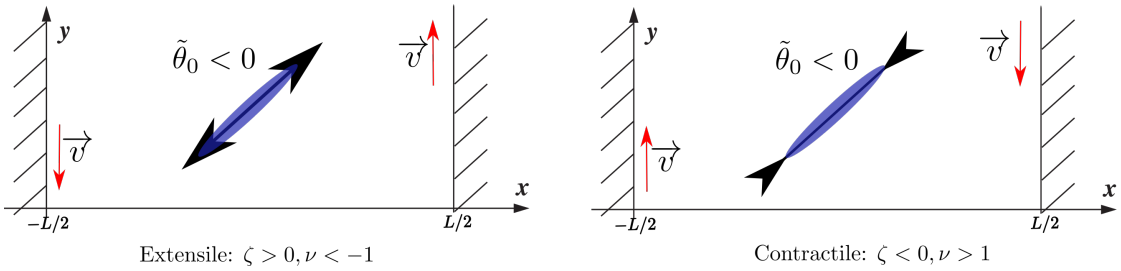

Figure 2.9: Direction of the shear flow depending on the sign of the tilt. We represented a negative tilt in the definition given by eq. (2.31). For extensile nematics on the left panel, $\zeta > 0$ and the velocity at the right edge induced by the gradient of orientation is positive. Inversely for contractile nematics on the right panel, $\zeta < 0$ and the velocity at the right edge is negative.

Tilt far from the transition length

Suppose that in a very large width $L \gg L_c$ the tilt saturates and there is a homogeneous uniform tilted state. There would be no flow in the middle of the stripe, but a gradient of orientation and flow close to the boundaries, on a length of the order of L_c. This uniform tilt θ_∞ is given by the fixed points of (2.24):

$$\theta_\infty = \frac{\pi}{2} \pm \frac{1}{2}\arccos\left(\frac{1}{\nu}\right) \tag{2.35}$$

From eq. (2.35) we see that the tilt and shear are set by the flow-alignment parameter ν. We recover the flow-tumbling instability, for $|\nu| < 1$ the nematic is unstable to a shear-flow perturbation. The tilt-angle θ_∞ is an increasing function of ν: at the smallest possible value $|\nu| = 1$ there is no tilt and when $\nu \gg 1$ the nematic orients perpendicular to the stripe direction.

However, in order to observe that state one would need to have a stabilizing effect for the first unstable mode. Otherwise one expects higher modes to become unstable as the width of the stripe is increased. Experimentally [1], for unknown reasons no higher-modes perturbation are observed, but no saturated tilt either. By using abrasions in the stripe acting as contact-guidance, the behavior of the cells in large stripes was stabilized and these results are presented in sections 2.4 and 2.5

2.3 Application to active cell nematics

2.3.1 Cell division and extrusion

One of the most striking feature of fluids made of cells compared to non-living fluids is the fact that the number of cells is not necessarily conserved because of cell divisions, apoptosis and extrusion events. This leads to an absence of mass conservation in the monolayer of cells. Obviously physically the mass is conserved and the existence of source terms is due to the fact that we consider a fluid made of only one constituent, cells. This implies that cells can appear *ex nihilo* and that after extrusion or apoptosis they completely disappear. To avoid this peculiarity one can consider a two-component fluid made of cells and interstitial fluid [31, 75]. In this model, cells can grow and divide, and become interstitial fluid after cell death. Ranft *et al.* [75] show that, for the hydrodynamics, permeation effect (the transfer from interstitial fluid to cells and vice-versa) matter above a certain screening length λ that is of the order of a few millimeters to centimeters. In the experiments considered, the width of the stripe is of the order of tens of micrometers to a millimeter, and we consider the one-constituent approximation to be valid.

In what follows I will consider mathematically extrusion and cell death as equivalent processes, as both reduce the mass density of cells in the monolayer. If we consider that cells divide at a rate k_d in the monolayer and are extruded at a rate k_a, then there is a net extrusion rate (resp. division) rate $k = k_a - k_d$ (resp. $-k$). Mass conservation in the monolayer is then given by:

$$\partial_t \rho + \partial_\alpha(\rho v_\alpha) = -k\rho \tag{2.36}$$

If we assume that cells are incompressible, then at confluency in the monolayer the net rate k has to be zero on average along the width $\int_{-L/2}^{L/2} \mathrm{d}x\, k(x) = 0$. If at steady-state the local net division rate is however non-zero, this creates local non-divergence-free flows.

Assuming that the density is constant along flow lines $\partial_t \rho + v_\alpha \partial_\alpha \rho = 0$, the divergence of the velocity is directly related to the net extrusion rate:

$$\partial_\alpha v_\alpha = -k \tag{2.37}$$

In the experiments presented in section 2.1, we do not focus on density changes but mostly on flows. There do not seem to be particular density effects and using (2.37) yields good results. Therefore, the simplifying incompressibility hypothesis is justified. Given the $y-$invariance in the problem, eq. (2.37) results in a "convergent" flow in the $x-$direction, perpendicular to the stripe:

$$\partial_x v_x = -k(x) \tag{2.38}$$

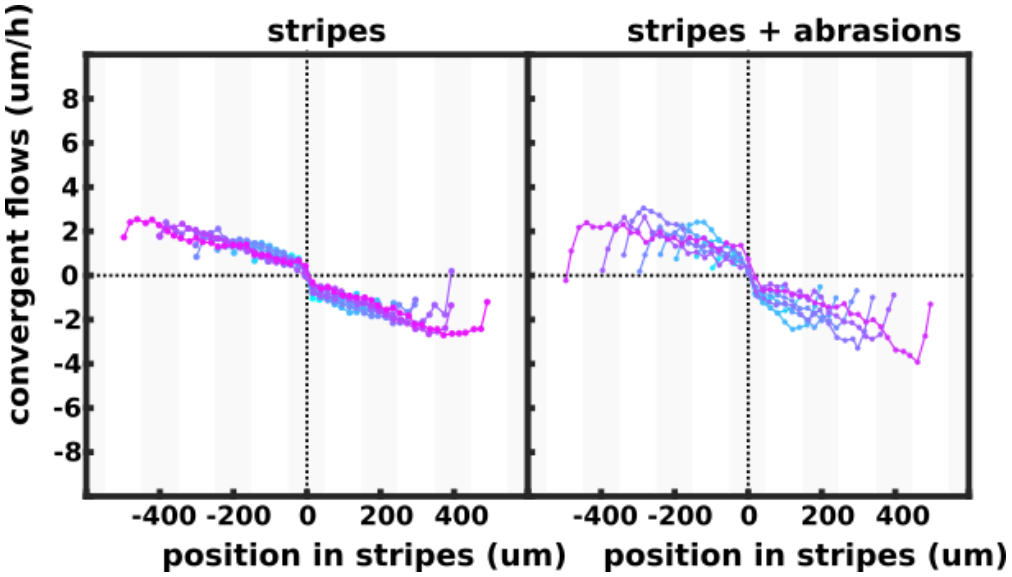

Figure 2.10: Experimental observation of convergent flows in the $x-$direction in the stripe. In both with and without abrasions, there is a linear behavior in most of the stripe with a negative slope suggesting mostly extrusion inside the stripe, and division close to the boundary. Preliminary figure, courtesy of Thibault Aryaksama.

The expression of $k(x)$ is not known *a priori* but it is the cause of the flow in the $x-$direction. The experimental observation of the flow on figure 2.10 indicates that the net extrusion rate is negative around each boundary of the stripe over a length $\lambda_d/2 \ll L$, and it is positive over distances $L - \lambda_d$. As a first approximation, we can assume that there is cell division outside of the stripe and that inside the stripe there is predominantly extrusion. This finds some biological basis in the fact that cells have a tendency to

divide more in low pressure environment and they have a tendency to be extruded in a high pressure environment [76–79]. Pressure-dependent division rates are discussed in more details in section 3.6.1. Intuitively, the free boundary has a lower pressure and cells have a tendency to divide near the boundary and to be extruded inside the stripe. We first look at what happens if cells are extruded uniformly in the stripe, i.e k constant. We discuss that a pressure-dependent extrusion rate do not modify the length for the active instability in appendix C.

Let us first focus on the case where there is uniform extrusion in the layer and assume that k is constant. This creates a compressional flow

$$v_x(x) = -kx \tag{2.39}$$

Let us now rewrite the equations of motion eqs. (2.16), (2.18) and (2.19) with the non-zero convergent flow (2.39):

$$0 = \eta\partial_x v_y - \frac{\zeta\Delta\mu}{2}\sin 2\theta + \frac{\nu}{2}(h_\parallel \sin 2\theta + h_\perp \cos 2\theta) - \frac{h_\perp}{2} \tag{2.40}$$

$$0 = \frac{h_\parallel}{\gamma} + \nu k\cos^2\theta - \frac{\nu}{2}\partial_x v_y \sin 2\theta, \tag{2.41}$$

$$\partial_t\theta - kx\partial_x\theta = \frac{h_\perp}{\gamma} - \frac{\nu k}{2}\sin 2\theta - \frac{\partial_x v_y}{2}(\nu\cos 2\theta - 1). \tag{2.42}$$

As done in section 2.2.2 this can be recast into a single non-linear differential equation for the angle θ:

$$\begin{aligned}(\partial_t\theta - kx\partial_x\theta)(4\eta + \gamma\nu^2\sin 2\theta^2) = \frac{h_\perp}{\gamma}\left(4\eta + \gamma(\nu^2 - 2\nu\cos 2\theta + 1)\right) - \zeta\Delta\mu\sin 2\theta(\nu\cos 2\theta - 1)\\ - \frac{\nu k}{2}\sin 2\theta\left(4\eta + 2\gamma\nu(\nu-1)\cos\theta^2\right).\end{aligned} \tag{2.43}$$

If we make linear perturbation around $\frac{\pi}{2}$, $\theta(x,t) = \pi/2 + \delta\theta(x,t)$, at steady state the perturbation $\delta\theta(x)$ satisfies

$$A\partial_x^2\delta\theta + kx\partial_x\delta\theta + (\nu k + C)\delta\theta = 0, \tag{2.44}$$

with

$$A = \frac{K}{\gamma}\left[1 + \frac{\gamma(\nu+1)^2}{4\eta}\right]; \quad C = -\frac{\zeta\Delta\mu(\nu+1)}{2\eta} \tag{2.45}$$

From eq. (2.43), we see that the critical length L_c given by eq. (2.27) above which a steady-state perturbation exists is modified by the existence of a convergent flow. We define the critical length in the presence of extrusion as L_c^k. There are two length scales in this system:

- $L_d(k) = \sqrt{\frac{A}{k}} = \left(\frac{K}{\gamma k}\left[1 + \frac{\gamma(\nu+1)^2}{4\eta}\right]\right)^{1/2}$, associated to cellular division;
- $L_c = \pi\sqrt{\frac{A}{C}} = \pi\left(\frac{K\left[\frac{4\eta}{\gamma}+(\nu+1)^2\right]}{-2\zeta\Delta\mu(\nu+1)}\right)^{1/2}$, the critical length for the active Freedericksz transition when there are no cell divisions nor deaths, defined by eq. (2.27).

If the division rate is "small", i.e if

$$\varepsilon = \frac{L_c}{L_d(k)} = \pi\left(-\frac{2\eta k}{\zeta\Delta\mu(\nu+1)}\right)^{1/2} \ll 1, \tag{2.46}$$

the critical length above which there is a transition L_c^k is given by:

$$L_c^k = L_c\left(1 - \frac{\varepsilon^2}{2}(\nu - 1/2) + O(\varepsilon^3)\right) \tag{2.47}$$

Depending on the sign of the flow-alignment parameter ν, the critical length in the presence of extrusion L_c^k is either larger or smaller then the critical length L_c:

- If $\nu > 1$, compression flows induced by extrusion favor the tilt. In this case, the effect of the compression flows is additive to the effect of the active stress, and the transition length $L_c^k < L_c$. This will be the case for contractile disc-like active nematics, where $\zeta < 0, \nu > 1$. In this case, since the convergent flow created by extrusion destabilizes the orientation parallel to the stripe, there is even an instability of the uniform state at zero activity. We show on fig. 2.11 a phase diagram showing the stability of the uniform state as a function of the two lengths L_c and $L_d(k)$.
- On the contrary if $\nu < -1$, compression flows stabilize the parallel state. In this case, the effect of compression flows is in competition with the active stress and the transition length $L_c^k > L_c$. This will be the case for extensile rod-like active nematics, where $\zeta > 0, \nu < -1$.

2.3.2 Interaction with the substrate

In ref. [1], Duclos, Blanch-Mercader *et al.* looked at the effect of friction because of two observations: firstly the shear velocity was screened over a finite length compared to gradients of orientation. Then, a type of cells - NIH 3T3 - did not show any active instability even for large stripes of width around a millimeter. As introduced in section 1.1.1, cells have to interact with their substrate to perform motion. From a theoretical perspective, this means that the momentum is no longer conserved. Coming back to the construction of the hydrodynamic theory of section 1.2, this technically

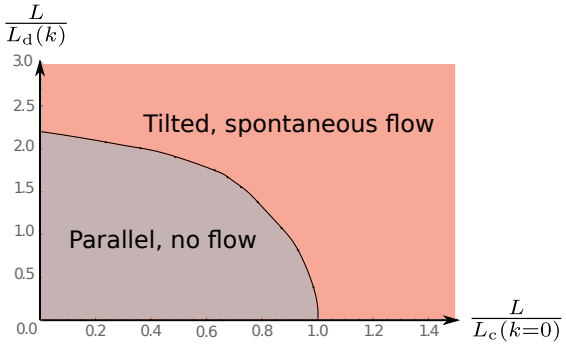

Figure 2.11: Phase diagram of the nematic in the stripe as a function of the two dimensionless lengths $L/L_d(k)$ and L/L_c in the contractile case ($\zeta < 0, \nu > 1$). We see that there is a tilted state that exist even at low activity $L \ll L_c$. The phase diagram is determined by numerical resolution of eq. (2.43).

means that momentum is no longer a hydrodynamic variable and the stress (the flux of momentum) is no longer relevant. However, one can adopt a more practical approach as was done in [1] and consider a hydrodynamic theory were momentum is no longer conserved but is retained as a hydrodynamic variable. This method is non systematic but depends on the scales of observation. Even though theoretically the momentum is not conserved at large length, momentum can be relevant at smaller length scales. This is the case in these experiments, were momentum is screened over lengths of the order of $50-100\mu m$ and is still relevant. A hydrodynamic theory with dissipation at an interface is considered in ref. [80].

Modification of the critical length

In section 2.2.2 we gave a hand-waving argument for the instability of active nematic stripes. This argument is based on a positive feedback loop between gradients of orientation that create a flow that in turn creates gradients of orientation. However, one can imagine that if momentum is screened over short lengths compared to the active length L_c characteristic of the active instability, the feedback loop is destroyed and the instability no longer exists. Let me now detail the calculations with an interaction with the substrate. This calculation is adapted ref. [1].

Duclos, Blanch-Mercader *et al.* model this friction by a viscous drag f_α proportional to the velocity:

$$f_\alpha = -\xi v_\alpha \tag{2.48}$$

We consider that there is no cell divisions nor extrusions, to look at the effect of friction alone. In that case, $v_x = 0$ and force balance in the $y-$direction is

$$\partial_x \sigma^t_{xy} = \xi v_y \tag{2.49}$$

The total stress no longer vanishes due to the free surface and must remain a variable of the problem. Given eq. (2.49), the shear becomes $\partial_x v_y = \partial_x^2 \sigma^t_{xy}/\xi$ and eqs. (2.16), (2.18) and (2.19) become:

$$\sigma^t_{yx} = \frac{\eta}{\xi}\partial_x^2 \sigma^t_{yx} - \frac{\zeta\Delta\mu}{2}\sin 2\theta + \frac{\nu}{2}(h_\parallel \sin 2\theta + h_\perp \cos 2\theta) - \frac{h_\perp}{2} \tag{2.50}$$

$$0 = \frac{h_\parallel}{\gamma} - \frac{\nu}{2\xi}\partial_x^2 \sigma^t_{yx} \sin 2\theta, \tag{2.51}$$

$$\partial_t \theta = \frac{h_\perp}{\gamma} - \frac{1}{2\xi}\partial_x^2 \sigma^t_{yx}(\nu \cos 2\theta - 1). \tag{2.52}$$

By performing a Fourier expansion at linear order (calculation detailed in section 2.4.4 with an external field), $\theta(x,t) = \pi/2 + \theta_0 e^{\omega t - iqx}$ and $\sigma^t_{xy}(x,t) = \sigma^t_{xy_0} e^{\omega t - iqx}$, one can determine a mode equation:

$$\omega = -q^2\left(\frac{K}{\gamma} + \frac{(\nu+1)}{2\xi(1+\frac{\eta}{\xi}q^2)}\left(\zeta\Delta\mu + q^2(\nu+1)\frac{K}{2}\right)\right) \tag{2.53}$$

We can see from eq. (2.53) that there is another length scale on top of the active length scale given by (2.27): there is also a length associated to friction that screens hydrodynamic interactions on scales of the order of $\sqrt{\frac{\eta}{\xi}}$. The critical wavevector q_c^ξ, above which there is an instability when there is friction is:

$$q_c^{\xi 2} = \frac{-2\zeta\Delta\mu(\nu+1)}{K\left(4\eta/\gamma + (\nu+1)^2\right)} - \frac{4\xi}{4\eta + \gamma(\nu+1)^2} \tag{2.54}$$

We can introduce the lengthscale L_f associated to friction:

$$L_f = \pi\sqrt{\frac{4\eta + \gamma(\nu+1)^2}{4\xi}} \tag{2.55}$$

The critical length $L_c^\xi = \pi/q_c^\xi$ above which a nematic stripe is unstable when there is friction is given by:

$$\frac{1}{(L_c^\xi)^2} = \frac{1}{L_c^2} - \frac{1}{L_f^2} \tag{2.56}$$

From eq. (2.56) one sees that if the friction length L_f is greater than the active length L_c, there is no instability and the parallel state is always stable. In other words, if the hydrodynamic interaction are screened over lengths that are smaller than the active length, quantitatively $L_f < L_c$, then the active instability cannot develop in the system. If $L_f > L_c$ then an instability will develop for stripes wider than the critical length L_c^ξ given by (2.56)

2.4 Effects of a perpendicular external field

2.4.1 A passive and active Freedericksz transition

In section 2.1, we presented the effects of abrasions on a free layer shown on fig. 2.3. The abrasions are geometrical cues like that orients the cells in their direction. In that sense, it acts like an external orientation field. Interestingly, the presence of abrasions stabilizes the orientation of the cells over large distances: the picture on fig. 2.3 is of a square which sides are about $500\mu m$ is length, and there is almost perfect alignment on the whole field of view. In order to model the abrasions, we take a phenomenological approach "à la Landau": in the Frank distortion energy, a term must be added to account for the preferred alignment direction with the orientation of the abrasions. By analogy with a magnetic field, the orientation of the abrasions can be modeled by a vector field **H**. The orientation of **H** is determined by the orientation of the abrasions. The magnitude however of **H** is not something that is controlled experimentally. Because of the nematic symmetry and the fact that the abrasions are not directed, the terms associated to the field **H** in the free energy must be even in **p** and **H**. There is an added energy density

$$f_a = -\frac{\chi}{2}(\mathbf{p}\cdot\mathbf{H})^2 \tag{2.57}$$

The formulation given by eq. (2.57) is a reference to the magnetic free-energy density of the passive Freedericksz transition eq. (2.4), although the physical interpretation of the quantities is not the same. We introduced a susceptibility χ by analogy with magnetism but the only physical quantity is χH^2, which is interpreted as an energy density of orientation induced by the abrasions. The schematic for the theoretical model is shown on fig. 2.12. Keeping the one-constant approximation for the Frank constants, similarly

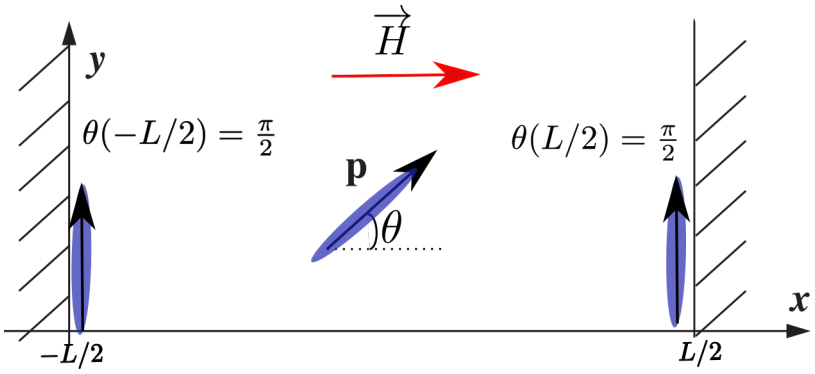

Figure 2.12: Schematic representation of the stripe with the abrasions modeled by an external field **H** perpendicular to the direction of the stripe. The same boundary conditions as in section 2.2.2 are applied.

to eq. (2.8) the distortion energy as a function of the polarization angle θ is given by:

$$F = \int dx\, dy \left[\frac{K}{2}(\nabla\theta)^2 - \frac{\chi}{2} H^2 \cos^2\theta - \frac{1}{2} h_{\parallel}^0 p^2 \right] \tag{2.58}$$

Changing the free energy changes the out-of-equilibrium dynamics given by eqs. (2.16), (2.18) and (2.19) only by changing the value of the molecular field **h**. The parallel component of the molecular field $h_{\parallel}$ is not important to the dynamics of the orientation, but the perpendicular component $h_{\perp}$ is modified by the external field:

$$h_{\perp} = K\partial_x^2\theta - \frac{\chi}{2}\sin(2\theta)\, H^2 \tag{2.59}$$

2.4.2 Changes in the critical length : cooperation of passive and active effects

Critical Length

Since both the active stress and the external field destabilize the nematic in stripes at finite length, we expect the critical length above which the uniform state is unstable to be smaller than in stripes without abrasions.

The non-linear equation accounting for the evolution of the angle θ eq. (2.20) remains the same. However the PDE controlling the evolution of the angle is modified:

$$\partial_t\theta = \frac{1}{4\eta + \gamma\nu^2\sin^2 2\theta}\left[\frac{K\partial_x^2\theta - \frac{\chi}{2}\sin(2\theta)\, H^2}{\gamma}\left(4\eta + \gamma(\nu^2 - 2\nu\cos 2\theta + 1)\right) \right. \\ \left. -\zeta\Delta\mu\sin 2\theta(\nu\cos 2\theta - 1)\right] \tag{2.60}$$

The stability of the uniform state $\theta = \pi/2$ is determined by looking at the stability of the perturbation $\delta\theta = \theta - \pi/2$, that satisfies at linear order:

$$\partial_t\theta = \frac{1}{4\eta}\left[\frac{K\partial_x^2\theta + \chi H^2\theta}{\gamma}(4\eta + \gamma(\nu+1)^2) - 2\zeta\Delta\mu(\nu+1)\theta \right] \tag{2.61}$$

Therefore, there is a critical wavenumber q_c^H below which the perturbation $\delta\theta$ grows with time and the uniform state is no longer stable:

$$(q_c^H)^2 = \frac{-2\zeta\Delta\mu(\nu+1)}{K(4\eta/\gamma + (\nu+1)^2)} + \frac{\chi}{K}H^2 \tag{2.62}$$

The anchoring condition $\theta(-L/2) = \theta(L/2) = \pi/2$ gives a critical length L_c^H defined by $L_c^h q_c^H = \pi$. From eq. (2.62), we see that there are two length scales, the active length

scale L_c given by eq. (2.27) and a passive "magnetic" length given by $L_H = \pi/H\sqrt{K/\chi}$, as in section 2.2.1. The critical length L_c^H is given by

$$\frac{1}{{L_c^H}^2} = \frac{1}{{L_c}^2} + \frac{1}{{L_H}^2} \tag{2.63}$$

We see in the value of the critical length L_c^H that there is an added effect from the active stress and from the field. A uniform active nematic under a perpendicular orientation field is destabilized at shorter lengths compared to both a passive nematic under orientation field and an active nematic without orientation field.

Weakly non-linear perturbation: amplitude of the tilt and of the flow

Let us now look at the effect of the external field $\mathbf{H}$ on the shear v_y. The external field $\mathbf{H}$ changes the free energy and consequently the molecular field $h_\perp$. However, the presence of a shear flow is a purely active effect. For a passive system, presented in section 2.2.1, the field does not induce flow since the tilt created in the stripe minimizes the free energy. Therefore, the external field $\mathbf{H}$ does not "directly" affect the shear. Indeed, the shear is still given by eq. (2.30), because $h_\perp$ is still given by eq. (2.20), even in the presence of the external field.

The flow v_y is however modified because the value of the tilt angle is modified by the external field. The tilt angle $\theta(x)$ close to the transition length, for a width L such that $L - L_c^H \ll L_c^H$, is given by non-linear terms in eq. (2.60) (details in appendix B):

$$\theta(x) = \frac{\pi}{2} + \tilde{\theta}_0^H \sqrt{\frac{L - L_c^H}{L_c^H}} \cos\left(\frac{\pi x}{L}\right) + O\left(\frac{L - L_c^H}{L_c^H}\right) \tag{2.64}$$

and

$$\tilde{\theta}_0^H = 2\sqrt{\frac{\left(4\frac{\eta}{\gamma} + (\nu+1)^2\right)^2 - 2\frac{\zeta\Delta\mu}{\chi H^2}(\nu+1)\left(4\frac{\eta}{\gamma} + (\nu+1)^2\right)}{\left(4\frac{\eta}{\gamma} + (\nu+1)^2\right)^2 - 2\frac{\zeta\Delta\mu}{\chi H^2}\left(4\frac{\eta}{\gamma}(1+4\nu) + 1 + \nu^2(3+4\nu)\right)}} \tag{2.65}$$

The $y-$component of the velocity is therefore given by :

$$v_y = \frac{2L_c^H \tilde{\theta}_0^H \pi K}{L_c^2(\nu+1)\gamma}\sqrt{\frac{L - L_c^H}{L_c^H}} \sin\left(\frac{\pi x}{L_c^H}\right) + O\left(\frac{L - L_c^H}{L_c^H}\right) \tag{2.66}$$

The amplitudes (2.65) and (2.66) as well as the value of the critical length can help us to determine hydrodynamic parameters for cells, that are not accessible from cell properties.

2.4.3 Tilt angle in large stripes

Let us now turn back to the angle at large widths, where we see experimentally a tilted homogeneous state far from the boundaries. There is a competition between the abrasions represented by the external field and the active stress. The abrasions, which are perpendicular to the stripe, favor a perpendicular orientation. However, the active stress favors an orientation dependent on the flow-alignment parameter ν given by eq. (2.35). What is the result of this competition? We can imagine two scenarios: either the tilt is a combination of the effect of the field and the active stress, or there is a threshold for the field where the nematic orients completely parallel to the field. To answer this question, we come back to the non-linear equation (2.60) verified by the angle θ, which gives at steady state:

$$\partial_x^2\theta = \frac{\chi H^2}{2K}\sin 2\theta + \frac{\zeta\Delta\mu}{K}\frac{\gamma(\nu\cos 2\theta - 1)}{4\eta + \gamma(\nu^2 - 2\nu\cos 2\theta + 1)}\sin 2\theta \tag{2.67}$$

The RHS of eq. (2.67) can be written as the derivative of an effective potential $V[\theta(x)]$, and eq. (2.67) becomes:

$$K\partial_x^2\theta(x) = -\frac{\delta V[\theta(x)]}{\delta\theta(x)} \tag{2.68}$$

With the following potential:

$$V[\theta] = \frac{\chi H^2}{4}\left[\cos 2\theta\left(1 - \frac{\zeta\Delta\mu}{\chi H^2}\right) - \frac{\zeta\Delta\mu}{\chi H^2}\frac{(4\eta/\gamma + \nu^2 - 1)}{2\nu}\ln\left(4\eta/\gamma + \nu^2 - 2\nu\cos 2\theta + 1\right)\right] \tag{2.69}$$

Given eq. (2.68) we can make a time analogy with a mechanical problem, where θ is the position of a particle moving in the potential V and the position is the stripe is the time in this analogy. Since there is a finite width of the stripe L and anchoring conditions $\theta(L/2) = \theta(-L/2)$, in this analogy the particle in the potential moves in a finite time and must start and end at the same position. Therefore, the "equilibrium" positions are not simply given by the minimum of the potential V.

For small times the particle does not move if it is at a minimum of potential V. Indeed, if the time is smaller than the characteristic oscillation time of the potential, the particle does not have time to move and to come back to its original position. This corresponds to the case where the uniform state $\theta = \pi/2$ is stable. What I call the characteristic oscillation time in terms of lengths is exactly the critical length above which the uniform state is no longer stable.

For times larger than the characteristic oscillation time, the particle has the time to explore the potential and to come back to its initial position. This corresponds to the case

where the uniform state $\theta = \pi/2$ is no longer stable, a tilt develops when "exploring" the potential.

For much larger times than the characteristic oscillation time, the particle explores the potential until it reaches the vicinity of a maximum value of the potential, where it is "slowed" down and spends most of its time before coming back to its original position. This corresponds to the situation of very large widths considered in section 2.2.3. In this case, the tilt in the middle of the stripe θ_∞ is given by the maximum of the potential V. The potential $V[\theta]$ has a periodicity of π because of the nematic symmetry, and is represented for two different values of the magnitude of the field H between $\theta = -\pi/2$ and $\theta = \pi/2$ on fig. 2.13.

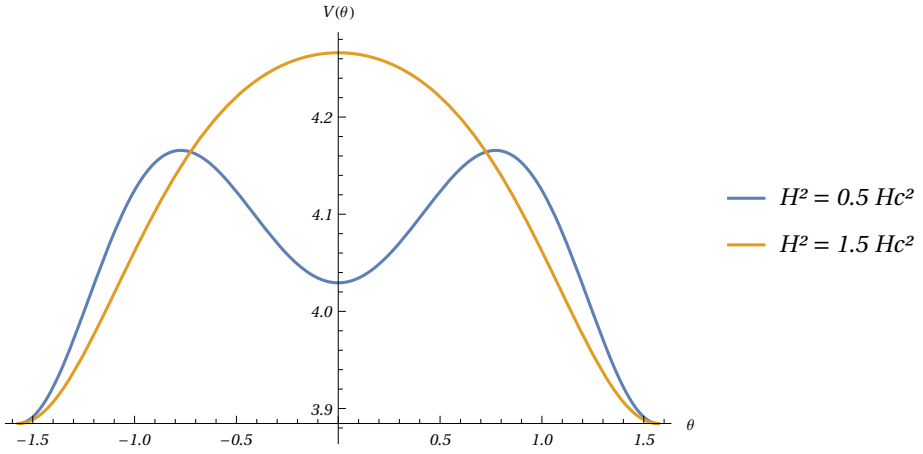

Figure 2.13: Representation of the potential $V[\theta]$ in units of χH^2 as a function of θ for a perpendicular field below the critical $H^2 = H_c^2/2$ field and a field above the critical width $H^2 = 3H_c^2/2$. For $H^2 = 3H_c^2/2$ the maximum is at $\theta = 0$ meaning the nematic is parallel to the field in the large stripe limit. For $H^2 = H_c^2/2$ it is not the case and the maximum is set by eq. (2.72).

We are looking for the extrema of the potential $V[\theta]$, given by the following equation:

$$0 = \left(\frac{\chi H^2}{2\gamma}(4\eta + \gamma(\nu^2 - 2\nu\cos 2\theta + 1)) - \zeta\Delta\mu(\nu\cos 2\theta - 1)\right)\sin 2\theta \tag{2.70}$$

For $-\pi/2 \leq \theta \leq \pi/2$, there are three obvious solutions, $\theta = 0$ and $\theta = -\pi/2, \pi/2$ which correspond respectively to being perpendicular or parallel to the stripe direction. There is potentially a third solution to eq. (2.70) if there is a solution to

$$\frac{\chi H^2}{2}(4\eta/\gamma + \nu^2 - 2\nu\cos 2\theta + 1) - \zeta\Delta\mu(\nu\cos 2\theta - 1) = 0 \tag{2.71}$$

Working with the dimensionless variables $x = \frac{\chi H^2}{\zeta \Delta\mu}$ and $a = \frac{1}{2}(4\eta/\gamma + \nu^2 + 1)$, a solution of eq. (2.71) is a solution of

$$\cos 2\theta = f(x) = \frac{1 - ax}{\nu(1 - x)} \tag{2.72}$$

There is a solution to (2.72) when x is such that $-1 \leq f(x) \leq 1$. Knowing that $a > |\nu|$, $-1 \leq f(x) \leq 1$ when the magnitude of the field H is smaller than a critical value H_c defined by:

$$\chi H_c^2 = 2\zeta\Delta\mu \frac{1 - \nu}{(4\eta/\gamma + (\nu - 1)^2)} \tag{2.73}$$

The critical value for the field H_c exists because the RHS of (2.73) is always positive. Indeed, starting from the assumption that an active instability exists, this means that either $\zeta\Delta\mu > 0$ and $\nu < -1$ (extensile case), or $\zeta\Delta\mu < 0$ and $\nu > 1$ (contractile case).

The conclusion is that when there is a field H perpendicular to the stripe, there is a critical value of this field H_c given by (2.73) above which the nematic aligns with the field in the large width limit. Below this critical field, the nematic orients given a particular angle θ given by (2.72), that depends on the ratio between the field and the active stress and on hydrodynamic parameters. This can be seen in fig. 2.13 where the potential V is plotted for values of H smaller and greater than H_c. A plot of the angle at the middle of the stripe $\theta(0)$ as a function of the normalized width of the stripe L/L_c^H, for different values of the magnitude of the external field H is given in fig. 2.14.

2.4.4 Interaction with the substrate and external field

We saw in section 2.3.2 that an interaction with the substrate modeled by a viscous drag can result in the destruction of the spontaneous flow instability because of hydrodynamic screening. We adapt in this section the calculations of section 2.3.2 to the case when an external field is present. Compared to the active instability presented in section 2.2.2, the passive instability presented in section 2.2.1 do not require a coupling between flow and orientation to exist. Therefore, the passive instability is unhindered by a finite hydrodynamic screening length. However, how does viscous drag affect the critical length L_c^H given by eq. (2.63), which is a combination of active and passive effects?

With the external field, the constitutive equations do not change, there is only a change in the value of the molecular field $\mathbf{h}$. Therefore, eqs. (2.50) to (2.52) are unchanged, and the value of $h_\perp$ is given by eq. (2.59). If we perform a linear expansion around the uniform state $\theta(x,t) = \pi/2 + \delta\theta(x,t)$ and $\sigma^t_{yx}(x,t) = \delta\sigma^t_{yx}(x,t)$, the parallel molecular field $h_\parallel$ given by eq. (2.51) is non-linear in the perturbations $\delta\theta, \delta\sigma^t_{yx}$. There

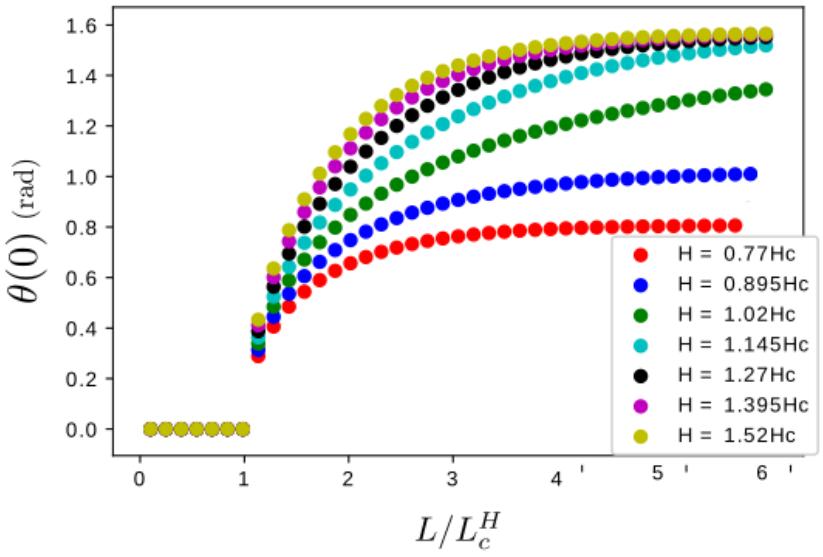

Figure 2.14: Middle angle $\theta(0)$ as a function of the normalized width L/L_c^H for different values of H. Angle calculated by solving numerically eq. (2.60) at steady state, using a relaxation method. The length is normalized by each value of L_c^H depending on H, so the bifurcation is always at $L/L_c^H = 1$. Other parameters are $\eta/\gamma = 1$ and $\nu = -1.3$.

are two remaining equations:

$$\delta\sigma_{yx}^t = \frac{\eta}{\xi}\partial_x^2\delta\sigma_{yx}^t + \zeta\Delta\mu\delta\theta - \frac{\nu+1}{2}(K\partial_x^2\delta\theta + \chi H^2\delta\theta) \tag{2.74}$$

$$0 = \frac{K}{\gamma}(\partial_x^2\delta\theta + \chi H^2\delta\theta) + \frac{\nu+1}{2\xi}\partial_x^2\delta\sigma_{yx}^t. \tag{2.75}$$

Performing a Fourier expansion $\delta\theta(x,t) = \theta e^{\omega t+iqx}$ and $\delta\sigma_{yx}^t(x,t) = \sigma_{yx}^t e^{\omega t+iqx}$, eqs. (2.74) and (2.75) become

$$-\left(1+\frac{\eta}{\xi}q^2\right)\sigma_{yx}^t + \left(\zeta\Delta\mu + \frac{\nu+1}{2}(Kq^2 - \chi H^2)\right)\theta = 0 \tag{2.76}$$

$$\sigma_{yx}^t = -\frac{2\xi}{q^2(\nu+1)}\left(\omega + \frac{K}{\gamma}q^2 - \frac{\chi H^2}{\gamma}\right) \tag{2.77}$$

This gives for the rate ω

$$(1+\frac{\eta}{\xi}q^2)\omega = (1+\frac{\eta}{\xi}q^2)\left(\frac{\chi H^2}{\gamma} - \frac{K}{\gamma}q^2\right) - q^2\frac{(\nu+1)}{2\xi}\left(\zeta\Delta\mu + \frac{\nu+1}{2}(Kq^2 - \xi H^2)\right) \tag{2.78}$$

Therefore there is an instability if the quantity $g(q)$ defined by eq. (2.79) is positive for finite wavenumbers.

$$g(q) = -q^4\left(\frac{\eta}{\gamma}K + \frac{K}{4}(\nu+1)^2\right) + q^2\left(\chi\frac{\eta}{\gamma}H^2 - \xi\frac{K}{\gamma} + (\frac{\chi H^2(\nu+1)}{2} - \zeta\Delta\mu)\frac{\nu+1}{2}\right) + \frac{\xi}{\gamma}\chi H^2 \tag{2.79}$$

$$= aq^4 + bq^2 + c \tag{2.80}$$

g is a second order polynomial for the variable q^2. Given the fact that $a < 0$ and $c > 0$, the discriminant of g is positive and the roots $q_1^2 < q_2^2$ of g are real. Since $q_1^2 q_2^2 = c/a < 0$, $q_1^2 < 0$ and $q_2^2 > 0$. Therefore, g is positive for $q^2 < q_2^2$ and the critical wavenumber below which the uniform state is unstable $q_c^{H,\xi}$ is given by $q_c^{H,\xi} = q_2$. The critical wavenumber $q_c^{H,\xi}$ is given by the positive root of g:

$$q_c^{H,\xi 2} = \frac{-b - \sqrt{b^2 - 4ac}}{2a} \tag{2.81}$$

$$= \frac{1}{2\left(\frac{\eta}{\gamma}K + \frac{K}{4}(\nu+1)^2\right)}\left[\chi\frac{\eta}{\gamma}H^2 - \xi\frac{K}{\gamma} + (\frac{\chi H^2(\nu+1)}{2} - \zeta\Delta\mu)\frac{\nu+1}{2}\right.$$
$$\left. + \left(\left(\chi\frac{\eta}{\gamma}H^2 - \xi\frac{K}{\gamma} + (\frac{\chi H^2(\nu+1)}{2} - \zeta\Delta\mu)\frac{\nu+1}{2}\right)^2 + 4\left(\frac{\eta}{\gamma}K + \frac{K}{4}(\nu+1)^2\right)\frac{\xi}{\gamma}\chi H^2\right)^{1/2}\right] \tag{2.82}$$

Interestingly, contrary to section 2.3.2, for all finite ξ there is a length $L_c^{H,\xi}$ defined by $L_c^{H,\xi} q_c^{H,\xi} = \pi$, such that for widths larger than $L_c^{H,\xi}$ a uniform state is no longer stable. We recover from eq. (2.82) the wavenumber q_c^{ξ} given by eq. (2.54) when $H = 0$. By taking the limit $\xi \to +\infty$, or more physically considering the hydrodynamic screening length $\sqrt{\eta/\xi}$ much smaller than the active length L_c given by eq. (2.27), we recover the critical wavenumber of the passive Freedericksz transition presented in section 2.2.1:

$$\lim_{\xi\to\infty} q_c^{H,\xi} = H\sqrt{\frac{\chi}{K}} \tag{2.83}$$

Contrary to the case where there is no external field, for all values of the active stress $\zeta\Delta\mu$, there is a finite length $L_c^{H,\xi}$ above which a gradient of orientation develops inside the stripe. Although we are not able to determine a value for the amplitude of the tilt angle or the shear when there is friction, we expect a finite gradient of velocity to develop if the activity is finite. This velocity gradient can however be screened by the friction length. From this consideration, T. Aryaksama observed the behavior of NIH-3T3 cells that do not exhibit an active transition [1] when there are no abrasions. Duclos,

Blanch-Mercader *et al.* attribute this behavior to the friction that inhibits the active instability. We see on fig. 2.15 that NIH-3T3 cells develop a gradient of orientation when there is abrasions, as expected by this theory. However, the measured velocity at the edge is not significant enough to claim there is a spontaneous flow. A possible explanation is that the activity of NIH-3T3 cells being low, the resulting shear velocity may be too small compared to the fluctuations in the cell monolayer.

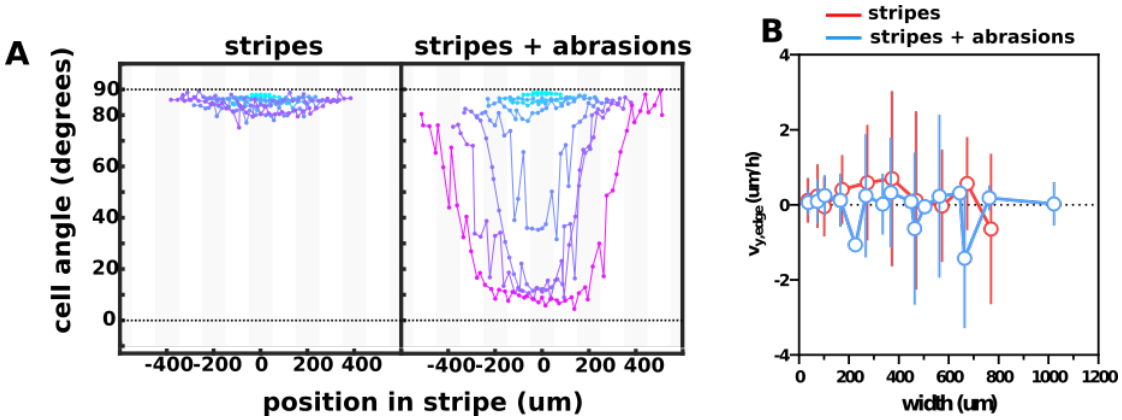

Figure 2.15: Evolution of the orientation (A) and the velocity at the edge (B) of NIH-3T3 fibroblasts with the width of the stripe, with and without abrasions. Without abrasions, as reported Duclos *et al.* in [1], NIH-3T3 cells do not show any instability. With abrasions, NIH-3T3 cells develop a gradient of orientation as expected by the calculations of this section. However, the velocity at the edge is not significant. Courtesy of Thibault Aryaksama.

2.5 Controlling the orientation of the external field

2.5.1 Experimental set up

Experimentally the abrasions do not allow to control precisely the magnitude of the field H. Indeed, changes in the mechanical procedure to perform the abrasions did not lead to significant results in the behavior of the tilt and the flow. In addition, quantitatively relating changes in abrasions to changes in the magnitude of the field is a complicated task.

In order to vary the field, one can however change the orientation of the abrasions and therefore theoretically change the orientation of the field. Changing the angle of the field provides an added control parameter to probe hydrodynamic parameters of wet active nematics. In particular, as explained later on in section 2.5.2, there is a competition

between the field and the active stress in the large width limit, which provides a way of measuring the flow-alignment parameter ν.

A schematic representation of the experiment is presented in fig. 2.16. We consider an external field $\mathbf{H}$ making an angle α with the $x-$axis, and anchoring conditions $\theta(-L/2) = \theta(L/2) = \pi/2$. Considering the angle of the external field, the distortion free

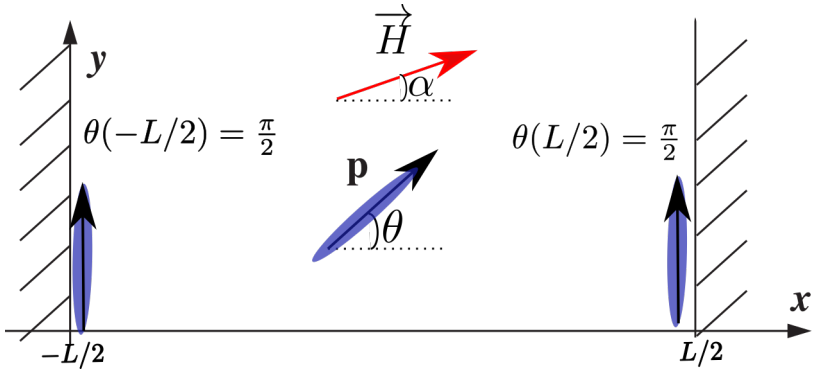

Figure 2.16: Schematic representation of the abrasions modeled by an external field with an angle α with respect to the $x-$axis.

energy (2.58) becomes:

$$F = \int dx\, dy \left[\frac{K}{2}(\nabla\theta)^2 - \frac{\chi}{2}H^2 \cos^2(\theta - \alpha) - \frac{1}{2}h_{\parallel}^0 p^2 \right] \tag{2.84}$$

and the perpendicular molecular field (2.59) becomes:

$$h_{\perp} = K\partial_x^2\theta + \frac{\chi H^2}{2}\sin 2(\alpha - \theta) \tag{2.85}$$

2.5.2 Effect of the orientation of the external field on the tilt angle: measuring the flow-alignment parameter ν

We saw in section 2.4.3 that when the field is perpendicular to the stripe, a competition between the external field and the active stress arises through the existence of a critical field H_c given by (2.73). For fields greater than the critical field $H > H_c$, the nematic aligns parallel to the field in the large width limit. What happens when the orientation of the field is changed? To answer this question we can proceed in the same way as in section 2.4.3, and consider the potential associated to the steady-state equation satisfied by the angle $\theta(x)$:

$$\partial_x^2\theta = \frac{\chi H^2}{2K}\sin 2(\theta - \alpha) + \frac{\zeta\Delta\mu}{K}\frac{\gamma(\nu\cos 2\theta - 1)}{4\eta + \gamma(\nu^2 - 2\nu\cos 2\theta + 1)}\sin 2\theta \tag{2.86}$$

which can be re-written

$$K\partial_x^2\theta = -\frac{\delta V_\alpha[\theta]}{\delta\theta} \tag{2.87}$$

with the potential $V_\alpha[\theta]$ given by:

$$V_\alpha[\theta] = \frac{\chi H^2}{4}\left(\cos 2(\alpha-\theta) - \frac{\zeta\Delta\mu}{\chi H^2}\left(\frac{(4\eta/\gamma+\nu^2-1)}{2\nu}\ln(4\eta/\gamma+\nu^2-2\nu\cos 2\theta+1)+\cos 2\theta\right)\right) \tag{2.88}$$

As explained in section 2.4.3, the tilt angle at large widths is given by the maxima of V_α. The potential V_α is represented on fig. 2.17 for different values of α. The extrema

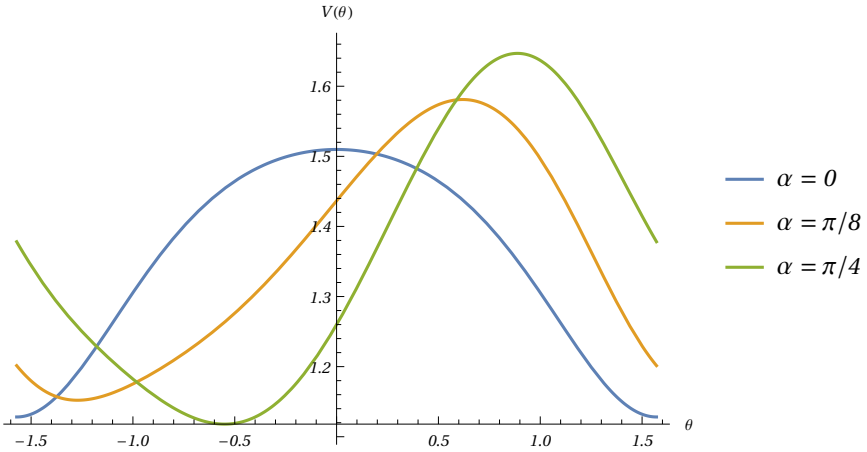

Figure 2.17: Potential $V_\alpha[\theta]$ in units of χH^2 as a function of θ for three values of the angle, $\alpha = (0, \pi/8, \pi/4)$. The field is taken as $H^2 = 1.5H_c^2$, even if the value H_c is defined for $\alpha = 0$. We can see that when $\alpha \neq 0$, $\theta = 0, \pi/2$ are no longer extrema of V_α.

of V_α follow the equation:

$$0 = \frac{\chi H^2}{2\zeta\Delta\mu}\sin 2(\alpha-\theta) - \frac{\nu\cos 2\theta - 1}{4\eta/\gamma+\nu^2-2\nu\cos 2\theta+1}\sin 2\theta \tag{2.89}$$

One of the first thing to notice is that, when α is different from 0 or $\pi/2$, $\theta = \alpha$ is no longer a general solution to (2.89) because of the active stress. When the field makes a finite angle α with the stripe there is a competition for the orientation between the external field χH^2 and the active stress $\zeta\Delta\mu$. Even when $\chi H^2 \gg \zeta\Delta\mu$, the nematic does not align perfectly with the field. Let us calculate this perturbation in the limit $\zeta\Delta\mu \ll \chi H^2$. In this limit, we can search for θ in the form $\theta = \alpha + \delta\theta + O\left(\left(\frac{\zeta\Delta\mu}{\chi H^2}\right)^2\right)$, and plugging back this development into eq. (2.89) yields

$$\delta\theta = \theta - \alpha = -\frac{\zeta\Delta\mu}{\chi H^2}\frac{\sin 2\alpha(\nu\cos 2\alpha - 1)}{4\eta/\gamma+\nu^2-2\nu\cos 2\alpha+1} + O\left(\left(\frac{\zeta\Delta\mu}{\chi H^2}\right)^2\right) \tag{2.90}$$

A plot of $\delta\theta$ is given in fig. 2.18. From eq. (2.90), we see that there is a value of α for

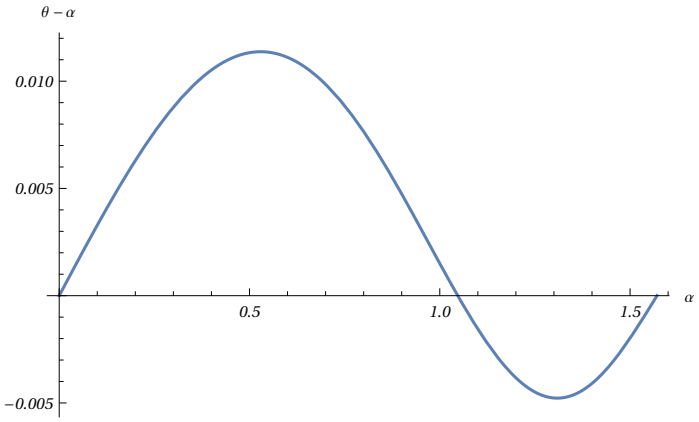

Figure 2.18: $\theta - \alpha$ in rad as a function of α as given by (2.90). The parameters are $\frac{\zeta\Delta\mu}{\chi H^2} = 0.07, \eta/\gamma = 1, \nu = -2$

which $\delta\theta = 0$, given by

$$\cos 2\alpha = \frac{1}{\nu} \tag{2.91}$$

Once α_c is identified as the value of the external field angle when $\delta\theta = 0$, the flow-alignment parameter ν is given by

$$\nu = \frac{1}{\cos 2\alpha_c} \tag{2.92}$$

There is a competition for the orientation in the stripe between the external field and the active stress resulting in a finite perturbation $\delta\theta$ at finite $\zeta\Delta\mu/(\chi H^2)$. However, there is no competition when the direction of the external field is aligned with the direction imposed by the shear flow created by the active force, given by eq. (2.92). This provides a method to calculate ν independently from the other hydrodynamic parameters.

2.6 Comparaison with experiments: parameter estimation

The experimental results presented in this section are preliminary. We propose a method in section 2.6.1 but the precise estimation of hydrodynamic parameters from the data is yet to be done. I present the experimental results in section 2.6.2 and estimate some parameters. These parameters are however sometimes estimated without information on their precision. Although this is not rigorous, it it the best we can do at this time. We proceed with the goal to obtain the order of magnitude of the parameters.

2.6.1 Constraints imposed by the Buckingham-π theorem

The Buckingham-π theorem [81] deals with dimensional analysis. If a system is described by n physical variables that depend on p fundamental physical units, then there are $n-p$ dimensionless variables (the Π variables) and p dimensioning variables. Every mathematical function of the n variables can be described by a function of $n-p$ variables. Let us detail this theorem in practice for an active nematic with an external field. In a minimal theory for active nematics presented in section 1.2, by adding an external field there are six physical variables:

1. Activity $\zeta\Delta\mu$
2. Shear viscosity η
3. Rotational viscosity γ
4. Flow alignment parameter ν
5. Frank elastic constant K
6. Field χH^2

Those six parameters are expressed by three fundamental physical units:

1. Length, and our choice for a reference lengthscale is given by the critical length (2.27)
2. Time which, once the length unit is determined, is given by the typical velocity of the shear flow $v_0 = 2\pi K/(L_c(\nu+1)\gamma)$
3. Mass or more physically a force once the length and time units are given.

The experimental setup that was used cannot measure forces, therefore whatever the number of measured quantities and comparison with the theory, an unknown parameter remains, either $\zeta\Delta\mu$, χH^2, γ, η or K, because all depend on a mass or force scale.

Once a unit of length and a unit of time are given, if we were also able to measure a force, three dimensionless variables would remain and could be inferred by fitting experimental results with the theory. We choose the three following dimensionless variables:

1. $\zeta\Delta\mu/(\chi H^2)$ the ratio between the active stress and the field
2. η/γ the ratio between shear and orientational viscosities
3. ν the flow-alignment parameter

An experimental plot of $\delta\theta$ given by eq. (2.90) and figure 2.18 gives directly ν through (2.92).

η/γ can then be inferred by fitting the amplitude of the tilt angle close to the transition when there is no field (2.32).

Finally, we can infer $\zeta\Delta\mu/(\chi H^2)$ by fitting the curve $\theta(0) - \alpha$ as a function of α for large widths compared to the width of instability using (2.90) or using a numerical fit if $\zeta\Delta\mu \ll \chi H^2$ is not verified.

Now that we have established the ideal procedure to measure as many hydrodynamic parameters as possible with the theoretical study provided in this chapter, let us try to apply this procedure on the experiments performed by Thibault Aryaksama in the group of Pascal Silberzan.

2.6.2 Experimental results

Strong effect of the abrasions

If we look at the angle in the middle of the stripe for C2C12 cells as a function of the width of the stripe, as shown on fig. 2.4, after $\sim 400\mu$m the angle is fixed at $\theta = 0$, parallel to the abrasions. Thus, modeling the abrasions with an external field, the magnitude of the field must be greater than the critical field given by eq. (2.73). Therefore, the effect of the abrasions is strong compared to the effect of the active stress, at least in large stripes.

Effect of the field on the critical width

If we want to look at the effect of the field on the critical width, we have to look at what happens for small stripes. Indeed, a previous experiment also done in the group of P. Silberzan [1] finds a critical width around 30μm for C2C12 cells. The experimental data for stripes between 20 and 180μm for the central angle $\theta(0)$ and the velocity at the right edge $v_y(L/2)$ are represented on fig. 2.19. We can see from figure 2.19 that around 80μm a tilt in the middle of the stripe and a flow at the edges start to appear.

An important feature is that there is no clear indication that the tilt and the flow appear for different lengths in the case where there are abrasions, compared to when there are none. However, calculations in presence of an external field (2.62) indicate that the critical length above which a tilt and a flow appear must be smaller in the presence of the field. This is especially true since we know from figure 2.4 that the effect of the field is strong in the sense of $H > H_c$ given by (2.73).

However, looking at the data for widths between 20μm and 300μm on fig. 2.20, we see that the curve of the central angle, in the case of abrasions, departs from the behavior of the middle angle without abrasions around 200μm. To explain this change of behavior, we make the hypothesis that the effect of the abrasions is not felt until the

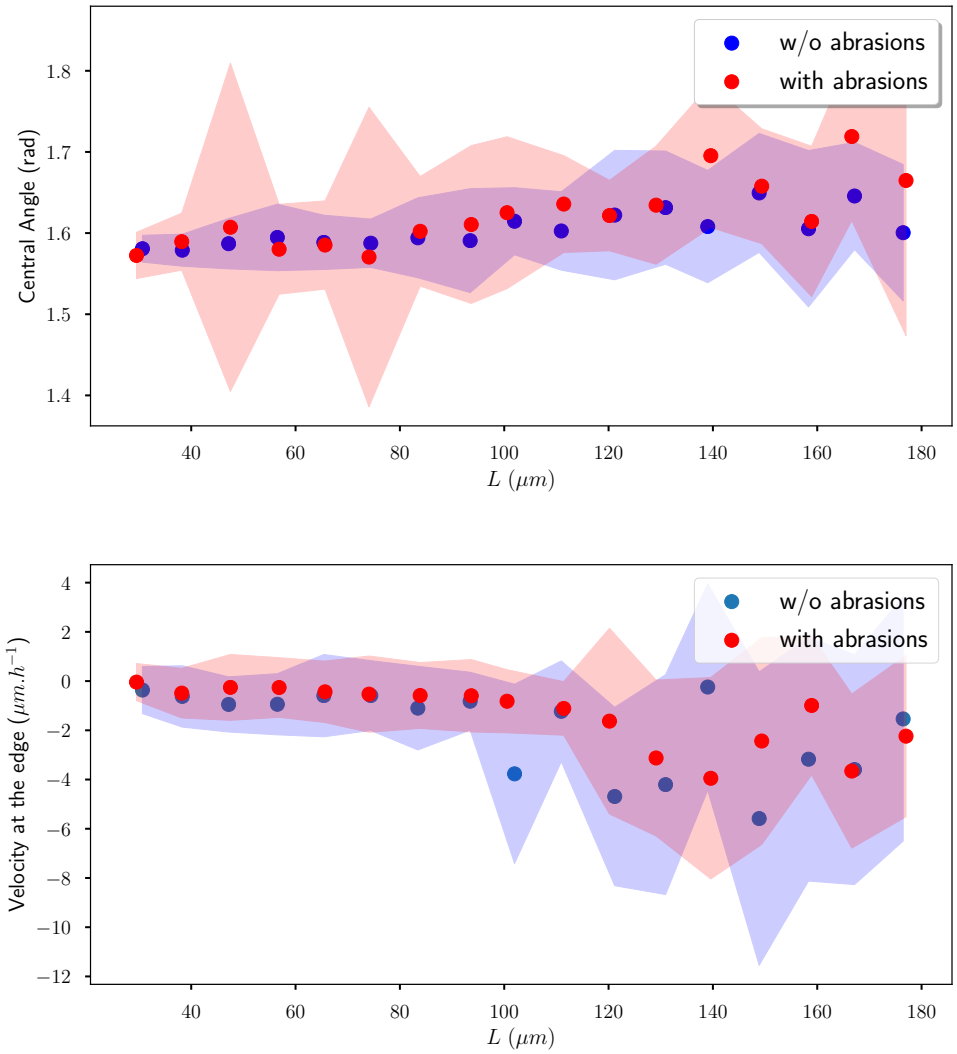

Figure 2.19: Stripes with a width between 30 and 180μm. On the top the central angle in rad and on the bottom the velocity at the right edge in $\mu m.h^{-1}$. The angle is greater than $\pi/2$ and the velocity at the right edge negative, consistent with an extensile behavior (see fig. 2.9). Experiments in a 10μm window are averaged to give a single data point, with a standard deviation represented by the colored area. We see, contrary to fig. 2.20, that with and without abrasions the evolution of the middle angle and of the velocity is the same, suggesting a non-linear effect of the abrasions on the cells. Courtesy of Thibault Aryaksama for experimental data

stripe has a certain width, here 200μm. This length is to be compared with the cell

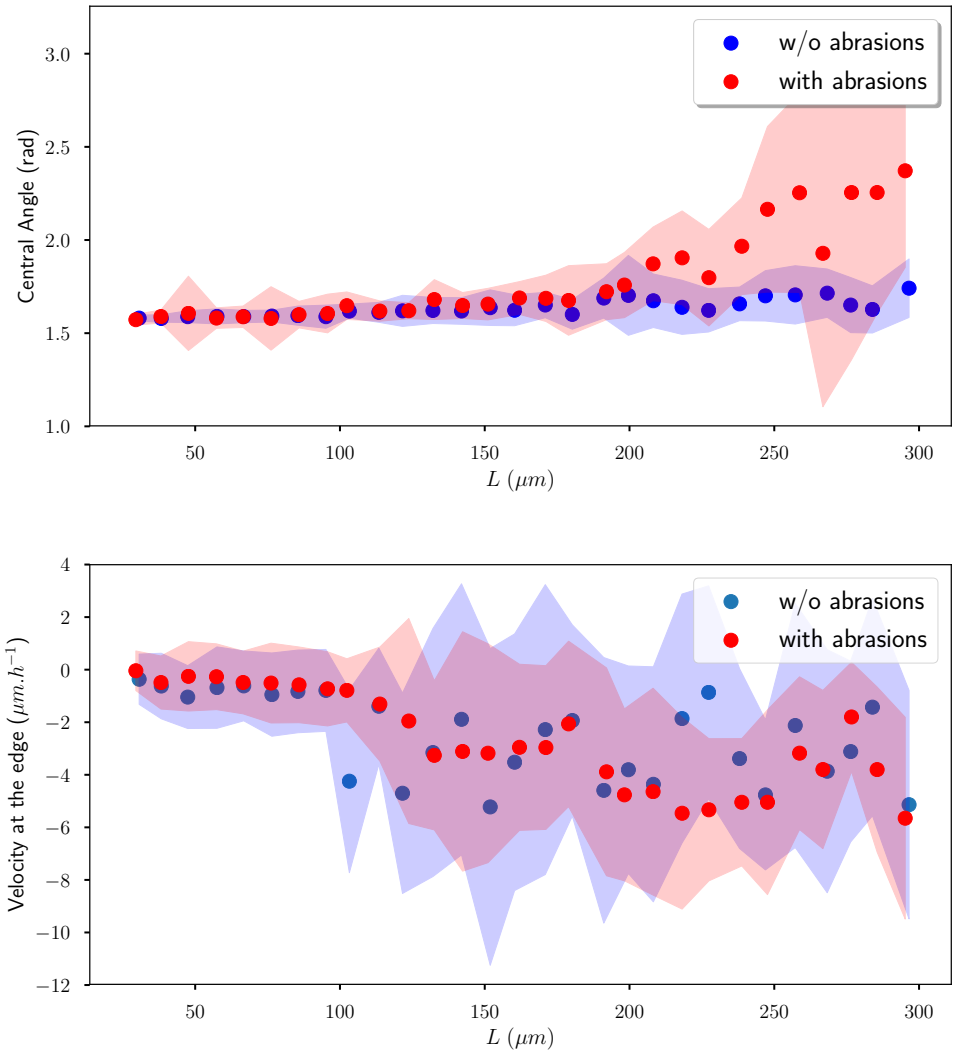

Figure 2.20: Stripes with a width between 30 and 300μm. We can see that the curve for the central angle has a change of behavior just before 200μm while the velocity is not significantly changed. An hypothesis for this change of behavior of the angle is that the cells start to orient with the abrasions after a certain intrinsic length that is of the order of 200μm. Courtesy of Thibault Aryaksama for experimental data

length, about 30 – 50μm. This means that below a certain width for the stripe, of about five times the cell size, it is as if the cells did not see the abrasions, in the sense that cells do not align preferentially in the direction of the abrasions when the confinement is too strong. The fact that the orientation of cells via contact guidance has an intrinsic

length scale is something that was previously reported in ref. [72] and so it seems a fair hypothesis to explain the behavior of the central angle on figure 2.20 with our theoretical analysis.

Flow Alignment parameter

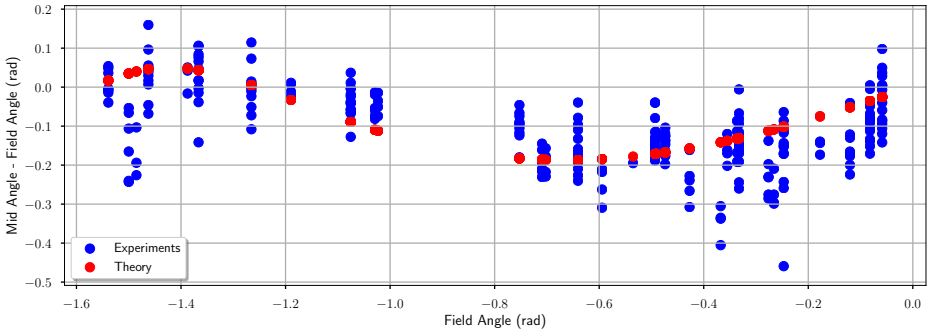

Figure 2.21: Difference between the central angle and the angle made by the abrasions as a function of the angle made by the abrasions, in radians. The point where the curve crosses the $x-$axis gives the flow alignment parameter. With a crossing angle α_c such that $-1.35 \leq \alpha_c \leq -1.15$ rad, we deduce from eq. (2.92) that $-1.5 \leq \nu \leq -1.1$

The flow alignment parameter can be determined directly from the observation of the central angle when the angle of the abrasions is varied, as detailed in section 2.5.2. The deviation of the central angle from the angle made by the abrasions, as a function of the angle made by the abrasions, is represented in fig. 2.21. Looking at the crossing of the curve $\theta(0)-\alpha$ with the $x-$axis, we deduce the flow alignment parameter to be $-1.5 \leq \nu \leq -1.1$. This value is close to values that can be found in the literature for passive nematics [82]. This value is similar to a value found in C2C12 cells by measurement on topological defects [83, 84], and in the range of values found in epithelial monolayers of *drosophilia* wings [85]. A fit is made in fig. 2.21 using eq. (2.90) with a value of $\nu = -1.3$, but there are two free variables, $\zeta\Delta\mu/(\chi H^2)$ and η/γ and we were not able to deduce η/γ from the amplitude of the tilt. Therefore, we cannot deduce a value for $\zeta\Delta\mu/(\chi H^2)$.

Fitting bifurcation curves

We compare the experimental data of the central angle and of the velocity at the edge, without abrasions, to their theoretical expressions (2.31) and (2.33). We perform a fit of the data using a square-root function starting at the critical length that is set at $L_c = 81\mu$m, represented in fig. 2.22. The flow-alignment parameter ν is given by

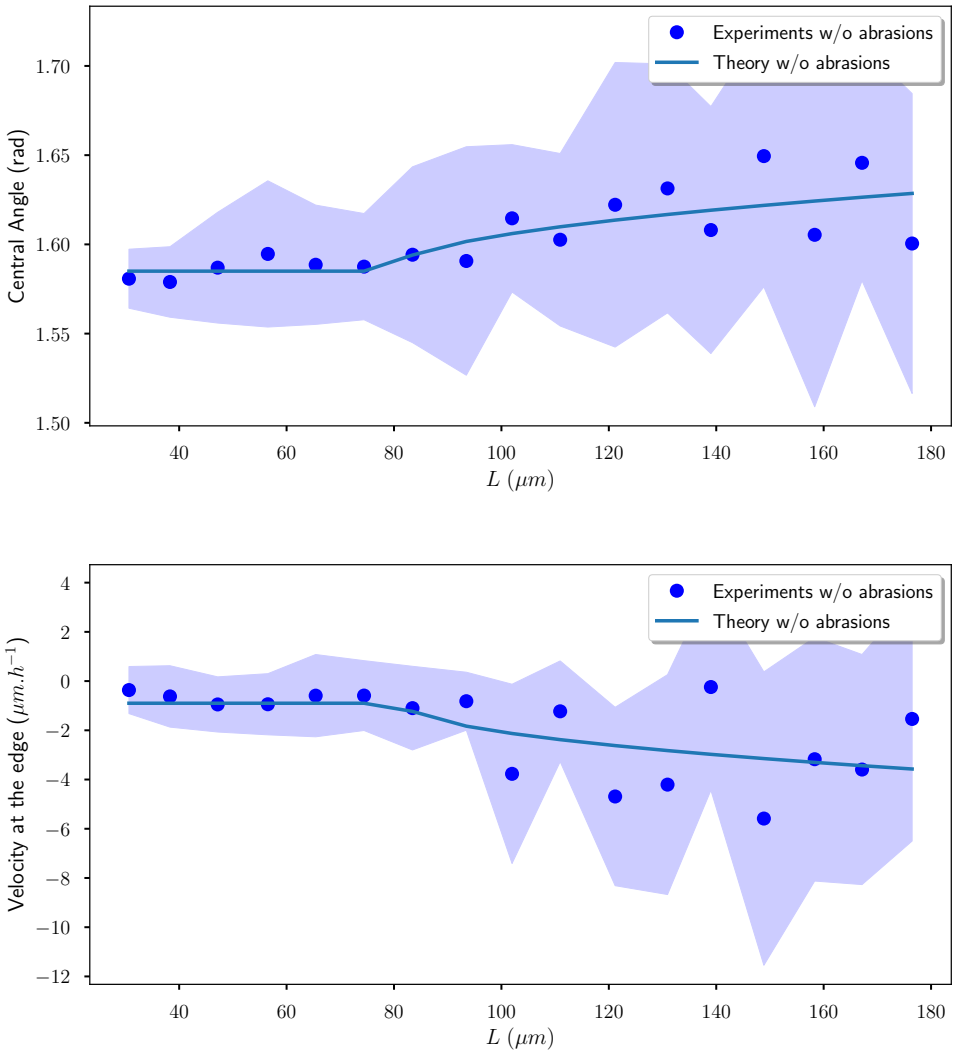

Figure 2.22: The experimental data are represented by points, while the colored areas represent the standard deviation. The theoretical fits are in solid line. On the top figure, the central angle is fitted with a square-root function $\sqrt{(L - L_c)/L_c}$ for $L > L_c$. On the bottom, the same is done on the velocity at the edges.

$\nu = -1.3 \pm 0.2$, and the only remaining variable in eq. (2.32) is η/γ. However, extracting η/γ from the expression given by eq. (2.32) with the value of $\tilde{\theta}_0$ found numerically is not possible. This is possibly due to non-linear terms that are not taken into account in the theory and modify the expression (2.32). The numerical fit finds a negative value for η/γ knowing the value of ν, which is a physical non-sense. A possible explanation

for this anomaly can be in the validity of the weakly non-linear perturbation giving eq. (2.32). On fig. 2.23 are represented the points from the numerical resolution of the nonlinear PDE (2.24), and in solid line the square-root function with the amplitude given by eq. (2.32). It shows that the weakly non-linear perturbation is not valid for lengths $L \gtrapprox 1.2L_c$ and could explain the anomaly. Another explanation can come from

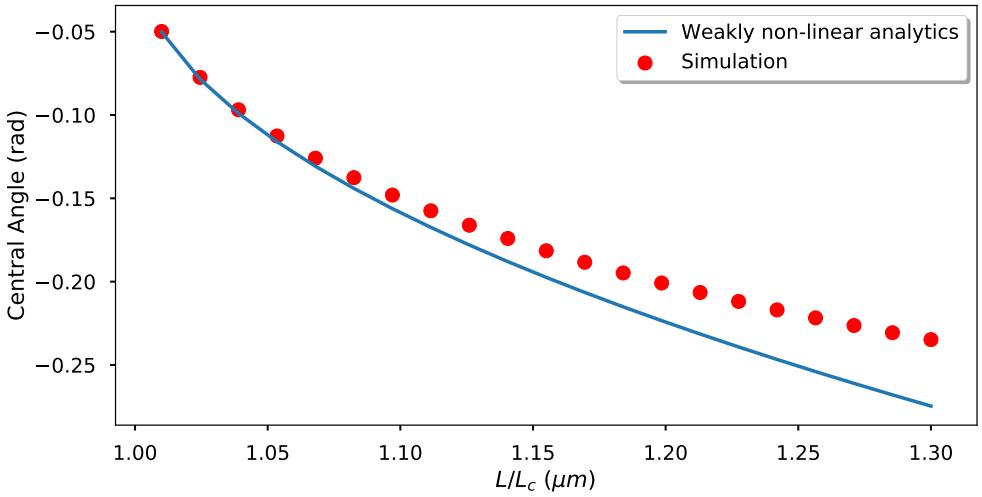

Figure 2.23: The points represent the central angle as a function of the width obtained by numerical resolution of eq. (2.24) at steady state, using a relaxation method. The solid line represents a square-root function $a\sqrt{(L-L_c)/L_c}$ for $L > L_c$ with the amplitude a given by eq. (2.32). We see that the weakly-linear approximation deviates from the simulated values for $L/L_c \geq 1.1$.

very different values of the two viscosities η and γ. For a concentrated solution of rigid rod-like polymers in the nematic phase, η and γ are of the same order of magnitude deep in the nematic phase [86]. It might however not be the case for cells because of active processes, and it is possible to be in the case $\eta \ll \gamma$ (the case $\eta \gg \gamma$ would lead to a large critical length).

By performing the ratio of the amplitudes given by the fits of the velocity and of the angle, we find a value of

$$\frac{K}{\gamma} = 2 \times 10^2 \ \mu m^2.h^{-1} \tag{2.93}$$

I do not give an error estimation on eq. (2.93) because this value must be taken as an order of magnitude more than a precise estimation. Moreover, this is preliminary results and an error of estimation on K/γ relies on an error estimation on the critical length which has not yet been done.

2.7 Discussion

Let me start by a word of caution: although the theoretical developments in this chapter are valid on their own, their comparison to the experimental results is preliminary and is subject to improvements and changes. Very few simulations have been performed at this point and this discussion can be enriched in the future.

In this section, we started by developing a theory for an active nematic confined in a stripe when an external field is imposed. We saw that when the field is perpendicular to the stripe, a situation identical to the passive Freedericksz transition, there is an added effect of the field and the active stress and the critical length above which a tilt and spontaneous flow develop is smaller. We saw that the spontaneous shear flow that develops above the critical length is not directly affected by the presence of the external field - although it is affected through changes in the orientation due to the external field. This confirms that the apparition of a shear flow is a signature of activity in the system.

We also saw that depending on the value of the external field the tilt angle could, in the large-stripe limit, either align with the field if the field is greater than a critical value that depends on the active stress, or take a value that depends on the ratio between the active stress and the field. Experimentally, the presence of the abrasions stabilizes the tilt angle for large stripes. Indeed, a tilt is observed even for stripes of widths of the order of a millimeter. This is of the order of ten times the critical length above which a tilt appears. In simulations, depending on material parameters the first mode (corresponding to the experimental observation) becomes unstable at a certain point. An explanation for the stability of the tilt is that, for the comparison with theory, fields of view with topological defects are removed from the experimental data. Therefore a selection of the stable first modes is made. This stability is not necessarily a general feature.

By changing the orientation of the abrasions, we found a way to measure the flow alignment parameter ν by looking at which angle the cells perfectly align with the abrasions. When the abrasions and the cells are aligned, the abrasions are in the same direction as the tilt imposed by the shear induced by the active stress.

By comparing the experimental results to the theory, we are able to determine two parameters that are used for adimensioning the equations, the critical length and the velocity. A unit force is missing which cannot be determined by these experiments. We are able to determine the flow-alignment parameter ν but cannot determine the two remaining dimensionless parameters: the ratio between the active stress and the external field $\zeta\Delta\mu/(\chi H^2)$, and the ratio between the two viscosities η/γ.

There are theoretical as well as experimental limitations to the precision of these results. On the theoretical side, we are able to make the estimation of the parameters through analytical expressions from an ideal hydrodynamic theory of active nematics. Indeed, when comparing the theory with experimental data, we did not take into consideration cell divisions and deaths nor interactions with the substrate. This is because

when taking into account these effects, we no longer have analytical results on the amplitudes (eqs. (2.32) and (2.33)), nor an effective potential description (eqs. (2.68) and (2.87)). Therefore the analytical expression for the central angle when the field is varied eq. (2.90) is lost. Eventually, we could make the parameter estimation using numerical fits in the non-linear regime and performing a multi-parameter optimization problem. The other problem is more fundamental in the sense that the theory that we developed has no strong basis for being valid for the non-linear dynamics. Indeed, this close-to-equilibrium theory based on linear phenomenological relations through the Onsager procedure is well suited to describe what happens at small activity, where we depart from equilibrium, or in the large stripe limit, which is close to a uniform equilibrium state, but there is no reason to believe it is well suited to infer parameters when there are large active effects. However, there is a history of strong accuracy of linear hydrodynamic theories being valid far from equilibrium. One example being the Navier-Stokes equation that describe accurately liquids even with strong perturbations. The hydrodynamics of liquid crystals from which the derivation of 1.2 is based on yields good results even under strong perturbations [35]. Because the accuracy of the active hydrodynamic theory is not well confirmed for strong perturbations, we prefer neglecting certain effects and no go into an exploration of the parameter space numerically, in order to retain analyticity.

On the experimental side, the velocity field is very noisy in the sense that the standard deviation of the velocity is of the order of the average velocity. This makes the precise identification of the critical length difficult.

Chapter 3

Active defects on a substrate

3.1 Introduction to topological defects in nematics

3.1.1 Overview

In this chapter, we are going to examine some hydrodynamic consequences of activity for specific configurations of the director field called topological defects. In the previous chapter we only considered, experimentally and theoretically, continuous deformation of the director. However, configurations where the orientation of the director is singular exist and are called defects. A mathematical definition of defects is given in section 3.1.2. The existence of defects in liquid crystals has been long known and defects were first observed by Otto Lehmann in 1904 [87] and Georges Friedel in 1922 [88]. Theoretical interest in defects came later with Frank and Kleman [34, 89], because of their mechanical properties. Defects are by nature places of higher stress, and can give information on the intrinsic symmetries of the basic constituent of the media, because they are optically identifiable. For example in liquid crystals the nature of defects can inform on the nature of the phase, for example if the liquid crystal is in a polar or nematic phase. The word nematic actually comes from the greek $\nu\tilde{\eta}\mu\alpha$, which means "thread", because of the observation of black lines of defects in nematic phases.

The hydrodynamics of nematics (even though the simplest form of liquid crystals in terms of symmetries) is very complex notably because of the coupling between the dynamics of the director and the flow. The dynamics of defects in nematics is still a relevant topic today [90–93]. Defects have been observed in living systems as early as 1968 by Elsdale [94] in fibroblast cells that organized into what he called groups - patches of aligned cells - and frontiers that can be interpreted as topological defects.

Since this precursor observation of islands of ordered nematic phases separated by defects, there has been a growing interest in topological defects in cellular architectures. The presence of defects can inform on the material properties of cells [28, 83, 84] and on their symmetries, whether polar or nematic [33]. It has been reported that topological

defects are also preferential sites for extrusion [12, 36, 37], multilayering [95], and play a role in cellular organization [96–98].

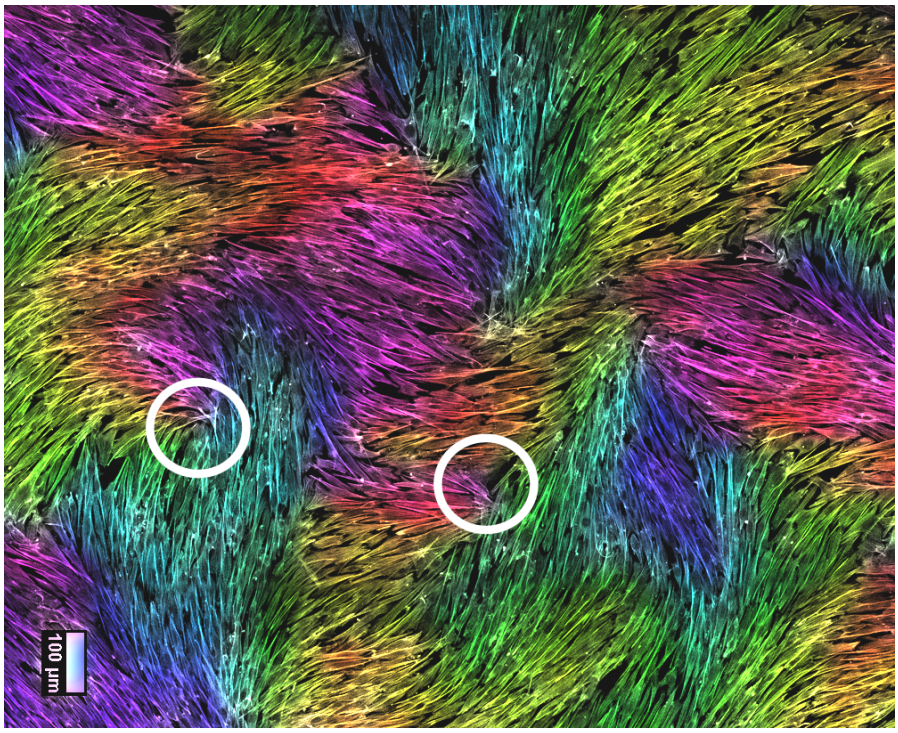

Figure 3.1: Picture of a monolayer of C2C12 cells showing several topological defects. The orientation of cells is colored for visual cues, and the two white circles show a $+1/2$ defect on the left and a $-1/2$ defect on the right. Courtesy of Trinish Sarkar.

Topological defects are particularly interesting in the context of active matter, because defects create gradients of orientation (see figs. 3.1 and 3.2). As seen in chapter 2, a gradient of orientation create an active force due to the gradient of active stress. Therefore, topological defects are special locations where active forces are generated. Because of this, spontaneous motion develops in the vicinity of topological defects. Different types of defects have different symmetries (see fig. 3.2), and depending on these symmetries active forces created by the defects can lead to self-advection or rotation [23, 26, 33, 39, 40, 99–101]. Because of activity, active topological defects can have a significantly different behaviors compared to their passive counterparts. In passive systems, the presence of defects can depend on the preparation of the system and on boundary conditions. As expressed in sections 3.1.2 and 3.1.3, topological defects can be classified by their topological charge and in passive systems their interactions are reminiscent of electrostatic interactions: defects of opposite charge attract each other and defects of the same charge repel each other. This leads in passive systems to annihi-

lation of defects and relaxation to a state of minimal number of defects. The dynamics of active defects is more complicated and, in the context of this work, I will focus on active nematics. Firstly, defects can appear in the system because of activity. This can be understood in the context of the active instability studied in chapter 2: activity destabilizes uniform configurations of the director [41, 102]. At high activity, strong gradients of orientation can appear and transform into topological defects, a process called "wall unzipping" [35, 39, 91, 99, 103, 104]. Although in the system of contractile C2C12 cells that is studied in this work there is no clear creation of defects, the density of defects has been related to activity in extensile MDCK cells [37]. Secondly, existing defects of opposite charges do not necessarily attract each other due to active self-advection. This can lead to an effective repulsion between defects [39, 99], and the number of defects does not necessarily decrease. This proliferation of defects and the flows created by their orientations can lead to chaotic flows, a state called active turbulence possible even at low Reynolds numbers [44, 45, 59, 103, 105–107].

Active topological defects are interesting from the point of view of phase transitions. Due to the proliferation of defects and the possible separation of defects at high activity, this leads to a phase transition at constant temperature, similar to a Berezinskii-Kosterlitz-Thouless transition [108]. With increasing activity, active nematics can go from an ordered nematic phase to a chaotic phase with topological defects [54, 100]. When activity is increased further, there is even existence of a novel thermodynamic polar phase due to the polarity of $+1/2$ defects [54, 109].

In this manuscript, I will focus on the flow created by isolated nematic defects in two dimensions. One of the main difficulties to calculate the flow created by a topological defect is the coupling between the flow and the orientation that creates a "backflow". Previous analytical results exist for the flow created by half-integer defects when momentum is conserved and the backflow is neglected [39]. Pismen in ref. [40] takes into account the backflow in his calculation, for a dry system (without hydrodynamic interactions). In section 3.3, we calculate the flow created by an isolated positive half-integer topological defect and its self-advection velocity when there is friction, by neglecting the backflow. Motivated by experimental observations presented in section 3.2, we calculate in section 3.4 the stall force to arrest a positive half-integer active defect. In section 3.5, we include part of the backflow by taking into account the torques created by the Frank distortion energy. In particular, we look at the effect of this torque on the arrest force. In section 3.6 we look at the effect of cell division on the flow created by a defect. Finally, in section 3.7 we look at the effect of the active flow on the nematic director.

3.1.2 Topological charge and energy

Defects are classified topologically by defining a strength S also called topological charge [35, 89]. The topological charge of a singular point is defined from the amount

of rotation that the director makes when going around a full circle around this point (see fig. 3.2). If the director makes an angle φ with a reference axis, then the variation of the director $\Delta\varphi$ after a rotation of 2π is $\Delta\varphi = 2\pi S$. Therefore S can only be integer or half-integer for nematics because $\mathbf{p}$ and $-\mathbf{p}$ are equivalent. For polar systems, S is an integer.

Coming back to the Frank free energy of nematics eq. (2.5), one can obtain the orientation field of a passive topological defect by minimizing the free energy. We define the orientational field angle $\varphi(r, \theta)$ in polar coordinates in a frame that has the defect's core as its origin and with respect to a chosen reference axis in accordance with the symmetries of the particular defect (see figs. 3.7 and 3.9). Taking the one Frank constant approximation the free energy is

$$F = \int \frac{K}{2}(\nabla\varphi)^2 \, r dr \, d\theta \tag{3.1}$$

Therefore minimizing the free energy (3.1) requires

$$\frac{\delta F}{\delta \varphi} = K\nabla^2\varphi = 0 \tag{3.2}$$

The solutions to (3.2) that do not depend on the distance to the defect r verify

$$\frac{d^2\varphi}{d\theta^2} = 0 \tag{3.3}$$

Solutions to (3.3) are

$$\varphi(r, \theta) = A\theta + B \tag{3.4}$$

where A, B are constants. A corresponds to the amount of rotation of the director and can be expressed by the strength S. With the expression (3.4), a rotation of 2π around the defect induces a change in the angle of the director of $\Delta\varphi = 2\pi A$. Therefore, the strength S is exactly A, and in the one-constant approximation a defect of strength S has an orientation

$$\varphi(r, \theta) = S\theta + B \tag{3.5}$$

Except for defects of strength $S = 1$, B can always be chosen to be zero by rotating the axis of the frame. For integer defects $S = 1$, $B = 0$ corresponds to asters, $B = \pi/2$ corresponds to circles and other values to spirals, as shown in fig. 3.2. Relaxing the one-constant approximation yields more complex expressions for the orientation field [28, 73].

I made an important simplification to derive eq. (3.5) that must be clarified: I considered in the free energy (3.1) a perfectly ordered nematic, with a director of modulus one that can be represented only by its orientation angle φ. This ideal situation is valid deep in the nematic phase, but close to a topological defect it is not. To be rigorous, one must

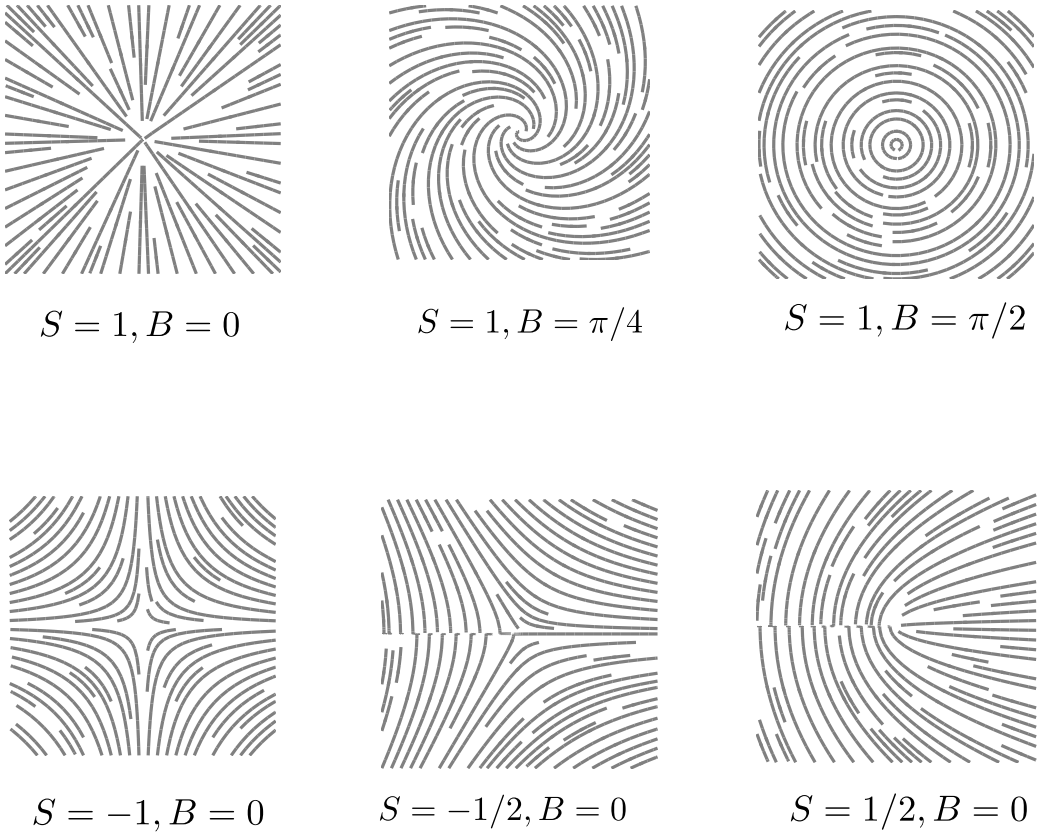

Figure 3.2: Different types of defects depending on the strength S and the offset B.

take into account $\mathbf{p}^2$ terms in the free energy. In that case, one finds a healing length ε that depends on parameters of the free energy, for which the modulus of $\mathbf{p}$ vanishes linearly for lengths smaller than ε [40, 110]. In this work, we do not want to describe precisely what happens close to the core. We either consider a vanishing healing length and consider a point-like core, or we consider that there is a region ε for which there is no nematic order, $\mathbf{p}^2 = 0$ for $r < \varepsilon$, and a region of perfect nematic order for $r > \varepsilon$, $\mathbf{p}^2 = 1$. In that case, we will say that we consider a finite-sized core.

Taking a circle of size R around the core of a defect, the free energy stored in the defect configuration of eq. (3.5) is:

$$F = \int \frac{K}{2} S^2 \frac{1}{r^2} r \mathrm{d}r \, \mathrm{d}\theta = \pi K S^2 \ln(\frac{R}{\varepsilon}) \tag{3.6}$$

Since the free energy depends on the square of the strength, lowest-strength defect are expected to be mostly observed, i.e half-integer defects for nematics and ±1 defects for polar systems.

3.1.3 Interaction between defects

The topological strength of a defect is called a charge because of the analogy with electrostatic charges. Like in electrostatics, topological charges of opposite signs attract each other while charges of the same sign repel each other. If two defects, a +1/2 and a -1/2, are separated by a distance d, the energy $E_{\pm}$ of the defect pair is [35, 39]:

$$E_{\pm} = 2\pi K S^2 \ln \frac{d}{\varepsilon} \tag{3.7}$$

The energy $E_{\pm}$ increases with the distance d. This creates an attractive force between the two defects of opposite charges. This result is valid only for passive defects, active defects can separate if the active force generated by the gradients of orientation overcomes the attractive force [39, 99].

3.2 Experimental observations

Trinish Sarkar in the group of Pascal Silberzan at Institut Curie performed experiments in a free monolayer of C2C12 myoblast cells (see fig. 3.1). The presence of half-integer topological defects confirms the nematic phase of C2C12 cells. Positive half defects have a motion from their head towards their tail, a motion consistent with a contractile active stress [33, 39], as seen in fig. 3.3.

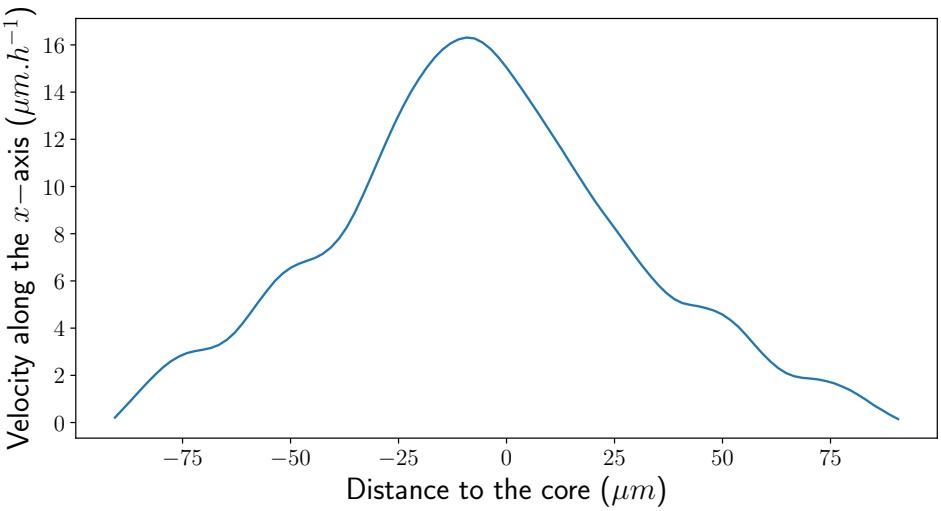

Figure 3.3: Velocity on the $x-$axis of $+1/2$ motile defects. The convention for the axis is the one of fig. 3.7. A positive value of the velocity is the signature of a motion from the head towards the tail. From data by Trinish Sarkar.

Results are preliminary and I will only indicate the general trend observed. In monolayers, positive half-integer defects have been observed as preferential sites for multilayering. Previous observations on MDCK cells [37] and NPC cells [36] report that topological defects are preferential sites for extrusion. In bacterial colonies, Copenhagen *et al.* [95] also report multilayering at positive half defects, and the bacteria are extensile.

The number of defects decays in the monolayer over time, but never vanishes, as seen in fig. 3.4. This is due to the absence of significant defect creation and the annihilation between defects of opposite charges. This suggests that the activity is sufficiently low to not create topological defects. Preliminary results suggest that there is a class of

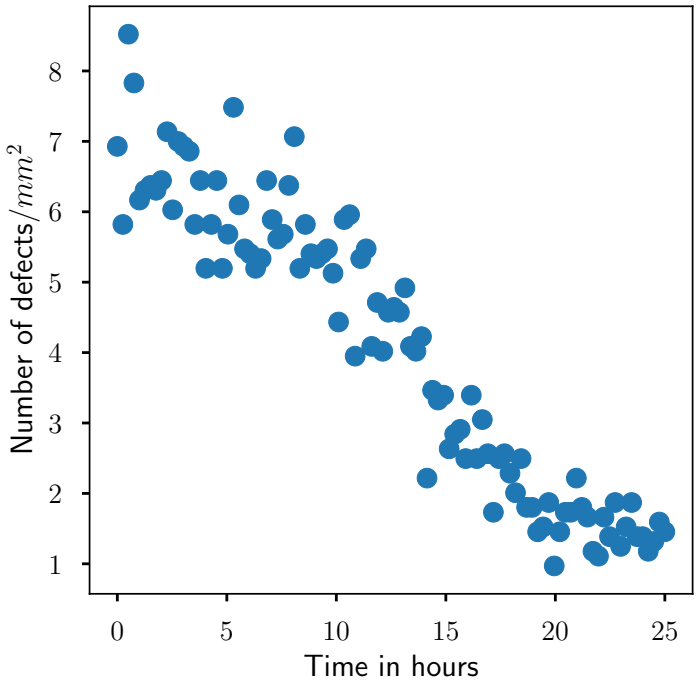

Figure 3.4: Number of defect per mm^2 as a function of time. Time zero is set close to confluency, and at 25h there is multilayering. We see that the number of defects does not vanish before multilayering. From data by Trinish Sarkar.

non-motile $+1/2$ defects and that new layers of cells form at these non-motile defects. The non-motile defects are not associated to jamming that can occur in confined monolayer of cells [111], because in this case, there is still a flow of cells around the defect. Instead, the defect itself is not moving, as seen on fig. 3.5.

The existence of motionless +1/2 defects is something not expected by the theory

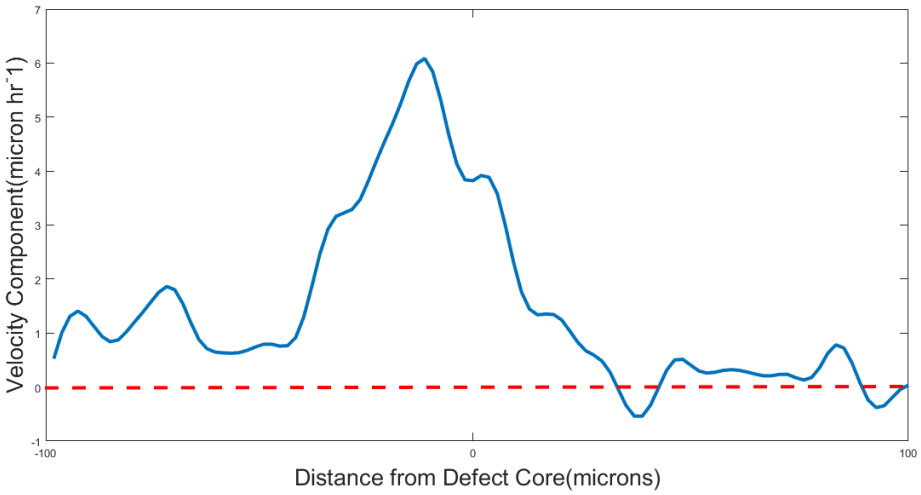

Figure 3.5: Velocity on the $x-$axis for non-motile defects as a function of the distance from the core. The velocity profile is no longer symmetric compared to fig. 3.3, and there is no motion at the tail of the defect. Courtesy of Trinish Sarkar.

and must be accounted for by a stabilizing force acting on the defect. Although the experimental apparatus used could not measure forces, information can be extracted by looking at the surface of focal adhesions that are related to force generation [24]. As seen in fig. 3.6, the largest focal adhesions are for cells located at the defect core, suggesting that the cells that are at the core contribute to the pinning of the defect.

3.3 Spontaneous flow without orientational dynamics

3.3.1 Active force created by defects

One of the main features of the hydrodynamics of active nematics is the presence of active forces whenever there are orientation gradients. Therefore, for an active nematic, the geometry of defects generates active forces. The active stress is given by eq. (1.29):

$$\sigma^{\text{act}}_{\alpha\beta} = -\zeta\Delta\mu\left(p_\alpha p_\beta - \frac{\delta_{\alpha\beta}}{2}\right) \tag{3.8}$$

Let us now compute the active stress and the active force density resulting from the distortion of the director for $+1/2$ and $-1/2$ defects in the one-constant approximation.

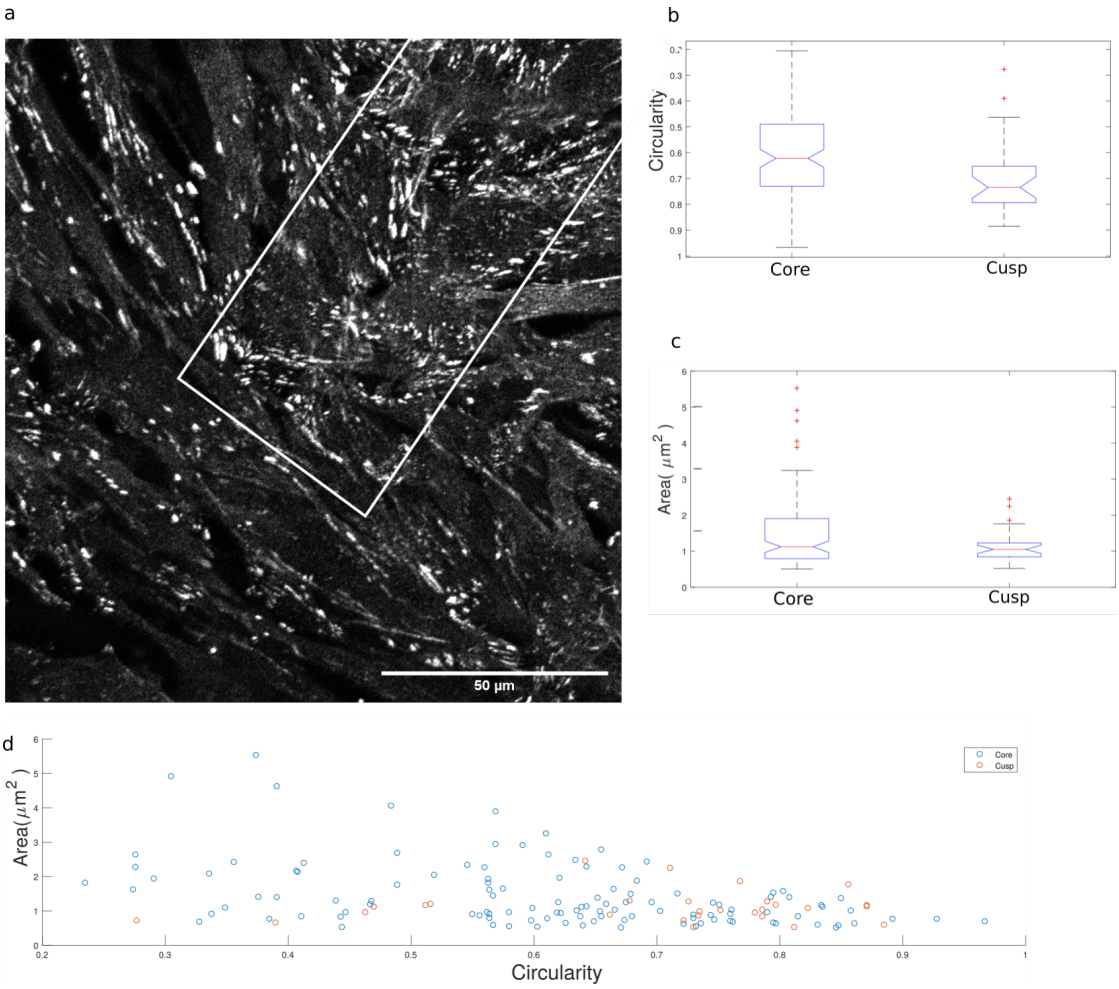

Figure 3.6: a. Zoom in on the core of a $+1/2$ topological defect. In white are shown the focal adhesions of the cells. The white frame indicates the cells of the core as opposed to the cusp. b. Circularity of the focal adhesions. Focal adhesions in the core are more elongated than the cells of the cusp (the $y-$axis is inverted and 1, the value of a perfect circle, is at the bottom). c. Area of focal adhesions. Inside the core, there are larger focal adhesions than for the cusp. d. Area and circularity of focal adhesions. Top left represents large elongated focal adhesions while the bottom right represents small circular focal adhesions. Blue dots are for the core, while red dots are for the cusp. There are predominantly blue dots in the top left quadrant of the figure, indicated larger elongated focal adhesions at the core, as seen in the white frame of a. Courtesy of Trinish Sarkar.

$+1/2$ defects

Let us consider a point-like $+1/2$ defect, in a reference frame centered at the core with the $x-$axis along the axis of symmetry of the defect, as in figure 3.7. At a point M, let us

define the polar coordinates r, the distance to the core, and θ the polar angle with respect to the $x-$axis. Let us call φ the angle that the nematic director makes with respect to the $x-$axis. In this cartesian frame, the director is $\mathbf{p} = \cos\varphi\ \mathbf{e_x} + \sin\varphi\ \mathbf{e_y}$. Because of

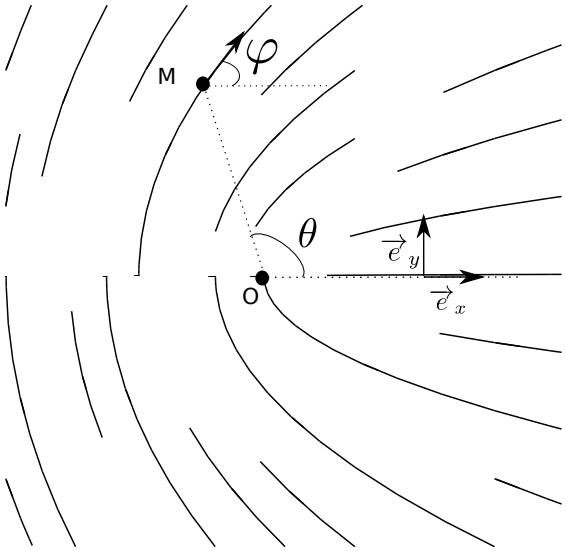

Figure 3.7: Schematic representation of $+1/2$ defect and reference axes.

the simple expression of the director angle φ in terms of the polar angle θ, $\varphi = \theta/2$ for a $+1/2$ defect, it is more convenient to work with polar coordinates with the core of the defect as origin and the $x-$axis as reference for the polar angle. In this polar frame, the director is $\mathbf{p} = \cos(\varphi - \theta)\ \mathbf{e_r} + \sin(\varphi - \theta)\ \mathbf{e}_\theta = \cos(\theta/2)\ \mathbf{e_r} - \sin(\theta/2)\ \mathbf{e}_\theta$. A matrix representation of the active stress $\sigma^{\mathrm{act}^+}_{\alpha\beta}$ in the $(\mathbf{e_r}, \mathbf{e}_\theta)$ basis is therefore

$$\sigma^{\mathrm{act}^+}_{\alpha\beta} = -\frac{\zeta\Delta\mu}{2}\begin{pmatrix} \cos\theta & -\sin\theta \\ -\sin\theta & -\cos\theta \end{pmatrix} \tag{3.9}$$

The force density $\mathbf{f}^{\mathrm{act}}_{+}$ due to activity of the $+1/2$ defect is given by

$$\mathbf{f}_{+}{}^{\mathrm{act}} = \nabla\cdot\sigma^{\mathrm{act}^+} = -\frac{\zeta\Delta\mu}{2r}\mathbf{e_x} \tag{3.10}$$

The geometry of $+1/2$ defects imposes a well-defined polarity. One can distinguish a tail region, where the cells on the axis $\theta = 0$ are parallel to the axis, and a head region, where the cells on the axis $\theta = 0$ are perpendicular to the axis. This acquired polarity is on the axis of symmetry of the defect. Therefore, it is natural to find that the active force density that depends on the gradient of orientation is oriented along the symmetry axis of the defect, as shown in fig. 3.7. The $1/r$ dependence comes from the orientation gradient and it is interesting to notice that the total active force of a defect diverges

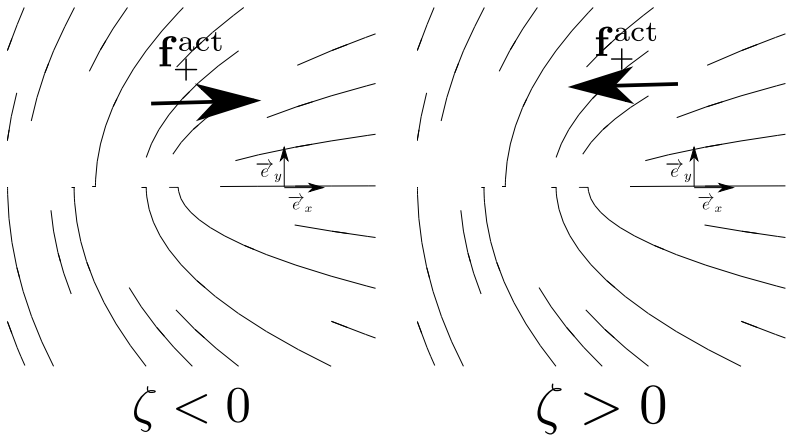

Figure 3.8: Force for $+1/2$ defect in the contractile ($\zeta < 0$) and extensile ($\zeta > 0$) cases.

linearly with the size of the system. The force (3.10) creates a spontaneous motion of an active $+1/2$ defect parallel to its symmetry axis. The direction of motion depends on the sign of the activity parameter ζ:

- For extensile cells, $\zeta > 0$ and $+1/2$ defects move towards their head
- For contractile cells, $\zeta < 0$ and $+1/2$ defects move towards their tail

The observation of the spontaneous motion of $+1/2$ defects because of the force density (3.10) and the direction of this motion (towards the head or the tail) has been used experimentally to confirm, first the nematic nature of cells, and then whether they are extensile or contractile [33, 36, 37, 95, 112].

-1/2 defects

If we now turn to $-1/2$ defects, there are three axes of symmetry with $2\pi/3$ angles between them. This means that there is no spontaneous polarity, and therefore no favored direction for the defect to move. Let us confirm this by computing the force as was done for $+1/2$ defects. We take a reference frame with one of the symmetry axes of the defect as the $x-$axis and work with polar coordinates (r, θ) centered at the core of the defect, as shown in fig. 3.9. For a $-1/2$ defect, $\varphi = -\frac{\theta}{2}$ and the director $\mathbf{p}$ is $\mathbf{p} = \cos(\varphi - \theta)\,\mathbf{e_r} + \sin(\varphi - \theta)\,\mathbf{e}_\theta = \cos(3\theta/2)\,\mathbf{e_r} - \sin(3\theta/2)\,\mathbf{e}_\theta$. A matrix representation of the active stress $\sigma_{\alpha\beta}^{\mathrm{act}^-}$ in the $(\mathbf{e_r}, \mathbf{e}_\theta)$ basis is therefore:

$$\sigma_{\alpha\beta}^{\mathrm{act}^-} = -\frac{\zeta\Delta\mu}{2}\begin{pmatrix} \cos(3\theta) & -\sin(3\theta) \\ -\sin(3\theta) & -\cos(3\theta) \end{pmatrix} \tag{3.11}$$

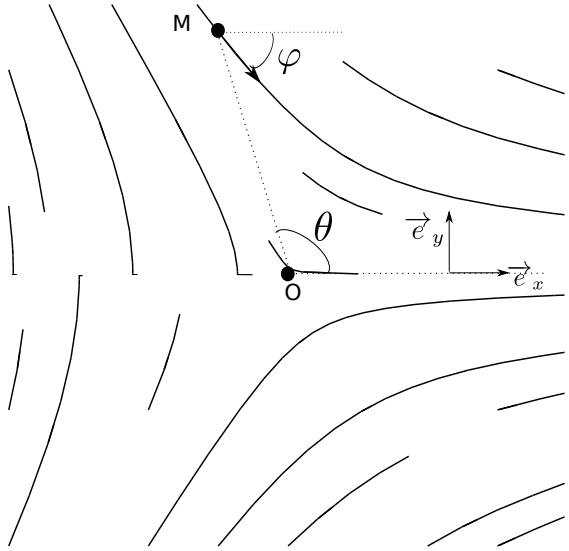

Figure 3.9: Schematic representation of $-1/2$ defect and reference axes.

The force density $\mathbf{f}_{-}^{\text{act}}$ due to the activity of the $-1/2$ defect is given by

$$\mathbf{f}_{-}{}^{\text{act}} = \nabla \cdot \sigma^{\text{act}^{-}} = -\frac{\zeta \Delta\mu}{2r}\left(-\cos(2\theta)\,\mathbf{e_x} + \sin(2\theta)\,\mathbf{e_y}\right) \tag{3.12}$$

Contrary to the $+1/2$ defect, the absence of acquired polarity results in a force density that depends on the polar angle θ, as shown in fig. 3.10. The 2θ dependence on the polar angle reflects the three axes of symmetry. The $1/r$ dependence of the force is recovered,

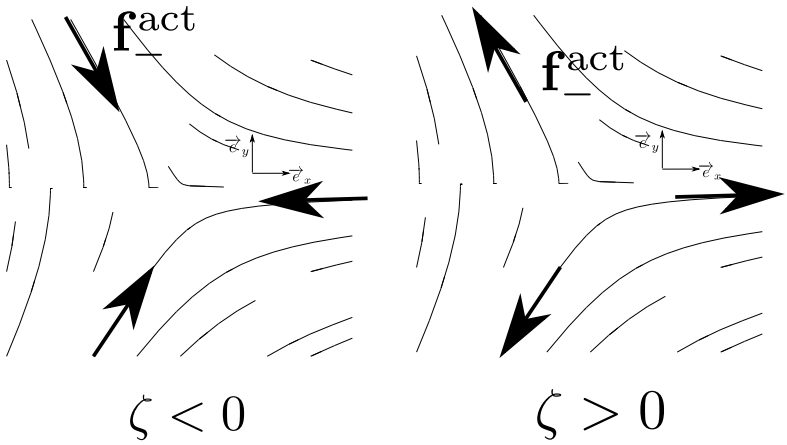

Figure 3.10: Force for $-1/2$ defect in the contractile ($\zeta < 0$) and extensile ($\zeta > 0$) cases.

but in this case because of the θ dependence the total force summed over a disk of size R vanishes.

- For extensile cells, $\zeta > 0$, the active force acts as a stretching force along the axes of the defect. This could explain the observation of cell depletion around extensile $-1/2$ defects that has been made in neural progenitor cells [36].
- For contractile cells, $\zeta < 0$, it is the opposite and the body force is contracting along the main axes of the defect.

3.3.2 Flows for a +1/2 defect on a substrate

After having made a hand-waving argument as to why $+1/2$ topological defects move spontaneously along their symmetry axis because of active forces, let me compute the flow created by an isolated $+1/2$ topological defect.

Force balance

We consider an isolated active $+1/2$ topological defect on an infinite surface. We consider this ideal situation because we are interested in the flow created by an individual defect, not necessarily pairs or assemblies of defects. We also consider that the defect interacts with the substrate through viscous drag. The friction force is given by $-\xi\mathbf{v}$ where ξ is a friction constant per unit area. When experimenting with cells, we work at low Reynolds number and inertia is negligible compared to viscous forces. At steady state, the velocity field $\mathbf{v}(r,\theta)$, pressure field $P(r,\theta)$ and orientation field $\varphi(r,\theta)$ are determined by the equations of motion eqs. (1.33) to (1.35) given in section 1.2.

To investigate the effect of the active force on the flow, we first look at the case where the rotation dynamics of the director is much faster than the dynamics of cell displacement. In terms of viscosities, this corresponds to the case where $\eta \gg \gamma$. In this approximation, on the scales of collective cell displacements, the rotational dynamics of the director is sufficiently fast as to satisfy $h_\perp = 0$ at all times. The distortion free energy is therefore minimized at all times. In this case, we keep the orientation $\varphi = \theta/2$ and the distortion free energy does not play a role in the dynamics. In this approximation, the molecular field $h_\alpha \sim \gamma$ is negligible compared to the viscous stress $\eta u_{\alpha\beta}$. In the limit $\eta \gg \gamma$, the flow-alignment coupling and the torques created by the antisymmetric stress are irrelevant, and eqs. (1.33) and (1.35) take a much simpler form:

$$\sigma^t_{\alpha\beta} = 2\eta u_{\alpha\beta} - \zeta\Delta\mu\left(p_\alpha p_\beta - \frac{\delta_{\alpha\beta}}{2}\right) - P\delta_{\alpha\beta} \tag{3.13}$$

$$h_\alpha = 0 \tag{3.14}$$

By considering the rotations of cells to be fast compared to their translations, the flow and the rotation of the director decouple. We can therefore consider that the orientation of the defect is fixed and corresponds to that of a passive defect, $\varphi = \theta/2$. If γ is finite, the flows created by the active force (3.10) modify the orientation of the defect and there

is an active component to the orientational field $\varphi = \theta/2 + \varphi^{\text{act}}(r, \theta)$ around the defect. This is situation is studied in section 3.7.

The orientation field $\varphi = \theta/2$ is only valid in the reference frame that has the defect core for origin. Therefore, force balance (1.34) must be written in the frame of the defect. The active force (3.10) creates spontaneous motion of the defect, and we define $\mathbf{v_0}$ as the self-advection velocity of the $+1/2$ defect. In the frame of the defect moving at constant velocity $\mathbf{v_0}$, the viscous drag is given by $-\xi(\mathbf{v} - \mathbf{v_0})$. Force balance then reads:

$$\eta\Delta\mathbf{v} - \nabla P - \xi(\mathbf{v} + \mathbf{v_0}) - \frac{\zeta\Delta\mu}{2r}\mathbf{e_x} = 0 \tag{3.15}$$

Force balance (3.15) is completed with the following boundary conditions, in the frame of the defect:

1. The defect core does not move in the frame centered at the defect core:

$$\mathbf{v}(0, \theta) = 0 \tag{3.16}$$

2. No velocity at infinity in the lab frame:

$$\mathbf{v}(+\infty, \theta) = -\mathbf{v_0} \tag{3.17}$$

Velocity and pressure field for an isolated defect

From the symmetries of the system, we can gather information on the solutions $\mathbf{v}(r, \theta)$ and $P(r, \theta)$. The configuration of the defect has the $x-$axis as a symmetry axis (by definition). Since the velocity and pressure fields result from the orientation gradients created by the geometry of the defect, the two fields must also have the $x-$axis as a symmetry axis. This means that the velocity of the defect $\mathbf{v_0}$ has to be on the $x-$axis: $\mathbf{v_0} = v_0\mathbf{e_x}$. For the scalar pressure field, $P(r, \theta)$ must be an even function of the polar angle θ. For the velocity vector, this means in cartesian coordinates that its $x-$component is even as a function of θ and its $y-$component is odd as a function of θ. In terms of polar coordinates, this means that the $r-$component of the velocity is even as a function of θ because the $\mathbf{e_x}$ dependence of $\mathbf{e_r} = \cos\theta\mathbf{e_x} + \sin\theta\mathbf{e_y}$ is even in θ but the $\mathbf{e_y}$ dependence is odd. The $\theta-$component of the velocity is odd as a function of θ because $\mathbf{e}_\theta = -\sin\theta\mathbf{e_x} + \cos\theta\mathbf{e_y}$ has the opposite signature with respect to θ compared to $\mathbf{e_r}$. There is obviously 2π periodicity in θ so if we look for solutions by separating the radial and azimuthal dependences, their Fourier decompositions read, given the symmetries:

$$P(r, \theta) = \sum_n P_n(r)\cos(n\theta) \tag{3.18}$$

$$v_r(r, \theta) = \sum_n v_r^n(r)\cos(n\theta) \tag{3.19}$$

$$v_\theta(r, \theta) = \sum_n v_\theta^n(r)\sin(n\theta) \tag{3.20}$$

Because we neglected the dynamics of the director field with respect to cell motion, we obtain for the force balance eq. (3.15) a linear Stokes equation with friction and an active force, which does not couple the different modes of eqs. (3.18) to (3.20). Mathematically, this is justified by the fact that (3.15) is a linear PDE with constant coefficients. Because the active force $\mathbf{f}_+^{\text{act}} = -\zeta\Delta\mu/(2r)\,(\cos\theta\mathbf{e_r} - \sin\theta\mathbf{e}_\theta)$ acts only on the first mode of the Fourier series, all other modes of the velocity and pressure fields vanish: $v_r^n, v_\theta^n, P_n = 0$ if $n > 1$. Now that we have used symmetry arguments to simplify the search for solutions, let us solve equation (3.15). We consider incompressible cells with no cell division, such that $\nabla \cdot \mathbf{v} = 0$. In two dimensions, due to the divergence-free velocity field, we can introduce the stream function $\psi(r,\theta)$ defined as $\nabla\times(\psi\mathbf{e_z}) = \mathbf{v}$, with $\mathbf{e_z} = \mathbf{e_r} \times \mathbf{e}_\theta$. Since $\mathbf{v} = v_r(r)\cos\theta\mathbf{e_r} + v_\theta(r)\sin\theta\mathbf{e}_\theta$, the stream function is of the form $\psi(r,\theta) = \psi(r)\sin\theta$. For simplicity of the notation, the superscript regarding the Fourier modes is dropped since only the first mode matters, and we use the same notation for the radial dependence of the stream function $\psi(r)$ and the stream function $\psi(r,\theta)$. We do the same for all physical quantities, as the azimuthal dependence is straightforward. When there is a potential ambiguity, we specify explicitly the arguments of the function.

By taking the curl of the force balance eq. (3.15), we obtain an equation for the stream function:

$$\Delta\left[\eta\Delta\psi - \xi\psi\right] = -\zeta\Delta\mu\frac{\sin\theta}{2r^2} \tag{3.21}$$

There is a characteristic length L given by $L = \sqrt{\eta/\xi}$, beyond which hydrodynamic interactions are screened. We introduce the dimensionless distance to the core of the defect $r' = r/L$ and define $\hat{\psi}(r',\theta) = \psi(Lr',\theta)$. Again, for simplicity of the notation, in the following we label $r = r'$ as a dimensionless length and $\hat{\psi} = \psi$. Using the dimensionless distance, we obtain:

$$\Delta\left[\Delta\psi - \psi\right] = -\alpha\frac{\sin\theta}{r^2} \tag{3.22}$$

with $\alpha = \zeta\Delta\mu/(2\xi)$. We can solve eq. (3.22) for $U = \Delta\psi - \psi$, which satisfies a Poisson equation:

$$\Delta U = -\alpha\frac{\sin\theta}{r^2} \tag{3.23}$$

The general solution to eq. (3.23) (given the azimuthal dependence) is:

$$U(r,\theta) = \Delta\psi(r,\theta) - \psi(r,\theta) = \left[Ar + \frac{B}{r} + \alpha\right]\sin\theta, \tag{3.24}$$

with A, B, integration constants. Since we are looking for $\psi(r,\theta) = \psi(r)\sin\theta$, we obtain an equation for the radial dependence of the stream function in reduced coordinates $\psi(r)$:

$$\frac{d^2\psi(r)}{dr^2} + \frac{1}{r}\frac{d\psi(r)}{dr} - \left(1 + \frac{1}{r^2}\right)\psi(r) = Ar + \frac{B}{r} + \alpha \tag{3.25}$$

The homogeneous solution ψ^0 to eq. (3.25) is given by the modified Bessel functions of the first kind I_1 and K_1:

$$\psi^0(r) = A_0 I_1(r) + B_0 K_1(r), \tag{3.26}$$

where A_0 and B_0 are integration constants. We look for a particular solution $\psi^p(r)$ of eq. (3.25) by using the method of variation of parameters. We look for a solution of the form

$$\psi^p(r) = C_I(r) I_1(r) + C_K(r) K_1(r) \tag{3.27}$$

To find a particular solution using the variation of parameters, one needs to add a condition on C_I, C_K

$$\frac{dC_I}{dr}(r) I_1(r) + \frac{dC_K}{dr}(r) K_1(r) = 0 \tag{3.28}$$

Plugging back eq. (3.27) into eq. (3.25), together with eq. (3.28), C_K and C_I follow a system of ODE:

$$\frac{dC_I}{dr}(r) I_1(r) + \frac{dC_K}{dr}(r) K_1(r) = 0 \tag{3.29}$$

$$\frac{dC_I}{dr}(r) \frac{dI_1}{dr}(r) + \frac{dC_K}{dr}(r) \frac{dK_1}{dr}(r) = Ar + \frac{B}{r} + \alpha \tag{3.30}$$

Using the Wronskian of modified Bessel functions $W(I_1, K_1) = I_1'(r)K_1(r) - I_1(r)K_1'(r) = -1/r$, we get:

$$\frac{dC_I}{dr}(r) = K_1(r) \left(Ar^2 + B + \alpha r \right) \tag{3.31}$$

$$\frac{dC_K}{dr}(r) = -I_1(r) \left(Ar^2 + B + \alpha r \right) \tag{3.32}$$

When integrating eqs. (3.31) and (3.32), we have a choice of integration constants that eventually redefines the values of the integration constants A_0, B_0. We choose constants that become convenient for boundary conditions in $r = +\infty$ and $r = 0$:

$$C_1(r) = -\int_r^{+\infty} K_1(u)(Au^2 + \alpha u + B)\, du \tag{3.33}$$

$$C_K(r) = -\int_0^{r} I_1(u)(Au^2 + \alpha u + B)\, du \tag{3.34}$$

The full solution to eq. (3.25) is

$$\begin{aligned} \psi(r) = I_1(r) \left(A_0 - \int_r^{+\infty} K_1(u)(Au^2 + \alpha u + B)\, du \right) \\ + K_1(r) \left(B_0 - \int_0^{r} I_1(u)(Au^2 + \alpha u + B)\, du \right) \end{aligned} \tag{3.35}$$

To determine the integration constants A_0, B_0, A, B, we need to take into account the boundary conditions eqs. (3.16) and (3.17) for the velocity. In terms of the dimensionless distance r,

$$v_r(r) = \sqrt{\frac{\xi}{\eta}}\frac{\psi(r)}{r} \tag{3.36}$$

$$v_\theta(r) = -\sqrt{\frac{\xi}{\eta}}\frac{d\psi(r)}{dr} \tag{3.37}$$

which gives:

$$v_r(r) = \sqrt{\frac{\xi}{\eta}} r^{-1}\left[I_1(r)\left(A_0 - \int_r^{+\infty} K_1(u)(Au^2+\alpha u+B)\,du\right) + K_1(r)\left(B_0 - \int_0^r I_1(u)(Au^2+\alpha u+B)\,du\right)\right] \tag{3.38}$$

$$v_\theta(r) = -\sqrt{\frac{\xi}{\eta}}\left[\left(I_0(r) - \frac{I_1(r)}{r}\right)\left(A_0 - \int_r^{+\infty} K_1(u)(Au^2+\alpha u+B)\,du\right) - \left(K_0(r) + \frac{K_1(r)}{r}\right)\left(B_0 - \int_0^r I_1(u)(Au^2+\alpha u+B)\,du\right)\right] \tag{3.39}$$

Boundary conditions

We now need to apply the boundary conditions eqs. (3.16) and (3.17) to the velocity field given by eqs. (3.38) and (3.39). There are possibly terms that give rise to divergences in $r = 0$ or for $r \gg 1$. Let us recall the asymptotic behavior of the modified Bessel functions of order one:

$$I_1(x) \underset{x\to 0}{\sim} \frac{x}{2} \tag{3.40}$$

$$K_1(x) \underset{x\to 0}{\sim} \frac{2}{x} \tag{3.41}$$

$$I_1(x) \underset{x\to +\infty}{\sim} \frac{e^x}{\sqrt{2\pi x}} \tag{3.42}$$

$$K_1(x) \underset{x\to +\infty}{\sim} \sqrt{\frac{\pi}{2x}}e^{-x} \tag{3.43}$$

The exponential growth of I_1 at infinity imposes $A_0 = 0$, in order to to have a finite self-advection velocity v_0. The hyperbolic divergence of K_1 in zero imposes $B_0 = 0$. A

finite value for B leads to a logarithmic divergence at the origin, therefore $B = 0$. We are left with the following velocity field:

$$v_r(r) = -\sqrt{\frac{\xi}{\eta}} r^{-1} \left[I_1(r) \int_r^{+\infty} K_1(u)(Au^2 + \alpha u)\, du + K_1(r) \int_0^r I_1(u)(Au^2 + \alpha u)\, du \right] \tag{3.44}$$

$$v_\theta(r) = \sqrt{\frac{\xi}{\eta}} \left[\left(I_0(r) - \frac{I_1(r)}{r} \right) \int_r^{+\infty} K_1(u)(Au^2 + \alpha u)\, du - \left(K_0(r) + \frac{K_1(r)}{r} \right) \int_0^r I_1(u)(Au^2 + \alpha u)\, du \right] \tag{3.45}$$

Given eqs. (3.44) and (3.45) and eqs. (3.42) and (3.43), the velocity in the far field is given by

$$\lim_{r \to +\infty} v_r(r) = -\sqrt{\frac{\xi}{\eta}} A \tag{3.46}$$

$$\lim_{r \to +\infty} v_\theta(r) = \sqrt{\frac{\xi}{\eta}} A \tag{3.47}$$

The boundary condition eq. (3.17) of vanishing velocity in the lab frame at infinity imposes:

$$A = \sqrt{\frac{\eta}{\xi}} v_0 \tag{3.48}$$

In the frame of the defect, the velocity needs to be zero at the core of the defect. This implies $v_r(0) = v_\theta(0) = 0$. The integrals in eqs. (3.44) and (3.45) are well defined in 0 and

$$\int_0^{+\infty} K_1(u) u^2\, du = 2 \tag{3.49}$$

$$\int_0^{+\infty} K_1(u) u\, du = \frac{\pi}{2} \tag{3.50}$$

Since $r^{-1} I_1(r) \underset{r \to 0}{\longrightarrow} 1/2$ and $I_0(r) \underset{r \to 0}{\longrightarrow} 1$,

$$\lim_{r \to 0} v_r(r) = -\sqrt{\frac{\xi}{\eta}} \frac{1}{2} \left(2A + \alpha \frac{\pi}{2} \right) \tag{3.51}$$

$$\lim_{r \to 0} v_\theta(r) = \sqrt{\frac{\xi}{\eta}} \frac{1}{2} \left(2A + \alpha \frac{\pi}{2} \right), \tag{3.52}$$

which imposes $A = -\alpha\pi/4$. Therefore, we get the velocity of the defect $v_0 = A\sqrt{\xi/\eta}$, recalling that $\alpha = \zeta\Delta\mu/(2\xi)$:

$$\mathbf{v_0} = -\frac{\pi}{8}\frac{\zeta\Delta\mu}{\sqrt{\xi\eta}}\mathbf{e_x} \tag{3.53}$$

As one expects from a linear hydrodynamic theory, the velocity is proportional to the activity $\zeta\Delta\mu$. For a contractile nematics, $\zeta < 0$, a defect move towards its tail. For extensile nematics, $\zeta > 0$, a defect move towards its head. The velocity decreases as the viscosity or the friction coefficients increase. The scaling for the velocity of the defect can be known only from dimensional analysis: by neglecting the dynamics of the director, there is only one time scale $\tau = \eta/\zeta\Delta\mu$ and one length scale $L = \sqrt{\eta/\xi}$. Therefore, the velocity of the defect has to be proportional to $\zeta\Delta\mu/\sqrt{\xi\eta}$. The velocity field in physical units created by a $+1/2$ topological defect when neglecting the dynamics of orientation of the director is:

$$\begin{aligned} v_r(r) = -\frac{\zeta\Delta\mu}{\sqrt{\xi\eta}}\frac{L}{r}\Bigg[& I_1(\frac{r}{L})\int_{\frac{r}{L}}^{+\infty} K_1(u)(-\frac{\pi}{8}u^2+\frac{1}{2}u)\,du \\ & + K_1(\frac{r}{L})\int_0^{\frac{r}{L}} I_1(u)(-\frac{\pi}{8}u^2+\frac{1}{2}u)\,du\Bigg] \end{aligned} \tag{3.54}$$

$$\begin{aligned} v_\theta(r) = \frac{\zeta\Delta\mu}{\sqrt{\xi\eta}}\Bigg[& \left(I_0(\frac{r}{L}) - \frac{LI_1(\frac{L}{r})}{r}\right)\int_{\frac{r}{L}}^{+\infty} K_1(u)(-\frac{\pi}{8}u^2+\frac{1}{2}u)\,du \\ & - \left(K_0(\frac{r}{L}) + \frac{LK_1(\frac{L}{r})}{r}\right)\int_0^{\frac{r}{L}} I_1(u)(-\frac{\pi}{8}u^2+\frac{1}{2}u)\,du\Bigg] \end{aligned} \tag{3.55}$$

The velocity field is represented in fig. 3.11.

A feature of the flow of eqs. (3.54) and (3.55) is the existence of two vortices of opposite signs. The vorticity scalar field $\omega(r,\theta)$ defined by $\omega\mathbf{e_z} = \nabla\times\mathbf{v}$ is represented in fig. 3.12. In the far field $r \gg L$, we find that the radial velocity in the lab frame scales as $\zeta\Delta\mu/(\xi r)$ and the vorticity scales as $\zeta\Delta\mu/(\xi r^2)$, as seen in fig. 3.13. This relatively "slow" decay of the velocity, even in the presence of friction through viscous drag, can be attributed to the divergence of the total active force with system size. The $1/r$ dependence of the velocity in the far field makes the total friction force diverge with system size, and the total force vanishes. This scenario of an isolated defect with a macroscopic size does not exist in practice and these divergences with respect to the system size disappear when considering a dipole flow created by a pair of half integer defects of opposite strengths [40].

Compared to previous results, Pismen in ref. [40] considers a lubrification approximation that cancels hydrodynamic interactions and studies the dynamics of the director in the far field, i.e does not consider $\gamma = 0$. Giomi *et al* in ref. [39] consider a case

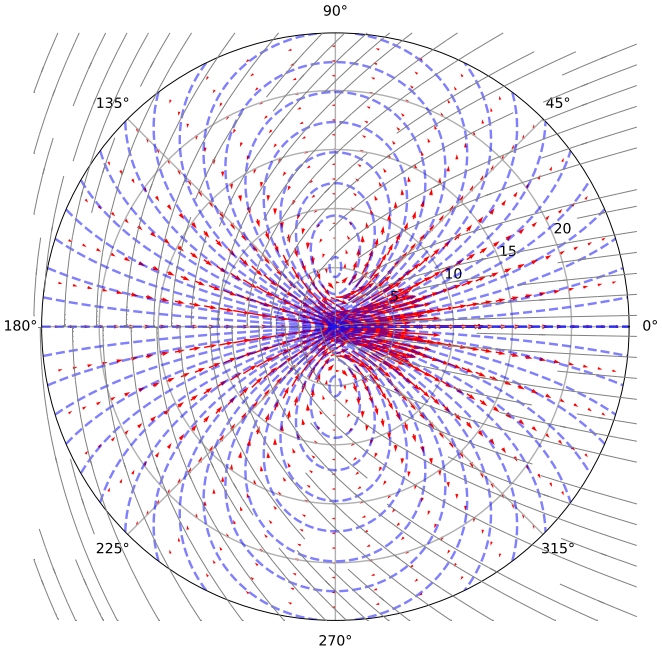

Figure 3.11: Velocity field in the lab frame around a contractile ($\zeta < 0$) $+1/2$ topological defect. The distance is in units of the length $L = \sqrt{\eta/\xi}$ and the flow is plotted up to $r/L = 25$, where the flow has already decays significantly compared to the core value. The blue dashed line are the stream line of the flow and the red arrows are the velocity vectors. The velocity decays with increasing distance to the core. There are vortices of opposite direction that are characteristic of the active flow around a $+1/2$ defect. The extensile flow profile $\zeta > 0$ can be obtained reversing the direction of the velocity vector field.

without interactions with the substrate ($\xi = 0$) and without orientation dynamic ($\gamma = 0$). The obtained results depend therefore on the system size, which is typically set by the distance between defects. In our calculation, by considering an interaction with the substrate that screens hydrodynamic interactions over a typical length scale $L = \sqrt{\eta/\xi}$, and by neglecting the dynamics of the director, we obtain an analytical solution that can be in principle compared to experiments.

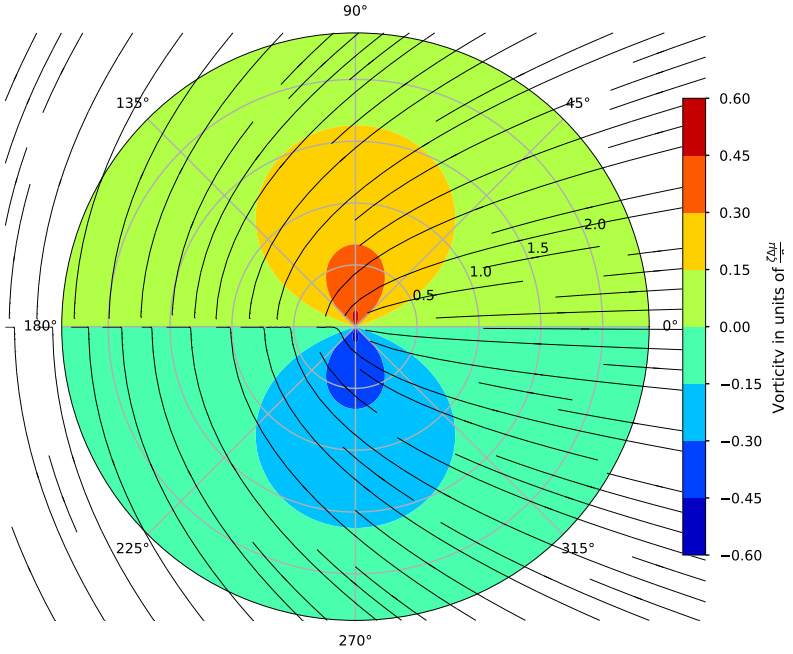

Figure 3.12: Vorticity map in units of $\zeta\Delta\mu/\eta$ around a contractile $\zeta > 0$ $+1/2$ topological defect. The dark solid line represent the orientation of the director around the defect. The distance is in units of the length $L = \sqrt{\eta/\xi}$ and the vorticity is plotted up to $r/L = 2.5$ where the vorticity has decayed significantly. The antisymmetry of the vorticity with respect to the $x-$axis is signature of this flow. For an extensile defect $\zeta > 0$, the vorticity map is given by reversing the sign of the vorticity.

Pressure field

Once the velocity field has been determined by eqs. (3.54) and (3.55), the pressure field $P(r, \theta)$ is given by force-balance eq. (3.15):

$$P(r, \theta) = -\frac{\zeta\Delta\mu}{2}\cos\theta \tag{3.56}$$

The pressure given by (3.56) is defined up to a constant determined by some external pressure. The active stress creates a gradient of pressure between the head and the tail of a defect. For contractile nematics ($\zeta < 0$), as represented on fig. 3.14, there is a lower pressure at the head than at the tail of a defect. For extensile nematics ($\zeta > 0$) it is the opposite.

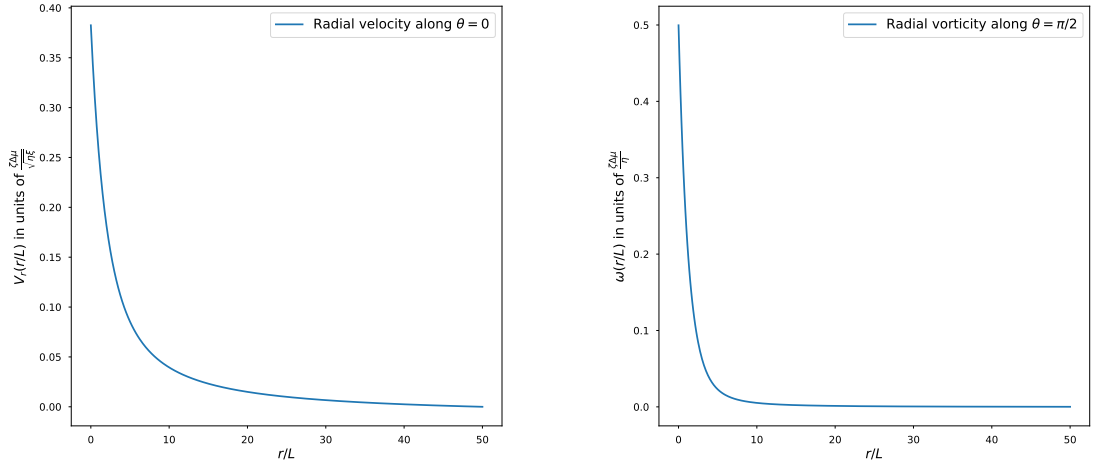

Figure 3.13: Radial parts of the velocity (left) in units of $\zeta\Delta\mu/\sqrt{\xi\eta}$ and of the vorticity (right) in units of $\zeta\Delta\mu/\eta$ as a function of the dimensionless length. Both functions decay over distances controlled by the behavior of modified Bessel functions.

3.4 Pinning of active defects

In this section, in the light of the experimental observations of motionless defects presented in section 3.2, we estimate the magnitude of a local force acting on the core necessary to stop the motion of a $+1/2$ defect. In this section, as presented in section 3.1.2, we consider the core of the defect to be a disk of finite radius ε. Inside the core, for $r < \varepsilon$, there is no nematic order ($\mathbf{p}^2 = 0$), and there is perfect nematic order for $r > \varepsilon$ ($\mathbf{p}^2 = 1$). This simplification approximation is justified because we do not focus on the dynamics inside the core.

We define $\mathbf{f}$ as the total force applied by the substrate on the core of the defect. Because the aim is not to describe what happens inside the core of the defect, the expression of the force density inside the core of the defect is of no importance. The only constraint we impose is that the total force be $\mathbf{f}$. We therefore consider that the substrate applies a force density $f/(2\pi\varepsilon r)\mathbf{e_x}$, where $f = |\mathbf{f}|$ is the constant total force. The force is applied only in the direction of the self-advection velocity $\mathbf{e_x}$. Force balance becomes:

$$\eta\Delta\mathbf{v} - \nabla P - \xi(\mathbf{v} + \mathbf{v_0}) - \frac{\zeta\Delta\mu}{2r}\mathbf{e_x} = 0, \qquad r > \varepsilon \tag{3.57}$$

$$\eta\Delta\mathbf{v} - \nabla P - \xi(\mathbf{v} + \mathbf{v_0}) - \frac{f}{2\pi\varepsilon r}\mathbf{e_x} = 0, \qquad r < \varepsilon \tag{3.58}$$

The velocity and pressure fields that satisfy the force balance eqs. (3.57) and (3.58) must also ensure the continuity of the stress and velocity at the core interface.

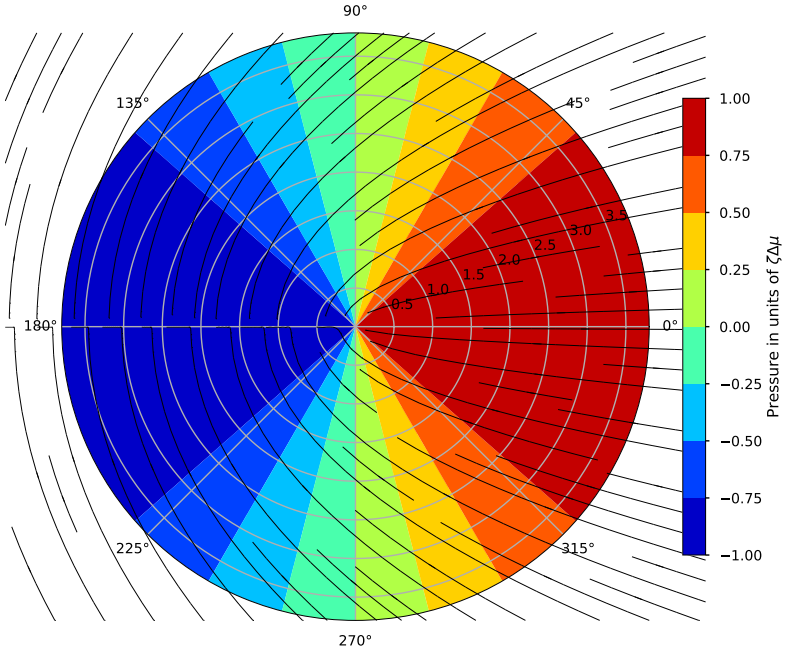

Figure 3.14: Pressure field in units of $\zeta\Delta\mu$ around a $+1/2$ defect in a contractile nematic.

Fields inside the core

The advantage of considering this form for the force density inside the core is that, formally, it is similar to the active force. Therefore, the results of the previous section can be used to determine the fields inside the core. Inside the core, all quantities have the superscript c. There is the same characteristic length L inside and outside of the core: $L = \sqrt{\eta/\xi}$. We can introduce the same dimensionless variable $r' = r/L$ for $r < \varepsilon$ and $r > \varepsilon$. Proceeding exactly as in section 3.3, we keep track of quantities inside the core with the superscript c. The stream function inside the core satisfies the following equation:

$$\frac{d^2\psi^c(r)}{dr^2} + \frac{1}{r}\frac{d\psi^c(r)}{dr} - \left(1 + \frac{1}{r^2}\right)\psi^c(r) = A^c r + \frac{B^c}{r} + \beta, \tag{3.59}$$

where $\beta = \frac{f}{2\pi\varepsilon\xi}$ is the analog, for the force imposed at the core of the defect, of $\alpha = \zeta\Delta\mu/(2\xi)$ in eq. (3.25). For simplicity, we took the liberty to keep the same names for the integration constants throughout this chapter. Following the calculations of sec-

tion 3.3, the velocity field inside the core is given by:

$$v_r^c(r) = \sqrt{\frac{\xi}{\eta}} r^{-1} \left[I_1(r) \left(A_0^c - \int_r^{+\infty} K_1(u)(A^c u^2 + \beta u + B^c)\, du \right) + K_1(r) \left(B_0^c - \int_0^r I_1(u)(A^c u^2 + \beta u + B^c)\, du \right) \right] \tag{3.60}$$

$$v_\theta^c(r) = -\sqrt{\frac{\xi}{\eta}} \left[\left(I_0(r) - \frac{I_1(r)}{r} \right) \left(A_0^c - \int_r^{+\infty} K_1(u)(A^c u^2 + \beta u + B^c)\, du \right) - \left(K_0(r) + \frac{K_1(r)}{r} \right) \left(B_0^c - \int_0^r I_1(u)(A^c u^2 + \beta u + B^c)\, du \right) \right] \tag{3.61}$$

The boundary conditions are imposed by eqs. (3.16) and (3.17). Therefore $v_r^c(r = 0) = v_\theta^c(r = 0) = 0$. This imposes that $B_0^c = B^c = 0$. Since this solution is valid for $r < \varepsilon/L$, we cannot discard A_0^c because of divergences far from the core, and A^c remains unknown. A_0^c, A^c are determined by imposing the continuity of the velocity and stress fields. The velocity field now reads:

$$v_r^c(r) = \sqrt{\frac{\xi}{\eta}} r^{-1} \left[I_1(r) \left(A_0^c - \int_r^{+\infty} K_1(u)(A^c u^2 + \beta u)\, du \right) - K_1(r) \int_0^r I_1(u)(A^c u^2 + \beta u)\, du \right] \tag{3.62}$$

$$v_\theta^c(r) = -\sqrt{\frac{\xi}{\eta}} \left[\left(I_0(r) - \frac{I_1(r)}{r} \right) \left(A_0^c - \int_{r'}^{+\infty} K_1(u)(A^c u^2 + \beta u)\, du \right) + \left(K_0(r) + \frac{K_1(r)}{r} \right) \int_0^r I_1(u)(A^c u^2 + \beta u)\, du \right] \tag{3.63}$$

To write the continuity of the stress at the interface of the core of the defect, one needs to compute the pressure field. Since $\nabla \cdot \mathbf{v} = 0$, we get an equation for the pressure field inside the core P^c by taking the divergence of eq. (3.58):

$$\Delta P^c(r, \theta) = \frac{f}{2\pi\varepsilon r^2} \cos\theta \tag{3.64}$$

Similarly to what has been done outside the core, we perform a mode expansion of the pressure field inside the core and only the first mode remains. We can give directly the pressure using the dimensionless variable r to be consistent, even though there is no intrinsic scale for the pressure field.

$$P^c(r, \theta) = \left[A_*^c r + \frac{B_*^c}{r} - \frac{f}{2\pi\varepsilon} \right] \cos\theta \tag{3.65}$$

By taking the curl and divergence of eq. (3.58), to determine respectively the velocity and pressure fields, we have introduced too many integration constants that must be linked by the force-balance eq. (3.58). After going back into physical units for the velocity, plugging back the velocity and pressure fields into the force-balance eq. (3.58) gives:

$$B_*^c = -\xi B^c \tag{3.66}$$

$$A_*^c = \xi(A^c - \sqrt{\frac{\eta}{\xi}} v_0) \tag{3.67}$$

Since $B^c = 0$ to avoid divergences of velocity at the center of the core this imposes $B_*^c = 0$. Vanishing velocity in $r = 0$ imposes $A_0^c = 0$

Fields outside the core

Outside the core, we have already calculated the full velocity field given by eqs. (3.38) and (3.39). The integration constants A_0, A, B, B_0 of eqs. (3.38) and (3.39) are modified because of the finite-size core. Vanishing velocity far from the core $r \gg L$ in the lab frame still imposes $A_0 = 0$ because of exponential divergences, and $A = \sqrt{\eta/\xi} v_0$ because of the finite velocity $-v_0 \mathbf{e_x}$ in the far field and eqs. (3.46) and (3.47). However, since this expression of the velocity is only valid outside the core, one can no longer take $B, B_0 = 0$.

Similarly to what is done inside the core, the pressure field outside the core $P(r, \theta)$ is given by

$$P(r, \theta) = \left[A_* r + \frac{B_*}{r} - \frac{\zeta \Delta\mu}{2} \right] \cos\theta \tag{3.68}$$

and the integration constants A_*, B_* are related to the constants of the velocity A, B by the force-balance eq. (3.57):

$$B_* = -\xi B \tag{3.69}$$

$$A_* = \xi(A - \sqrt{\frac{\eta}{\xi}} v_0) \tag{3.70}$$

Since $A = \sqrt{\eta/\xi} v_0$, eq. (3.70) gives $A_* = 0$.

Matching of the solutions

We are left with four independent constants B, B_0, A^c, v_0, which all depend on the hydrodynamic parameters and on the force f. There are four relations to be satisfied. There are two equations for the continuity of the velocity:

$$v_r(\varepsilon) = v_r^c(\varepsilon) \tag{3.71}$$

$$v_\theta(\varepsilon) = v_\theta^c(\varepsilon) \tag{3.72}$$

There is continuity of the normal and tangential force densities at the interface of the core. The normal force is given by $\sigma^t_{rr} = 2\eta\partial_r v_r - P$ and the tangential force is given by the stress $\sigma^t_{r\theta} = \eta\left((\partial_\theta v_r - v_\theta)/r + \partial_r v_\theta\right)$. The conditions for stress continuity are:

$$(2\eta\partial_r v_r - P)_{|\varepsilon} = (2\eta\partial_r v_r^c - P^c)_{|\varepsilon} \tag{3.73}$$

$$\eta\left(\frac{1}{r}(\partial_\theta v_r - v_\theta) + \partial_r v_\theta\right)_{|\varepsilon} = \eta\left(\frac{1}{r}(\partial_\theta v_r^c - v_\theta^c) + \partial_r v_\theta^c\right)_{|\varepsilon} \tag{3.74}$$

These four conditions form a linear system for the four unknows B, B_0, A^c, v_0. Solving this system, we determine the value of the stall force f, such that $v_0 = 0$.

$$f = \sqrt{\frac{\eta}{\xi}}\frac{\pi^2\zeta\Delta\mu}{1 - \log(\varepsilon\sqrt{\frac{\xi}{\eta}})} \tag{3.75}$$

On a side note, mathematically we have computed the partial (**f** is applied only in the $x-$direction) two-dimensional Green function (for $f = 1$) for a Stokes flow with viscous drag in real space with, in the lab frame, a finite velocity in the $x-$direction at the origin and no velocity in the far field.

At short distance $r \ll \sqrt{\eta/\xi}$, the viscous drag is negligible w.r.t to the shear forces. This explains the logarithmic dependence in the core size for the force to pin a defect, which comes from the Stokeslet flow (the flow of localized force represented by a Dirac function). In two dimensions, the Stokeslet has a logarithmic dependence on the distance to the origin [113]. Since a point force creates a flow that diverges logarithmically, we obtain the expression for the stall force given by eq. (3.75). The expression in eq. (3.75) is to be compared to the stall force needed when taking into account orientation dynamics, given by eq. (3.102) as we shall see later. The velocity field obtained with the presence of a stall or pinning force **f** is represented in fig. 3.15. The radial component of the velocity $v_r(r)$ is plotted in fig. 3.16.

3.5 Effect of orientation dynamics

3.5.1 Motivation, changes

In the previous section, we have neglected the orientational dynamics of the director. However, the displacement of a $+1/2$ topological defect due to the active force generates rotations of the director together with the displacement of the defect. When the core of the defect moves, because the velocity field decreases as the distance to the core increases, the motion of the defect is not a translation of the defect conformation, it is accompanied by a rotation of the directors around the defect, to account for the motion. Taking into account the rotational viscosity γ can affect the velocity of the defect computed in the previous section. Moreover, because the effect of the rotation is strongest

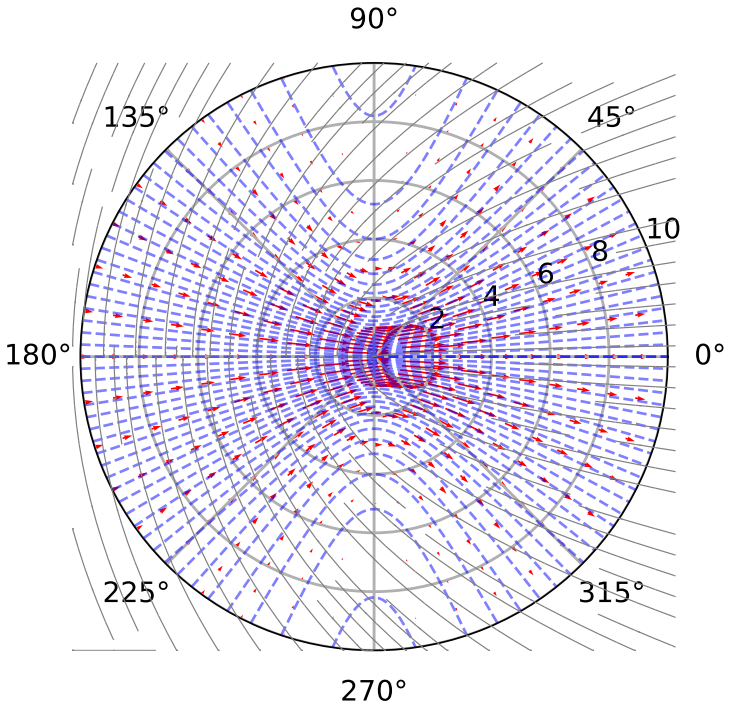

Figure 3.15: Velocity field around a contractile ($\zeta < 0$) $+1/2$ topological defect, with the pinning force $\mathbf{f}$ applied. The distance is in units of the length $L = \sqrt{\eta/\xi}$ and the flow is plotted up to $r/L = 25$. The blue dashed lines are the stream lines of the flow and the red arrows are the velocity vectors. The core is of size is set numerically to $\varepsilon = 10^{-3}L$. The radial velocity decays towards zero very fast in the vicinity of the core as seen in fig. 3.16 and, at this scale, it may seem that there is flow at the core, but the core does not move.

at the core, it can influence greatly the scaling of the force needed to pin a defect with respect to the size of the core given in eq. (3.75). The dynamics of the director acts on the total stress via three contributions:

1. The coupling between flow and orientation represented by the parameter ν
2. The Ericksen stress that is the equilibrium stress presented in section 1.2 and given in appendix A in the case of defects.
3. The torque caused by the distortion free energy, given by the antisymmetric part of the total stress.

To investigate the effect of the orientation dynamics on the velocity of the defect and on the pinning of the defect, we start by looking at the effect of the torque given by the

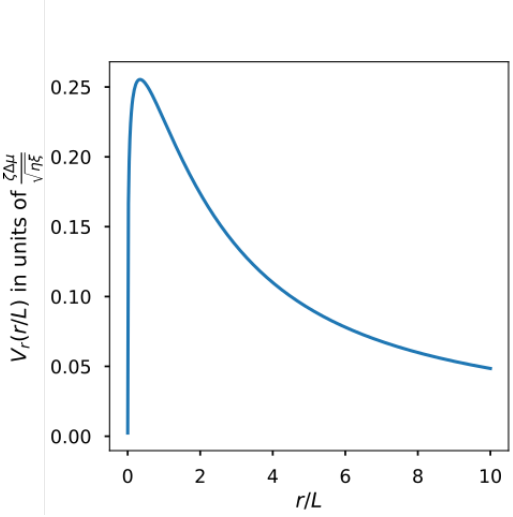

Figure 3.16: Radial velocity $v_r(r)$ with the presence of the pinning force $\mathbf{f}$, in units of $\zeta\Delta\mu/\sqrt{\xi\eta}$. There is a sharp decrease of the velocity in the vicinity of the core.

anti-symmetric part of the stress $\sigma^A_{\alpha\beta} = \left(h_\alpha p_\beta - h_\beta p_\alpha\right)/2$. In tensorial notations, the anti-symmetric part of the stress reads:

$$\sigma^A = \frac{1}{2}\begin{pmatrix} 0 & -h_\perp \\ h_\perp & 0 \end{pmatrix} \tag{3.76}$$

This expression is independent of the system of coordinates, although the expression of $h_\perp$ depends on it. The force density created by the anti-symmetric part of the stress is given by $\nabla \cdot \sigma^A = \nabla \times (h_\perp \mathbf{e_z})/2$. By definition $h_\perp$ is given by the variation of the free energy with respect to the angle of the director $h_\perp = -\delta F/\delta\varphi = K\nabla^2\varphi$. For passive systems at equilibrium, the defect configuration verifies by definition $h_\perp = 0$. However, in the active case, the steady-state configuration no longer minimizes the free energy and $h_\perp \neq 0$. In the active case, the molecular field is given by solving the dynamical constitutive equation for the director, coupled to the velocity field:

$$\partial_t p_\alpha + v_\beta \partial_\beta p_\alpha + \omega_{\alpha\beta} p_\beta = \frac{1}{\gamma} h_\alpha - \nu u_{\alpha\beta} p_\beta \tag{3.77}$$

We are interested in the steady state and put all time derivatives to zero. As a first approximation, we only consider the effects of the torques and consider that $\nu = 0$. By projecting eq. (3.77) onto q_α, the perpendicular vector to p_α, and introducing $\omega = (\nabla \times \mathbf{v}) \cdot \mathbf{e_z}$, we obtain $h_\perp$:

$$h_\perp = \frac{\gamma}{2}[\frac{v_\theta}{r} - \omega] \tag{3.78}$$

In terms of the stream function $\psi = (\nabla \times \mathbf{v}) \cdot \mathbf{e_z}$,

$$h_\perp = \frac{\gamma}{2}[\Delta\psi - \frac{\partial_r \psi}{r}] \tag{3.79}$$

3.5.2 Perturbative flow with passive defect orientation

Even when not considering the coupling between the flow and the orientation with $\nu = 0$, the flow induced by the active stress generates torques because of a non-zero $h_\perp$ given by eq. (3.78). The orientation of the director φ must satisfy:

$$K\nabla^2\varphi = \frac{\gamma}{2}[\Delta\psi - \frac{\partial_r \psi}{r}] \tag{3.80}$$

For a passive defect, there is no flow in the absence of external forcing, the flow is the result of the active stress that creates an active force density when there are gradients of orientation. Therefore, when writing a formal expansion in activity for the velocity, there is no zeroth order term, $\mathbf{v} = \zeta\Delta\mu\mathbf{v}^1 + \dots$. Let us write an expansion in the activity $\zeta\Delta\mu$ for the angle of the director $\varphi = \varphi^0 + \zeta\Delta\mu\varphi^1 + \dots$, or in terms of the director $\mathbf{p} = \mathbf{p}^0 + \zeta\Delta\mu\mathbf{p}^1$ or the active stress $\sigma^{\text{act}}_{\alpha\beta} = \zeta\Delta\mu p^0_\alpha p^0_\beta + (\zeta\Delta\mu)^2 p^1_\alpha p^1_\beta$. Considering this expansion in activity, to calculate the first-order term in velocity, one can consider that the orientation is the passive orientation. From the first-order velocity one can then calculate the first-order perturbation in activity to the orientation φ^1, which in turn gives the second-order velocity field $\mathbf{v}^2$.

Let us compute the first-order velocity $\mathbf{v}^1$ and drop the superscript for simplicity. At this point, we only consider the effect of the torques and not of the Ericksen stress that we set to zero. Force balance, when taking into account the torques due to the distortion free energy, reads:

$$\eta\Delta\mathbf{v} + \frac{1}{2}\nabla \times (h_\perp \mathbf{e_z}) - \nabla P - \xi(\mathbf{v} + \mathbf{v_0}) - \frac{\zeta\Delta\mu}{2r}\mathbf{e_x} = 0 \tag{3.81}$$

It is convenient to use the stream function to find the velocity field and to take the curl of eq. (3.81):

$$\Delta\left[(\eta + \frac{\gamma}{4})\Delta\psi - \frac{\gamma}{4r}\partial_r\psi - \xi\psi\right] = -\zeta\Delta\mu\frac{\sin\theta}{2r^2} \tag{3.82}$$

There is an effective viscosity $\bar{\eta} = \eta + \gamma/4$ that defines a characteristic length $\bar{L} = \sqrt{\bar{\eta}/\xi}$. There is a numerical coefficient made of the ratio between rotational and effective viscosities $\lambda = \gamma/(4\eta + \gamma)$. By considering the dimensionless unit length $r' = r/\bar{L}$ and renaming it r, eq. (3.82) reads:

$$\Delta\left[\Delta\psi - \frac{\lambda}{r}\partial_r\psi - \psi\right] = -\alpha\frac{\sin\theta}{r^2}, \tag{3.83}$$

where we recall that $\alpha = \zeta\Delta\mu/(2\xi)$. Equation (3.83) can be integrated two times and

$$\Delta\psi - \frac{\lambda}{r}\partial_r\psi - \psi = \left[A\, r + \frac{B}{r} + \alpha\right]\sin\theta \tag{3.84}$$

We have retained the same notation for the integration constants A, B to emphasize the similarity with the case where $\gamma = 0$ of section 3.3. Similarly to the case where there is no orientation dynamics $\gamma = 0$, by symmetry and due to the expression of the active force, $\psi(r,\theta) = \psi(r)\sin\theta$. Expanding eq. (3.84) one gets the evolution of the radial stream function $\psi(r)$:

$$\partial_r^2\psi + \frac{(1-\lambda)}{r}\partial_r\psi - (1 + \frac{1}{r^2})\psi = A\, r + \frac{B}{r} + \alpha \tag{3.85}$$

Equation (3.85) is similar to eq. (3.25) at $\gamma = 0$, and the difference is in the coefficient λ. Equation (3.85) is a transformed version of the modified Bessel equation given by Bowman [114], and the functions solving the homogeneous equation are $r^{\lambda/2}I_\nu(r)$ and $r^{\lambda/2}K_\nu(r)$, where $\nu = \sqrt{1+\lambda^2/4}$.

3.5.3 Flows

We proceed exactly as in section 3.3, where orientation dynamics was neglected ($\gamma, \lambda = 0$), and find the general solution for the stream function satisfying eq. (3.85):

$$\begin{aligned}\psi(r,\theta) = r^{\lambda/2}\Bigg[I_\nu(r)\left(A_0 - \int_r^{+\infty} r'^{-\lambda/2}K_\nu(r')(Ar'^2 + \alpha r' + B)\, dr'\right) \\ + K_\nu(r)\left(B_0 - \int_0^{r} r'^{-\lambda/2}I_\nu(r')(Ar'^2 + \alpha r' + B)\, dr'\right)\Bigg]\sin\theta,\end{aligned} \tag{3.86}$$

where A_0, A, B_0, B are integration constants. This gives the velocity field $\mathbf{v} = \sqrt{\xi/\bar{\eta}}\nabla\times(\psi\mathbf{e_z})$:

$$\begin{aligned}v_r = \sqrt{\frac{\xi}{\bar{\eta}}}\, r^{\lambda/2-1}\Bigg\{I_\nu(r)\left(A_0 - \int_r^{+\infty} r'^{-\lambda/2}K_\nu(r')(Ar'^2 + \alpha r' + B)\, dr'\right) \\ + K_\nu(r)\left(B_0 - \int_0^{r} r'^{-\lambda/2}I_\nu(r')(Ar'^2 + \alpha r' + B)\, dr'\right)\Bigg\}\cos\theta\end{aligned} \tag{3.87}$$

$$\begin{aligned}v_\theta = \sqrt{\frac{\xi}{\bar{\eta}}}\, r^{\lambda/2}\Bigg\{\left(\frac{\nu - \frac{\lambda}{2}}{r}I_\nu(r) - I_{\nu-1}(r)\right)\left(A_0 - \int_r^{+\infty} r'^{-\lambda/2}K_\nu(r')(Ar'^2 + \alpha r' + B)\, dr'\right) \\ + \left(\frac{\nu - \frac{\lambda}{2}}{r}K_\nu(r) + K_{\nu-1}(r)\right)\left(B_0 - \int_0^{r} r'^{-\lambda/2}I_\nu(r')(Ar'^2 + \alpha r' + B)\, dr'\right)\Bigg\}\sin\theta\end{aligned} \tag{3.88}$$

We are interested mostly in the effect of a finite rotational viscosity on the velocity of the defect. As in the previous section, the velocity of the defect is given by setting the boundary-condition eqs. (3.16) and (3.17) of finite velocity in the far field and vanishing velocity at the origin, in the frame of the defect. Far from the core $r \gg 1$ (in dimensionless units), the A_0 term diverges exponentially and therefore $A_0 = 0$. Because of the exponential behavior of the modified Bessel functions in the far field, the behavior of the velocity far from the core is unchanged by the presence of the coefficient λ. Therefore eqs. (3.46) and (3.47) giving the limit of the velocity field at large distance is still valid and

$$A = \sqrt{\frac{\bar{\eta}}{\xi}} v_0 \tag{3.89}$$

Close to the core $r \ll 1$, the velocity is asymptotically given by:

$$v_r(r) \underset{r\ll 1}{\approx} \sqrt{\frac{\xi}{\bar{\eta}}} \left(-\frac{B}{\lambda} + 2^{\nu-1}\Gamma(\nu) B_0 r^{\lambda/2-(\nu+1)} - \frac{2^{-\nu}}{\Gamma(\nu+1)} (C_1^\lambda \alpha + C_2^\lambda A) r^{\lambda/2+\nu-1} \right) \tag{3.90}$$

$$v_\theta(r) \underset{r\ll 1}{\approx} \sqrt{\frac{\xi}{\bar{\eta}}} \left(\frac{B}{\lambda} + 2^{\nu-1}\Gamma(\nu)(\nu - \frac{\lambda}{2}) B_0 r^{\lambda/2-(\nu+1)} + \frac{2^{-\nu}(\frac{\lambda}{2}+\nu)}{\Gamma(\nu+1)} (C_1^\lambda \alpha + C_2^\lambda A) r^{\lambda/2+\nu-1} \right) \tag{3.91}$$

with

$$C_1^\lambda = \int_0^\infty dr\, r^{1-\lambda/2} K_\nu(r) \tag{3.92}$$

$$C_2^\lambda = \int_0^\infty dr\, r^{2-\lambda/2} K_\nu(r) \tag{3.93}$$

Contrary to the behavior far from the core, the behavior close to the core is changed by orientation dynamics. In order to satisfy the condition of vanishing velocity at the core eq. (3.16), one has to take $B_0 = 0$ to avoid divergences. One must also take $B = 0$ to avoid a finite velocity at the core. However, now the term α that depends on the active stress, and the term A that depends on the velocity of the defect both behave as vanishing power laws close to the core $\sim r^{\lambda/2+\nu-1}$. Therefore, the velocity of the defect cannot be determined by eq. (3.16) alone. On top of ensuring vanishing velocity in $r = 0$, one has to verify that the antisymmetric stress does not diverge at the core of the defect. In other words, we need to ensure that the flow induced by the active stress does not make the total transverse stress $\sigma^t_{r\theta}$ diverge in $r = 0$. The transverse stress is given by an active

contribution $\sigma^{\text{act}}_{r\theta} = \zeta\Delta\mu\sin\theta$, a viscous contribution

$$\sigma^{v}_{r\theta}(r,\theta) = \sqrt{\frac{\xi}{\bar{\eta}}}\eta\left[\partial_r v_\theta + \frac{1}{r}\left(\partial_\theta v_r - v_\theta\right)\right] \tag{3.94}$$

$$= \frac{\xi}{\bar{\eta}}\eta\left[-\partial_r^2\psi(r) + \frac{1}{r}\partial_r\psi(r) - \frac{\psi(r)}{r^2}\right]\sin\theta \tag{3.95}$$

$$= \frac{\xi}{\bar{\eta}}\eta\left[-(1+\frac{2}{r^2})\psi(r) + \frac{2-\lambda}{r}\partial_r\psi(r) - (Ar+\alpha)\right]\sin\theta \tag{3.96}$$

and an antisymmetric contribution $\sigma^{A}_{r\theta} = -h_\perp$. Using eq. (3.84) verified by ψ and the expression of $h_\perp$ as a function of the stream function given by eq. (3.79),

$$\sigma^{A}_{r\theta} = -\frac{\xi}{\bar{\eta}}\frac{\gamma}{4}\left[\frac{\lambda-1}{r}\partial_r\psi(r) + \psi(r) + A\,r + \alpha\right]\sin\theta \tag{3.97}$$

Expressing the total tangential stress in terms of velocity for which we calculated the asymptotic expression, one gets

$$\sigma^{t}_{r\theta} = \sqrt{\xi\bar{\eta}}\left(2\frac{\lambda-1}{r}(v_\theta(r)+v_r(r)) - r v_r(r) - \sqrt{\frac{\xi}{\bar{\eta}}}A\,r\right)\sin\theta \tag{3.98}$$

From eqs. (3.90) and (3.91), since $0 < \lambda = \gamma/(\gamma+4\eta) < 1$ and $1 < \nu = \sqrt{1+\lambda^2/4} < \sqrt{5}/2$, the exponent $\lambda/2 + \nu - 2 < 0$. Contrary to the case $\lambda = 0$, there is a divergence of the tangential stress at the core of the defect, except when $A = -\alpha C_1^\lambda/C_2^\lambda$. This sets the defect self-advection velocity:

$$\mathbf{v_0} = -\frac{\zeta\Delta\mu}{\sqrt{\xi\bar{\eta}}}\frac{C_1^\lambda}{2C_2^\lambda}\mathbf{e_x} \tag{3.99}$$

with C_1^λ, C_2^λ given respectively by eqs. (3.92) and (3.93). The expression for the velocity when there is orientational dynamics is very similar to the case when it is neglected. The main difference is that there is an effective viscosity $\bar{\eta} = \eta + \gamma/4$ and a numerical coefficient C_1^λ/C_2^λ that depends on the ratio of the two viscosities η/γ. The ratio between the velocity when γ is finite given by eq. (3.99) and the velocity at $\gamma = 0$ given by eq. (3.53), is plotted on fig. 3.17. The way to determine the velocity of the defect in the case where there is orientational dynamics is different from the case there is none, and this difference is informative. In the case where there is no orientation dynamics, the velocity of the defect is such that, in the lab frame, the viscous dissipation balances the active stress and ensures that there is no flow far from the core. In this case, because of the added dissipation through γ, the velocity of the defect is set such that the torques

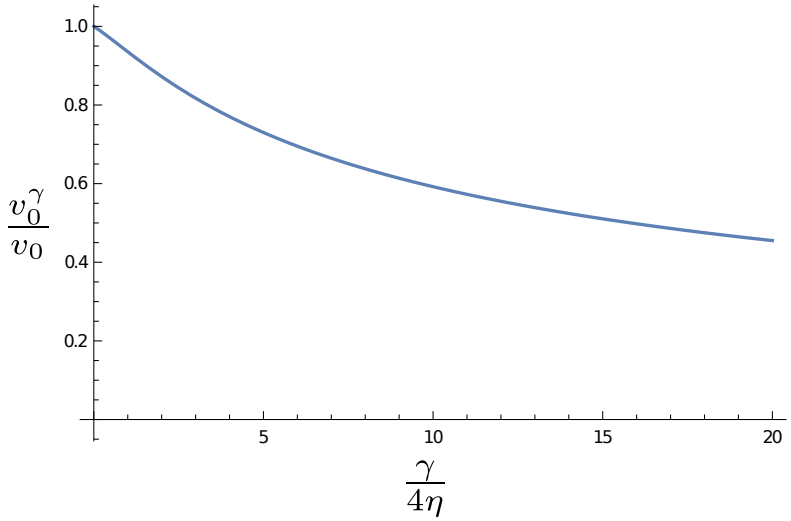

Figure 3.17: Ratio between the velocity at $\gamma \neq 0$ and the velocity at $\gamma = 0$ as a function of $\gamma/(4\eta)$. As $\gamma/(4\eta)$ increases the velocity decreases w.r.t to the case $\gamma = 0$, consistent with the added dissipation introduced by the rotational viscosity.

that now exist in the system do not diverge at the defect core. Knowing the effective viscosity $\bar{\eta}$, the scaling of the velocity as $\zeta\Delta\mu/\sqrt{\xi\bar{\eta}}$ can be expected from dimensional arguments as for the case $\gamma = 0$ in section 3.3. As plotted on fig. 3.17, taking into account the rotational viscosity effectively "slows" down the defect compared to the case $\gamma = 0$. To compare the velocity field computed in this section to the one when $\gamma = 0$ in section 3.3, we plot on fig. 3.18 the radial velocity $v_r(r)$ in units of $\zeta\Delta\mu/\sqrt{\xi\eta}$ for $\gamma = 0$ in blue and for an extreme value $\gamma/(4\eta) = 10^3$ in red.

3.5.4 Reduction of pinning force due to orientational dynamics

The added source of dissipation, from the orientational dynamics with rotational viscosity γ, changes the behavior of the velocity close to the core of the defect, and the stokeslet associated to the flow with orientational dynamics no longer has a logarithmic divergence. Let us see how this changes the scaling of the pinning force with respect to the size of the core. To do so, we proceed exactly as for $\gamma \ll \eta$ in section 3.4, and consider a defect core of finite size ε and different forces inside and outside of the defect core:

$$\eta\Delta\mathbf{v} + \frac{1}{2}\nabla\times(h_\perp\mathbf{e_z}) - \nabla P - \xi(\mathbf{v}+\mathbf{v_0}) - \frac{\zeta\Delta\mu}{2r}\mathbf{e_x} = 0, \qquad r > \varepsilon \tag{3.100}$$

$$\eta\Delta\mathbf{v} - \nabla P - \xi(\mathbf{v}+\mathbf{v_0}) - \frac{f}{2\pi\varepsilon r}\mathbf{e_x} = 0, \qquad r < \varepsilon \tag{3.101}$$

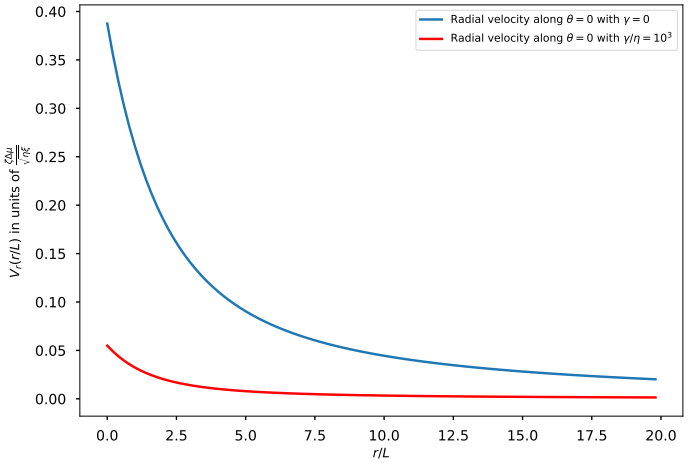

Figure 3.18: Radial velocity $v_r(r)$ in units of $\zeta\Delta\mu/\sqrt{\xi\eta}$ in the lab frame as a function of the distance r in units of $\sqrt{\eta/\xi}$. The blue curve represents the velocity without orientational dynamics at $\gamma = 0$ whereas the red curve represents the velocity in an extreme case where $\gamma/\eta = 10^3$. When $\gamma \gg \eta$ the value of the defect velocity decreases.

The pressure outside the core is unchanged because the torques due to the antisymmetric stress do not affect the pressure field. The fields outside the core and inside the core are therefore already known from the previous sections 3.4 and 3.5.3. Performing the same asymptotic matching as in section 3.4, we find the force f to apply at the core in order to pin a defect:

$$f = \sqrt{\frac{\bar{\eta}}{\xi}}\zeta\Delta\mu\left(\varepsilon\sqrt{\frac{\xi}{\bar{\eta}}}\right)^{\lambda/2+\nu-1} g(\lambda) \tag{3.102}$$

$$g(\lambda) = -3\frac{2^\nu C_1^\lambda(\lambda-2)\left[48(\nu-1)+2\lambda(\lambda(1+\lambda/2+\nu)-4)\right]}{(48-20\lambda^2+\lambda^4)\Gamma(\nu+1)} \tag{3.103}$$

Compared to the case where $\lambda = 0$, the force to pin a defect has a different scaling with respect to the size of the core ε. When taking into account the orientational dynamics, we find that the force necessary to pin a defect depends on the size of the core as a power-law with a positive exponent $\lambda/2 + \nu - 1 > 0$. We recall that $\lambda = \gamma/(4\eta + \gamma)$ and $\nu = \sqrt{1 + \lambda^2/4}$. Compared to the logarithmic dependence in eq. (3.75), there is a stronger dependence on the size of the core. The size of the core ε is to be compared to the characteristic length $\sqrt{\bar{\eta}/\xi}$. The presence of orientational dynamics lowers the force required to pin a defect, because there is an added source of dissipation due to the translation of the defect core, that requires rotations of cells to accommodate the defect

configuration. At this point in this work, it is too early to evaluate the magnitude of the force eq. (3.102). However, this informs on the possibility of pinning a defect. This results shows that, by creating strong gradients of orientations through a small core size ε, the force necessary to pin a defect decreases as a power-law. Even though no forces were measured in experiments, the distribution of focal adhesions on fig. 3.6 could be the signature of the pinning force.

3.6 Effects of cell division and cell death

3.6.1 Pressure-dependent cell-division rate

To describe the onset of multilayering, one has to look at the influence of cell divisions and extrusions or deaths in the monolayer. In the same fashion as was done in the stripes of section 2.3.1, we consider that cells appear "*ex nihilo*" and disappear from the monolayer when they are extruded or when they die. One of the motivation behind looking at the role of cell divisions is that the mechanical environment around the defect is not homogeneous because of active forces. The pressure given by eq. (3.56) varies between the head and the tail of the defect. This pressure difference can impact cell division and extrusion, and therefore inform on the onset of multilayering. If we give a simplistic picture of cell division and extrusion, compared to a reference pressure, a higher pressure hinders cell growth and therefore division. Inversely, a lower pressure facilitates cell growth and division. It has been shown that the growth of cell aggregates can be regulated by applying mechanical stress on spheroids [76–79]. The aforementioned papers introduce the concept of homeostatic pressure P_h, which is a reference pressure for the net division rate. When the pressure is above the homeostatic pressure there is more cell deaths then cell divisions on average and the spheroid shrinks, whereas when the pressure is below the homeostatic pressure cells divide more than they die on average, and the spheroid grows. In a monolayer of elongated cells like C2C12, this concept can become more complicated, and there can be potentially coupling between the anisotropic stress and the net cell division rate proportional to $\sigma_{\alpha\beta}p_\alpha p_\beta$, but as a first approximation, one can consider a linear relation between the net division rate k and the mechanical pressure P:

$$k(P) = -\frac{1}{\kappa}(P - P_h) \tag{3.104}$$

Taking account net cell divisions, mass conservation, or in this case mass balance, is given by:

$$\partial_t \rho + \nabla \cdot (\rho \mathbf{v}) = k(P)\rho \tag{3.105}$$

If we assume constant density $\partial_t \rho + \mathbf{v} \cdot \nabla \rho = 0$, then the incompressibility condition is given by

$$\nabla \cdot \mathbf{v} = k(P) \tag{3.106}$$

$$= -\frac{1}{\kappa}(P - P_h) \tag{3.107}$$

It is one of the particular features of the hydrodynamics of cells to have incompressible flows that are not divergence-free, because the total number of cells is not conserved locally. There are sources (divisions) and sinks (death or extrusion) of cells even if the cells are incompressible. More specifically, by taking a constant density of cells, the fact that the velocity is not divergence-free implies that the volume (or here surface) is not conserved. κ has the dimension of a viscosity and is called the bulk viscosity: κ is associated to the amount of inflow or outflow from a given volume due to pressure changes. At low κ, a small pressure change induces a large flow and it is the opposite at large κ.

The pressure field $P(r, \theta)$ given by eq. (3.56) is defined up to a constant that depends on a reference pressure. We consider this reference pressure to be the homeostatic pressure. Physically, this means that the reference state for which the net division rate vanishes is the uniform monolayer state, with no gradient of orientations. In that case, the pressure $P(r, \theta)$ of eq. (3.56) is the pressure difference induced by the defect compared to the homeostatic pressure P_h. For contractile cells ($\zeta < 0$), there is an increase of pressure at the tail of the defect and a decrease of pressure at the head of the defect with respect to the homeostatic pressure, and vice-versa for extensile cells ($\zeta > 0$). The low-pressure environment at the head of the defect promotes division while the high-pressure environment promotes extrusion. Let us look in details at the hydrodynamic effects of the pressure-dependent cell-division rate.

3.6.2 Changes in the flow due to cell division

To investigate the effect of this pressure-dependent cell-division rate, we consider for simplicity the simpler case where orientational dynamics are neglected, i.e $\eta \gg \gamma$. Force balance is given by eq. (3.15) and has to be supplemented with an equation for the divergence of the velocity (3.107) since the velocity field is no longer divergence-free. We write the velocity field as a sum of a curl-free part and a divergence-free part, also known as the Helmholtz decomposition [115]

$$\mathbf{v} = \nabla \times (\psi \mathbf{e_z}) + \nabla \phi \tag{3.108}$$

and ϕ is related to pressure via eq. (3.107), which implies

$$\kappa \Delta \phi = -(P - P_h) \tag{3.109}$$

It must be noted that the decomposition given by eq. (3.108) is not unique, as detailed in appendix E. Taking the curl and the divergence of the force-balance eq. (3.15) decouples the two fields ψ and ϕ, which follow:

$$\eta\Delta(\Delta\psi) - \xi\Delta\psi = -\frac{\zeta\Delta\mu}{2r^2}\sin\theta \tag{3.110}$$

$$(\eta+\kappa)\Delta(\Delta\phi) - \xi\Delta\phi = -\frac{\zeta\Delta\mu}{2r^2}\cos\theta \tag{3.111}$$

Working with the dimensionless variable $r' = r\sqrt{\xi/\eta}$, renamed r for simplicity, eqs. (3.110) and (3.111) become:

$$\Delta(\Delta\psi) - \Delta\psi = -\frac{\alpha}{r^2}\sin\theta \tag{3.112}$$

$$\Delta(\Delta\phi) - \frac{1}{a^2}\Delta\phi = -\frac{\alpha}{a^2r^2}\cos\theta \tag{3.113}$$

with $a = \sqrt{(\eta+\kappa)/\eta}$ the square root of the ratio between the longitudinal and the transverse viscosities and the same active coefficient $\alpha = \zeta\Delta\mu/(2\xi)$ as in the rest of the chapter. The function ψ that gives the divergence-free part of the velocity is unchanged and is given by eq. (3.35). For symmetry reasons exposed in section 3.3, $\phi(r,\theta) = \phi(r)\cos\theta$. The function $\phi(r)$ that gives the curl-free part of the velocity is very similar to $\psi(r)$, except that the effective viscosity is not the same. Therefore, the two functions evolve on different length scales:

$$\begin{aligned}\phi(r,\theta) = \Bigg[I_1(\frac{r}{a})\left(\tilde{A}_0 - \int_{\frac{r}{a}}^{+\infty} K_1(r')(\tilde{A}a^3r'^2 + \alpha r' + \tilde{B}a)\,dr'\right) \\ + K_1(\frac{r}{a})\left(\tilde{B}_0 - \int_0^{\frac{r}{a}} I_1(r')(\tilde{A}a^3r'^2 + \alpha r' + \tilde{B}a)\,dr'\right)\Bigg]\cos\theta\end{aligned} \tag{3.114}$$

The velocity is then given by

$$v_r(r,\theta) = \left(\frac{\psi(r)}{r} + d_r\phi(r)\right)\cos\theta \tag{3.115}$$

$$v_\theta(r,\theta) = -\left(\frac{\phi(r)}{r} + d_r\psi(r)\right)\sin\theta \tag{3.116}$$

Injecting the expression of the velocity and of the pressure into the force-balance eq. (3.15) relates the integration constants of ψ to those of ϕ with

$$B = a^2\tilde{B} \tag{3.117}$$

$$A + a^2\tilde{A} = \sqrt{\frac{\eta}{\xi}}v_0 \tag{3.118}$$

To determine the integration constants $A_0, \tilde{A}_0, A, \tilde{A}, B, \tilde{B}, B_0, \tilde{B}_0$ (the constants without tilde are the constants as given in eqs. (3.38) and (3.39) for the flow without orientation dynamics), we need to apply the boundary conditions eqs. (3.16) and (3.17): $A_0 = \tilde{A}_0 = 0$ to avoid exponential divergences with system size. A supplementary condition must be added to determine the velocity field, that the division rate $k(P)$ does not diverge with system size nor in $r = 0$. With this supplementary condition, we are able to set $B = B_0 = \tilde{B}_0 = \tilde{B} = 0$. The remaining integration constants are $A, \tilde{A}$, and the limits of the velocity are given by:

$$\lim_{r\to+\infty} v_r(r) = -\sqrt{\frac{\xi}{\eta}}(A + a^2\tilde{A}) \tag{3.119}$$

$$\lim_{r\to+\infty} v_\theta(r) = \sqrt{\frac{\xi}{\eta}}(A + a^2\tilde{A}) \tag{3.120}$$

$$\lim_{r\to 0} v_r(r) = -\sqrt{\frac{\xi}{\eta}}\frac{1}{2}\left(2(A + a^2\tilde{A}) + \alpha\frac{\pi}{2}(1 + \frac{1}{a})\right) \tag{3.121}$$

$$\lim_{r\to 0} v_\theta(r) = \sqrt{\frac{\xi}{\eta}}\frac{1}{2}\left(2(A + a^2\tilde{A}) + \alpha\frac{\pi}{2}(1 + \frac{1}{a})\right) \tag{3.122}$$

The boundary condition far from the core $r \gg \sqrt{\eta/\xi}$ that $\mathbf{v} = -\mathbf{v_0}$ is redundant with eq. (3.118). The boundary condition of vanishing velocity at the core of the defect eq. (3.16) gives $A + a^2\tilde{A} = -\alpha\pi/4(1 + 1/a)$, which gives for the velocity of the defect

$$\mathbf{v_0} = -\frac{\pi}{8}\frac{\zeta\Delta\mu}{\sqrt{\xi\eta}}\left(1 + \sqrt{\frac{\eta}{\eta + \kappa}}\right)\mathbf{e_x} \tag{3.123}$$

When $\kappa \ll \eta$, small deviations from the homeostatic state induce very large flow. In that case, we see from eq. (3.123) that the velocity of the defect is twice the velocity obtained when there is no cell division. For contractile cells, the active stress induces a motion of the defect in the direction of its tail. On top of that, the active stress creates, for contractile cells, a depression at the head of the defect and an excess pressure at the tail. This pressure difference promotes division at the head and extrusion at the tail. Equation (3.123) indicates that the asymmetric net division rate also promotes a motion of the defect towards its tail. For extensile cells, the role of the head and of the tail of a defect are reversed. Regarding the motion of the defect, the effects of the active stress and that of a pressure-dependent net division rate are additive. The flow considering cell division is shown in fig. 3.19, and the heterogeneous division rate is shown in fig. 3.20. Note that the divergence field of the flow is the same thing as the division rate

according to the incompressibility relation (3.106). This asymmetric cell division can be one of the mechanisms to explain why topological defects are preferential points for multilayering and extrusion in general. It can be noted that in ref. [36,37], Kawaguchi *et al.* and Saw *et al.* considered cell accumulation around $+1/2$ topological defects without making a distinction between the head and the tail of the defect. Density changes between the head and the tail are explored in ref. [95], for extensile bacteria in the context of a dry system without hydrodynamic interactions. Copenhagen *et al.* measure the divergence field around a $+1/2$ defect and find a mainly positive divergence at the tail and negative divergence at the head. This would be consistent with our predictions eq. (3.107), with the head and the tail reversed compared to fig. 3.20, since the bacteria considered in ref. [95] are extensile. In the experiments conducted by T. Sarkar, preliminary observations suggest an accumulation of cells at the head that could be what leads to multilayering.

3.7 Active corrections to the orientation of topological defects

3.7.1 Active perturbation to the orientation of the defect

In all the previous sections 3.3 to 3.6, in particular in the perturbation in activity presented in section 3.5.2, we computed the velocity field created by the active force due to an equilibrium configuration of a $+1/2$ topological defect. We computed in section 3.5.3 the velocity field induced by activity, considering orientation dynamics. We can now in turn calculate the influence of the flow on the director field. The perpendicular component of the molecular field $h_\perp$ is $h_\perp = K\nabla^2\varphi$ by definition. To first order in activity, $h_\perp$ is given by eq. (3.79). The angle of the director φ therefore satisfies:

$$K\nabla^2\varphi = \frac{\gamma}{2}\left[\Delta\psi - \frac{\partial_r\psi}{r}\right], \tag{3.124}$$

with ψ the stream function given by eq. (3.86). Given the azimuthal dependence of the stream function, we look for a solution to the eq. (3.124) of the form $\varphi(r,\theta) = \theta/2 + \varphi(r)\sin\theta$. Solving the Poisson eq. (3.124), we can get the radial function of the director angle, as a function of the velocity field induced by the active force given by eqs. (3.87) and (3.88):

$$\varphi(r) = \frac{\gamma}{2K}\left\{C\,r + r v_r(r) + \frac{1}{2}\left(r\int_0^r \frac{v_\theta(r')}{r'}\,dr' - \frac{1}{r}\int_0^r r' v_\theta(r')\,dr'\right)\right\} \tag{3.125}$$

Any divergence at the origin was removed by choosing appropriate integration constants, and C is an integration constant that must be determined given a value of the perturbation $\varphi(r)$ at a given point.

The angular field $\varphi(r,\theta)$ is computed in the frame of the defect, and the velocities in eq. (3.125) are the velocities given in the frame of the defect. In this frame, in the far field $r \gg \sqrt{\eta/\xi}$, $v_r \to -v_0$ and $v_\theta \to v_0$, where v_0 is the magnitude of the self-advection velocity of the defect given by eq. (3.99). Therefore, all the terms on the RHS of eq. (3.125) diverge at least linearly with the system size. Consequently, this solution cannot be valid at large lengths. This determines a cutoff length above which the expansion around the solution for a passive topological defect is no longer valid, and above which active effects dominate the orientation field.

3.7.2 Domain of validity of the passive orientation

Let us write the orientation angle $\varphi(r)$ given by eq. (3.125) in the far field. Knowing that $v_r \to -v_0$ and $v_\theta \to v_0$, the orientation angle in the far field is:

$$\varphi(r) \underset{r\gg\sqrt{\eta/\xi}}{\approx} \frac{\gamma}{2K} r \left\{ C + \frac{v_0}{2} \ln(\frac{r}{r_0}) \right\} \tag{3.126}$$

with r_0 a length that does not impact the behavior of the orientation angle. From eq. (3.126), the expression for the angle is valid only if the system size R is such that $R \ll K/(\gamma v_0)$. In terms of hydrodynamic parameters, given the scaling for v_0 in eq. (3.99),

$$R \ll \frac{\eta + \gamma/4}{\gamma} \sqrt{\frac{\xi}{\eta + \gamma/4}} \frac{K}{|\zeta \Delta\mu|} \tag{3.127}$$

On the right-hand-side of inequality (3.127), there is the characteristic length associated to the screening of hydrodynamic interactions by the viscous drag $L = \sqrt{(\eta + \gamma/4)/\xi}$, and an active length $L_a = \sqrt{K/|\zeta\Delta\mu|}$. The active length L_a, up to dimensionless parameters depending on the geometry, is the same length as in chapter 2. In chapter 2, this length is the typical length above which a band of active nematic spontaneously deforms and create a gradient of orientation. We also have on the RHS of inequality (3.127) the ratio between the effective viscosity $\eta + \gamma/4$ and the rotational viscosity γ. In terms of those lengths, inequality (3.127) can be rewritten

$$R \ll L_c^{\text{defect}} = \frac{\eta + \gamma/4}{\gamma} \frac{L_a^2}{L} \tag{3.128}$$

The inequality (3.128) gives a domain of validity for the passive orientation. For distances r much smaller than the length L_c^{defect}, the approximation $\varphi = \theta/2$ is valid to compute the flow induced by activity. However, the divergence of φ from eq. (3.126) implies that the flow created by the orientation field of a defect $\varphi = \theta/2$ destroys this orientation field at distances larger than L_c^{defect}. Therefore, the configuration of an active $+1/2$ defects should not exist above Lc^{defect}.

To ensure the existence of an isolated topological defects and satisfy inequality (3.128), it is sufficient to have $L_a \gg L$, or to be in the approximation of negligible orientation dynamics $\eta \gg \gamma$. When this condition is not satisfied, active topological defects lose orientational order over lengths greater then L_c^{defect}. Interestingly, L_a controls the low-Reynolds turbulent regime found in active nematics. There is a turbulent regime for lengths much larger than the active length L_a [44, 105, 116, 117]. We recover a form of this result here, but because of the interaction with the substrate via viscous drag, this active length must be compared to the screening length L and the ratio between the viscosities $(\eta + \gamma/4)/\gamma$.

3.8 $-1/2$ topological defects

Most of the focus of this work is on $+1/2$ defects. From an experimental point of view, this is where T. Sarkar observed multilayering and non-motile defects. From a theoretical viewpoint, $+1/2$ defects are particularly interesting because of their acquired polarity that explains the self-advection and the asymmetry in cell division described in section 3.6. Let me however show without much details how the calculations of this chapter can be adapted to compute the flow field for a $-1/2$ topological defects. We introduce the same physical quantities as in the previous sections, with a superscript $^-$ to differentiate them from the ones computed for a $+1/2$ defect. For simplicity, I consider the case where the rotational viscosity vanishes.

A schematic representation of a $-1/2$ defect with the reference axis is given on fig. 3.9. The active force density created by the defect configuration $\varphi = -\theta/2$ is given by eq. (3.12). Since there is no preferred direction of motion for a $-1/2$ defect, there is no self-advection velocity. Force balance is given by:

$$\eta\Delta\mathbf{v}^- - \nabla P^- - \xi\mathbf{v}^- - \frac{\zeta\Delta\mu}{2r}\left(-\cos(3\theta)\,\mathbf{e_r} + \sin(3\theta)\,\mathbf{e}_\theta\right) = 0 \tag{3.129}$$

The only boundary condition is

$$\mathbf{v}^-(+\infty,\theta) = 0 \tag{3.130}$$

The curl of eq. (3.129) gives:

$$\Delta\left[\eta\Delta\psi^- - \xi\psi^-\right] = \frac{3}{2}\zeta\Delta\mu\frac{\sin 3\theta}{r^2} \tag{3.131}$$

The characteristic length $L = \sqrt{\eta/\xi}$ is unchanged and in the dimensionless unit $r' = r/L$,

$$\Delta\left[\Delta\psi^- - \psi^-\right] = -\alpha^-\frac{\sin 3\theta}{r^2}, \tag{3.132}$$

with $\alpha^- = -3\zeta\Delta\mu/(2\xi)$. ψ^- is of the form $\psi^-(r,\theta) = \psi^-(r)\sin 3\theta$. Integrating eq. (3.132) gives for $\psi^-(r)$:

$$\frac{d^2\psi^-(r)}{dr^2} + \frac{1}{r}\frac{d\psi^-(r)}{dr} - \left(1 + \frac{3}{r^2}\right)\psi^-(r) = A^- r + \frac{B^-}{r} + \alpha^- \tag{3.133}$$

Homogeneous solution are given by the modified Bessel functions $I_3(r)$ and $K_3(r)$. The velocity field for an isolated $-1/2$, with vanishing velocity in the far field, in dimensionless units, is given by:

$$v_r = \frac{3\zeta\Delta\mu}{2\sqrt{\xi\eta}r}\left\{I_3(r)\int_r^{+\infty} K_3(r')r'\,\mathrm{d}r' + K_3(r)\int_0^r I_3(r')r'\,\mathrm{d}r'\right\}\cos 3\theta \tag{3.134}$$

$$v_\theta = \frac{3\zeta\Delta\mu}{2\sqrt{\xi\eta}}\left\{\left(\frac{3}{r}I_3(r) - I_2(r)\right)\int_r^{+\infty} K_3(r')r'\,\mathrm{d}r' + \left(\frac{3}{r}K_3(r) + K_2(r)\right)\int_0^r I_3(r')r'\,\mathrm{d}r'\right\}\sin 3\theta \tag{3.135}$$

I give on fig. 3.21 a representation of the division rate for a $-1/2$ defect following the lines of section 3.6

3.9 Discussion

In order to understand the role of topological defects in the multilayering of C2C12 cell monolayers, we looked at the flow created by an isolated active topological defect. We modeled the interaction between the cells and the substrate through a viscous drag with a friction coefficient ξ, and found that there is a characteristic length scale $L = \sqrt{\eta/\xi}$, over which hydrodynamic interactions are screened. The passive configuration of a defect given by eq. (3.5) has a gradient of orientation that creates an active force density. For $-1/2$ defects, because of the geometry of the defect, the total force density around a defect vanishes and a $-1/2$ defect does not move on average. The geometry of $+1/2$ topological defects creates however a force density along its axis of symmetry, which generates a self-advection of the defect. As a first approximation, the flow can be computed by neglecting the orientation dynamics with respect to the shear dynamics. In this approximation, the self-advection velocity of a $+1/2$ defect is proportional to $-\zeta\Delta\mu/\sqrt{\xi\eta}\mathbf{e_x}$ (eq. (3.53)). For contractile cells ($\zeta < 0$) a $+1/2$ defect moves towards its tail, and for extensile cells it moves towards its head ($\zeta > 0$). The motion of defects in C2C12 monolayers is consistent with a contractile behavior.

The total active force on an isolated defect diverges with the system size. As a consequence, despite the screening of hydrodynamic interactions by the characteristic length,

the velocity field decays in the far field as the inverse distance to the core. Therefore, the total friction force diverges with system size and the total force vanishes.

To understand the experimental observation of motionless $+1/2$ defects, we computed the stall force of a $+1/2$ defect and found that the force depends on the logarithm of the size of the defect core (eq. (3.75)). We identified that the orientation dynamics of the flow can be key for the stall force as the motion of a $+1/2$ defect requires rotation of cells to accommodate for the changes in the orientation field. By taking into account this effect, we found that the self-advection velocity of the defect decreases with the rotational viscosity γ (eq. (3.99)). Taking into account orientational dynamics, the stall force depends on the size of the core as a power law (eq. (3.102)). Compared to the logarithmic dependence at $\gamma \ll \eta$, there is a stronger dependence on the size of the core. If the core of the defect is small with respect to the characteristic length L, this force can become small compared to the active force. This work is still preliminary, and the comparison between the theoretical force given by eq. (3.102) and the force generated by the cells is yet to be done.

To understand the onset of multilayering, we modeled cell division and extrusion in the monolayer. As a first approximation, we considered the net division rate to be proportional to pressure: we considered a homeostatic state where the net division rate vanishes when there is no gradient of orientation. The configuration of a $+1/2$ defect creates a pressure difference between the head and the tail of the defect, and the sign of this difference depends on whether the cells are extensile or contractile. This pressure difference generates an asymmetric net division rate, and the flow is no longer divergence-free. The flow caused by this asymmetric division rate is favoring the motion of the defect. In the limit $\kappa \ll \eta$ where minute changes in pressure induce a large divergence of the flow, the self-advection velocity of a $+1/2$ defect is doubled.

Although a qualitative argument, the existence of trapped defects together with the flow induced by division can explain why $+1/2$ topological defects are preferential sites for multilayering or for extrusion. For contractile cells, the combination of these effects leads to an accumulation of cells at the head of the defect, because the net division rate is predicted to be positive on average at the head. For extensile cells, it should be the opposite. T. Sarkar tried to measure cell division in the monolayer but there was no strong evidence of division rate resembling the one predicted by the theory fig. 3.20. Experimentally, there is preliminary evidence of accumulation of cells at the head of non-motile $+1/2$ defects.

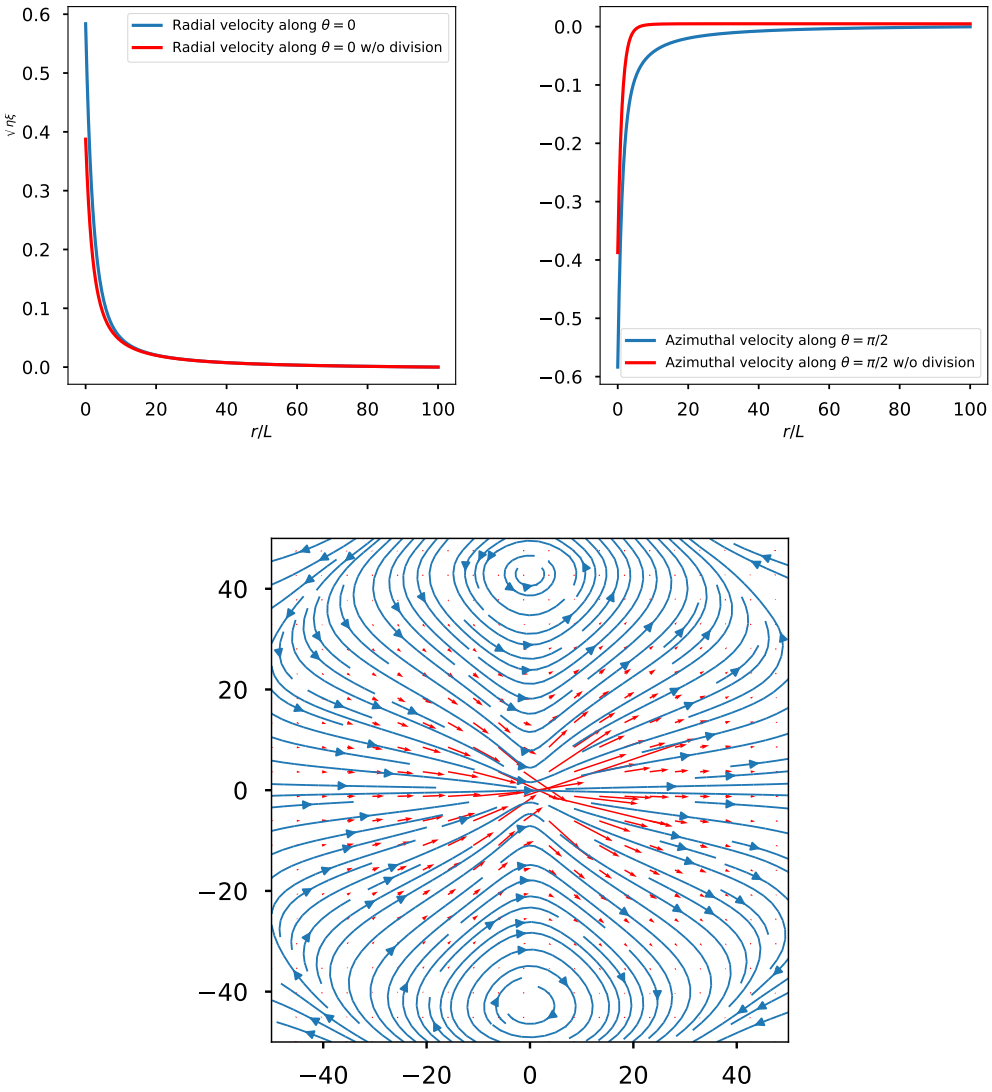

Figure 3.19: Changes in the radial (upper left) and azimuthal (upper right) velocity fields $v_r(r)$ and $v_\theta(r)$ due to cell division (blue curve, $\kappa = \eta$) compared to when there is no cell division (red curve), in units of $\zeta\Delta\mu/\sqrt{\xi\eta}$. The radial velocity is not very affected by cell division except that the velocity of the defect is increased by cell division. The azimuthal velocity is however changed, it decays slower when there is cell division, on the same length scale as the radial velocity. On the bottom panel is shown the streamlines of the velocity field in blue and the arrows of the velocity field in red. Because of cell division, there is a convergent flow towards the core from the head of the defect and a divergent flow towards the tail.

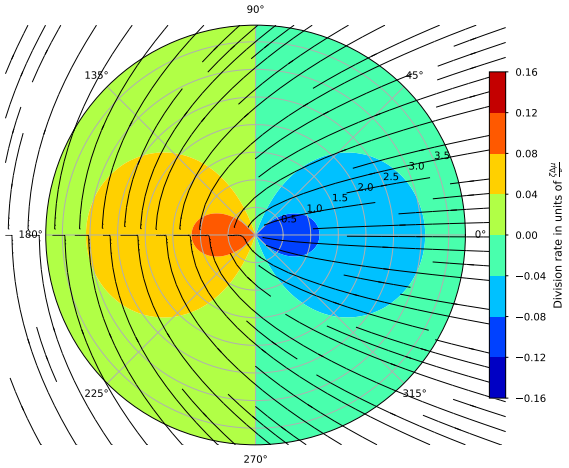

Figure 3.20: Division rate, or equivalently divergence of the velocity field, in units of $\zeta\Delta\mu/\kappa$, for a contractile system around a $+1/2$ topological defect. We see that at the head of the defect there is a positive net division rate, whereas at the tail of the defect there is a negative net division rate, i.e extrusion or death.

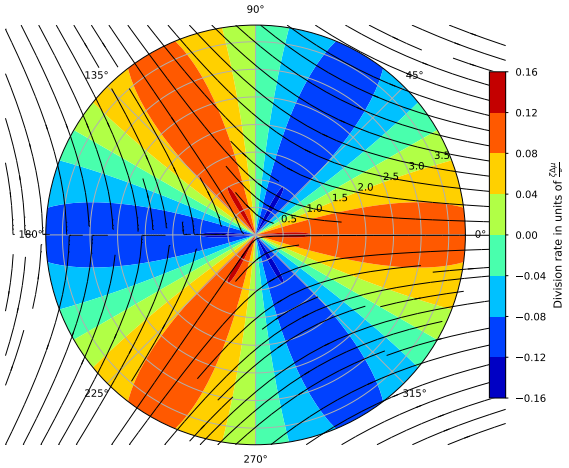

Figure 3.21: Division rate (or equivalently divergence of the velocity field) in units of $\zeta\Delta\mu/\kappa$ around a $-1/2$ topological defect for a contractile system.

Conclusion

This PhD thesis deals with the theoretical description of the collective motion and spatial organization of cells. In particular, we restricted our attention to elongated cells that form confluent monolayers. These cells orientationally order into a nematic phase characterized by a director $\mathbf{p}$, and can be described by the hydrodynamic theory of active nematics presented in section 1.2. This theory is similar to the hydrodynamic theory of passive nematics, with the addition of new terms due to the activity of the system. There is an active stress proportional to $p_\alpha p_\beta$, which can be either contractile or extensile. We presented in this work two manifestations of this active stress in two different geometries.

Chapter 2 dealt with a monolayer of active nematics confined in a stripe of width L and of quasi-infinite length, while chapter 3 focused on topological defects in an active monolayer, in particular positive half-integer defects. Although my work is theoretical, the questions addressed in this manuscript are all grounded in experiments.

In chapter 2, I presented in section 2.2.1 the active Freedericksz instability of a band of active nematics [41]: there is a critical width L_c, above which a uniform state parallel to the stripe is no longer stable. Above L_c, a gradient of orientation develops in the stripe and there is a shear flow. I presented in section 2.3 the specificities of cell nematics introduced by Duclos, Blanch-Mercader *et al.* in ref. [1]. The main differences with the hydrodynamic theory presented in section 1.2 are cell divisions and deaths that do not conserve the mass density, and the interactions with the substrate that do not conserve momentum. Both these effects can influence the stability of a monolayer of cells in a stripe and influence the value of the critical width L_c.

I then proceeded to describe new experimental work conducted in the group of Pascal Silberzan by Thibault Aryaksama in sections 2.4 and 2.5. By abrading the surface over which the cells are plated, one is able to favor the orientation of the cells, a process called contact-guidance. From a theoretical viewpoint, we modeled this effect by adding an external field favoring orientation. When this field is applied perpendicularly to the stripe, we showed that there is an additive effect between the active stress and the external field to destabilize the uniform state. The resulting critical width must be smaller than in the absence of external field, as shown in section 2.4.2. In section 2.4.3, we showed that depending on the magnitude of the external field, there is potentially a

competition for the tilt angle in large stripes.
Experimentally, cells align parallel to the abrasions in large stripes. According to our calculations, this means that the effect of the abrasions on the orientation of the cells is strong with respect to the active stress, in the sense of eq. (2.73). However, when comparing the critical length for the instability of the uniform state with and without abrasions, there is no clear difference between the two. We therefore make the hypothesis that there is a non-linear effect of the abrasions on the orientation. Below a certain width of the stripe, of the order of 200μm, the abrasions have no effect on the orientation.

In section 2.5, by varying the angle of the abrasions with respect to the direction of the stripes, we are able to quantify the competition between the orientation imposed by the active stress and the orientation imposed by the abrasions. Because of the active stress, cells do not align exactly with the abrasions when the abrasions are not perpendicular to the stripe. This competition allows for the direct measurement of the flow-alignment parameter ν.

These experiments in a relatively simple geometry are well suited to measure the hydrodynamic parameters of tissues. Section 2.6 deals with the estimation of the hydrodynamic parameters by comparing experimental data to analytical results. I present the theoretical limitations to such an approach in section 2.6.1. Apart from measuring the flow-alignment parameter ν and the diffusion coefficient K/γ, the estimation was not successful in giving unknown parameters to ref. [1], which deals with the same geometry. This is due notably to the difficulty in estimating the ratio of viscosities η/γ from the amplitudes of the tilt, which could be caused by the fact that $\eta \ll \gamma$.

Chapter 3 deals with topological defects in active cell monolayers. Although this chapter is more theoretical, it is still grounded in the experimental observations made by Trinish Sarkar in the group of Pascal Silberzan. I give an overview of passive and active topological defects and introduce their mathematical description in section 3.1. Section 3.2 details the physical questions raised by the experiments. The first question comes from the multilayering events that occur at positive half-integer topological defects. Surprisingly, there are motionless $+1/2$ defect in the monolayer even though $+1/2$ defects are supposed to be self-propelled due to an active force. Several hours after confluency, all non-motile $+1/2$ defects multilayer. To describe these effects, we first computed in section 3.3 the velocity and pressure field created by a $+1/2$ defect interacting with the substrate through viscous drag. To do so, we decoupled the orientation dynamics and considered only the flow created by a passive defect configuration. The interaction with the substrate allowed for the calculation of the pinning force necessary to stall the self-propelled motion of a $+1/2$ defect, detailed in section 3.4. In section 3.5, we considered the effect of torques created by the antisymmetric stress on the flow. We found that the self-propelled velocity decreases with the rotational viscosity γ. The pinning force is also lowered because of the rotational viscosity, as it depends as a power

law on the size of the core compared to a logarithmic dependence when the rotational viscosity vanishes. We were able in section 3.7 to estimate a length scale above which the passive orientation of a $+1/2$ defect is no longer stable due to the flow created by its orientation.

In section 3.6, we took into account the effect of cell division and death on the flow around a $+1/2$ topological defect. We related linearly the division rate to the pressure around the defect. The pressure difference between the head and the tail of the defect, due to the active force, drives an asymmetry in the net division rate. The effect of this asymmetric division rate is to push the defect in the same direction as the active force does. There is an additive effect between the flow associated to cell division and the flow associated to the active force. Together with the potential pinning of defects, this could explain why multilayering happens preferentially at $+1/2$ topological defects.

The perspectives of this work are numerous and bridge the two chapters of this thesis. For the parameter estimation in the stripe experiment, a more rigorous numerical approach could be used to estimate the parameters. An interesting feature to explore in the stripes is the presence of topological defect close to the boundary. We only looked in chapter 2 at continuous deformations of the director, but in general there are topological defects located close to the boundary of the stripe in the presence of abrasions, which account for the frustration between the direction of the stripes and the perpendicular abrasions. There seems to be a typical distance between pairs of defects along the length of the stripe. This is a phenomenon reminiscent of wall formation and "pincement" in the passive Freedericksz transition.

There are several possible extensions of the study that we have made on defects. Firstly, we have neglected two contributions, the flow-alignment parameter ν and the Ericksen stress. Taking into account the coupling between flow and orientation $\nu \neq 0$, all the modes of the angular Fourier expansion become coupled. The Ericksen stress poses other problems, but there are reasons to believe it does not change qualitatively the result. We have not computed the case of cell division together with the pinning force. The case where the rotational viscosity is much larger than the shear viscosity is a limit to explore, especially since some results of chapter 2 could suggest that this limit is relevant. In this limit, the flow is treated as a perturbation and the active force acts on the orientation field. It would also be interesting to calculate the flow and the effects of cell division for a configuration of two defects of opposite charges, a $+1/2$ and $-1/2$ defect.

A question raised by the observations of chapters 2 and 3 is the apparent extensile and contractile behaviors, for the same line of C2C12 myoblast cells, in the stripe geometry and for topological defects. The observation of the flow with respect to the tilt angle in stripes is consistent with an extensile active stress, while the motion of $+1/2$ defects in the free monolayer is consistent with a contractile active stress. This could be explained by active interactions with the substrate, as proposed by Maitra *et al.* in

ref. [68]. A different interaction with the substrate for a splay and a bend deformation could explain this apparent contradiction.

Bibliography

[1] G. Duclos, C. Blanch-Mercader, V. Yashunsky, G. Salbreux, J.-F. Joanny, J. Prost, and P. Silberzan, "Spontaneous shear flow in confined cellular nematics," *Nature Physics*, vol. 14, pp. 728–732, July 2018.

[2] E. Scarpa and R. Mayor, "Collective cell migration in development," *Journal of Cell Biology*, vol. 212, pp. 143–155, Jan. 2016.

[3] M. Behrndt, G. Salbreux, P. Campinho, R. Hauschild, F. Oswald, J. Roensch, S. W. Grill, and C.-P. Heisenberg, "Forces Driving Epithelial Spreading in Zebrafish Gastrulation," *Science*, vol. 338, pp. 257–260, Oct. 2012.

[4] D. Krndija, F. El Marjou, B. Guirao, S. Richon, O. Leroy, Y. Bellaiche, E. Hannezo, and D. Matic Vignjevic, "Active cell migration is critical for steady-state epithelial turnover in the gut," *Science*, vol. 365, pp. 705–710, Aug. 2019.

[5] C.-P. Heisenberg and Y. Bellaïche, "Forces in Tissue Morphogenesis and Patterning," *Cell*, vol. 153, pp. 948–962, May 2013.

[6] P. Friedl and D. Gilmour, "Collective cell migration in morphogenesis, regeneration and cancer," *Nature Reviews Molecular Cell Biology*, vol. 10, pp. 445–457, July 2009.

[7] P. Martin and R. Nunan, "Cellular and molecular mechanisms of repair in acute and chronic wound healing," *British Journal of Dermatology*, vol. 173, pp. 370–378, Aug. 2015.

[8] D. W. Thompson, *On Growth and Form*. Cambridge: Cambridge University Press, 1917.

[9] B. Ladoux and R.-M. Mège, "Mechanobiology of collective cell behaviours," *Nature Reviews Molecular Cell Biology*, vol. 18, pp. 743–757, Dec. 2017.

[10] T. Lecuit and P.-F. Lenne, "Cell surface mechanics and the control of cell shape, tissue patterns and morphogenesis," *Nature Reviews Molecular Cell Biology*, vol. 8, pp. 633–644, Aug. 2007.

[11] X. Trepat and E. Sahai, "Mesoscale physical principles of collective cell organization," *Nature Physics*, vol. 14, pp. 671–682, July 2018.

[12] T. Chen, T. B. Saw, R.-M. Mège, and B. Ladoux, "Mechanical forces in cell monolayers," *Journal of Cell Science*, vol. 131, p. jcs218156, Dec. 2018.

[13] C. Guillot and T. Lecuit, "Mechanics of Epithelial Tissue Homeostasis and Morphogenesis," *Science*, vol. 340, pp. 1185–1189, June 2013.

[14] L. Blanchoin, R. Boujemaa-Paterski, C. Sykes, and J. Plastino, "Actin Dynamics, Architecture, and Mechanics in Cell Motility," *Physiological Reviews*, vol. 94, pp. 235–263, Jan. 2014.

[15] T. Risler, "Cytoskeleton and Cell Motility," in *Encyclopedia of Complexity and Systems Science* (R. A. Meyers, ed.), pp. 1738–1774, New York, NY: Springer New York, 2009.

[16] P. Roca-Cusachs, V. Conte, and X. Trepat, "Quantifying forces in cell biology," *Nature Cell Biology*, vol. 19, pp. 742–751, July 2017.

[17] M. Gupta, B. R. Sarangi, J. Deschamps, Y. Nematbakhsh, A. Callan-Jones, F. Margadant, R.-M. Mège, C. T. Lim, R. Voituriez, and B. Ladoux, "Adaptive rheology and ordering of cell cytoskeleton govern matrix rigidity sensing," *Nature Communications*, vol. 6, p. 7525, Nov. 2015.

[18] M. Abercrombie, "The Croonian Lecture, 1978 - The crawling movement of metazoan cells," *Proceedings of the Royal Society of London. Series B. Biological Sciences*, vol. 207, pp. 129–147, Feb. 1980.

[19] V. Hakim and P. Silberzan, "Collective cell migration: A physics perspective," *Reports on Progress in Physics*, vol. 80, p. 076601, July 2017.

[20] E. Hannezo, J. Prost, and J.-F. Joanny, "Theory of epithelial sheet morphology in three dimensions," vol. 111, no. 1, pp. 27–32, 2014.

[21] R. Alert and X. Trepat, "Physical Models of Collective Cell Migration," *Annual Review of Condensed Matter Physics*, vol. 11, pp. 77–101, Mar. 2020.

[22] S. Alt, P. Ganguly, and G. Salbreux, "Vertex models: From cell mechanics to tissue morphogenesis," *Philosophical Transactions of the Royal Society B: Biological Sciences*, vol. 372, p. 20150520, May 2017.

[23] M. C. Marchetti, J. F. Joanny, S. Ramaswamy, T. B. Liverpool, J. Prost, M. Rao, and R. A. Simha, "Hydrodynamics of soft active matter," *Reviews of Modern Physics*, vol. 85, pp. 1143–1189, July 2013.

[24] L. Trichet, J. Le Digabel, R. J. Hawkins, S. R. K. Vedula, M. Gupta, C. Ribrault, P. Hersen, R. Voituriez, and B. Ladoux, "Evidence of a large-scale mechanosensing mechanism for cellular adaptation to substrate stiffness," *Proceedings of the National Academy of Sciences*, vol. 109, pp. 6933–6938, May 2012.

[25] J. Ranft, M. Basan, J. Elgeti, J.-F. Joanny, J. Prost, and F. Julicher, "Fluidization of tissues by cell division and apoptosis," *Proceedings of the National Academy of Sciences*, vol. 107, pp. 20863–20868, Dec. 2010.

[26] K. Kruse, J. F. Joanny, F. Jülicher, J. Prost, and K. Sekimoto, "Generic theory of active polar gels: A paradigm for cytoskeletal dynamics," *The European Physical Journal E*, vol. 16, pp. 5–16, Jan. 2005.

[27] G. Duclos, S. Garcia, H. G. Yevick, and P. Silberzan, "Perfect nematic order in confined monolayers of spindle-shaped cells," *Soft Matter*, vol. 10, no. 14, pp. 2346–2353, 2014.

[28] R. Kemkemer, D. Kling, D. Kaufmann, and H. Gruler, "Elastic properties of nematoid arrangements formed by amoeboid cells," *The European Physical Journal E*, vol. 1, no. 2, p. 215, 2000.

[29] M. Sadati, N. Taheri Qazvini, R. Krishnan, C. Y. Park, and J. J. Fredberg, "Collective migration and cell jamming," *Differentiation*, vol. 86, pp. 121–125, Oct. 2013.

[30] S. Ramaswamy, "The Mechanics and Statistics of Active Matter," *Annual Review of Condensed Matter Physics*, vol. 1, pp. 323–345, Aug. 2010.

[31] J.-F. Joanny and L. Brézin, *Tissues as Active Materials*. Les Houches school 2018 "Active Matter and non-equilibrium statistical physics", in press (2020).

[32] G. Gompper, R. G. Winkler, T. Speck, A. Solon, C. Nardini, F. Peruani, H. Löwen, R. Golestanian, U. B. Kaupp, L. Alvarez, T. Kiørboe, E. Lauga, W. C. K. Poon, A. DeSimone, S. Muiños-Landin, A. Fischer, N. A. Söker, F. Cichos, R. Kapral, P. Gaspard, M. Ripoll, F. Sagues, A. Doostmohammadi, J. M. Yeomans, I. S. Aranson, C. Bechinger, H. Stark, C. K. Hemelrijk, F. J. Nedelec, T. Sarkar, T. Aryaksama, M. Lacroix, G. Duclos, V. Yashunsky, P. Silberzan, M. Arroyo, and S. Kale, "The 2020 motile active matter roadmap," *Journal of Physics: Condensed Matter*, vol. 32, p. 193001, May 2020.

[33] G. Duclos, C. Erlenkämper, J.-F. Joanny, and P. Silberzan, "Topological defects in confined populations of spindle-shaped cells," *Nature Physics*, vol. 13, pp. 58–62, Jan. 2017.

[34] M. Kleman, "Defects in liquid crystals," *Reports on Progress in Physics*, vol. 52, pp. 555–654, May 1989.

[35] P. de Gennes and J. Prost, *The Physics of Liquid Crystals*. Oxford Science Publications, 1974.

[36] K. Kawaguchi, R. Kageyama, and M. Sano, "Topological defects control collective dynamics in neural progenitor cell cultures," *Nature*, vol. 545, pp. 327–331, May 2017.

[37] T. B. Saw, A. Doostmohammadi, V. Nier, L. Kocgozlu, S. Thampi, Y. Toyama, P. Marcq, C. T. Lim, J. M. Yeomans, and B. Ladoux, "Topological defects in epithelia govern cell death and extrusion," *Nature*, vol. 544, pp. 212–216, Apr. 2017.

[38] R. Mayor and C. Carmona-Fontaine, "Keeping in touch with contact inhibition of locomotion," *Trends in Cell Biology*, vol. 20, pp. 319–328, June 2010.

[39] L. Giomi, M. J. Bowick, P. Mishra, R. Sknepnek, and M. Cristina Marchetti, "Defect dynamics in active nematics," *Philosophical Transactions of the Royal Society A: Mathematical, Physical and Engineering Sciences*, vol. 372, p. 20130365, Nov. 2014.

[40] L. M. Pismen, "Dynamics of defects in an active nematic layer," *Physical Review E*, vol. 88, p. 050502, Nov. 2013.

[41] R. Voituriez, J.-F. Joanny, and J. Prost, "Spontaneous flow transition in active polar gels," *Europhysics Letters (EPL)*, vol. 70, pp. 404–410, May 2005.

[42] P. M. Chaikin and T. C. Lubensky, *Principles of Condensed Matter Physics*. Cambridge: Cambridge University Press, 1995.

[43] B. Weigelin, G.-J. Bakker, and P. Friedl, "Intravital third harmonic generation microscopy of collective melanoma cell invasion: Principles of interface guidance and microvesicle dynamics," *IntraVital*, vol. 1, pp. 32–43, July 2012.

[44] L. Giomi, "Geometry and Topology of Turbulence in Active Nematics," *Physical Review X*, vol. 5, p. 031003, July 2015.

[45] C. Blanch-Mercader, V. Yashunsky, S. Garcia, G. Duclos, L. Giomi, and P. Silberzan, "Turbulent dynamics of epithelial cell cultures," *Physical Review Letters*, vol. 120, p. 208101, May 2018.

[46] S. Ramaswamy, R. A. Simha, and J. Toner, "Active nematics on a substrate: Giant number fluctuations and long-time tails," *Europhysics Letters (EPL)*, vol. 62, pp. 196–202, Apr. 2003.

[47] V. Schaller and A. R. Bausch, "Topological defects and density fluctuations in collectively moving systems," *Proceedings of the National Academy of Sciences*, vol. 110, pp. 4488–4493, Mar. 2013.

[48] H. P. Zhang, A. Be'er, E.-L. Florin, and H. L. Swinney, "Collective motion and density fluctuations in bacterial colonies," *Proceedings of the National Academy of Sciences*, vol. 107, pp. 13626–13630, Aug. 2010.

[49] J. Toner, Y. Tu, and S. Ramaswamy, "Hydrodynamics and phases of flocks," *Annals of Physics*, vol. 318, pp. 170–244, July 2005.

[50] É. Fodor, C. Nardini, M. E. Cates, J. Tailleur, P. Visco, and F. van Wijland, "How far from equilibrium is active matter?," *Physical Review Letters*, vol. 117, p. 038103, July 2016.

[51] M. E. Cates and J. Tailleur, "When are active Brownian particles and run-and-tumble particles equivalent? Consequences for motility-induced phase separation," *EPL (Europhysics Letters)*, vol. 101, p. 20010, Jan. 2013.

[52] Y. Fily and M. C. Marchetti, "Athermal Phase Separation of Self-Propelled Particles with No Alignment," *Physical Review Letters*, vol. 108, p. 235702, June 2012.

[53] Y. Tu and J. Toner, "How birds fly together: Long-range order in a two-dimensional dynamical XY model," *arXiv:adap-org/9506001*, June 1995.

[54] S. Shankar and M. C. Marchetti, "Hydrodynamics of Active Defects: From order to chaos to defect ordering," *Physical Review X*, vol. 9, p. 041047, Dec. 2019.

[55] J. Deseigne, O. Dauchot, and H. Chatè, "Collective Motion of Vibrated Polar Disks," *Physical Review Letters*, vol. 105, p. 098001, Aug. 2010.

[56] J. R. Howse, R. A. L. Jones, A. J. Ryan, T. Gough, R. Vafabakhsh, and R. Golestanian, "Self-motile colloidal particles: From directed propulsion to random walk," *Physical Review Letters*, vol. 99, p. 048102, July 2007.

[57] X. Serra-Picamal, V. Conte, R. Vincent, E. Anon, D. T. Tambe, E. Bazellieres, J. P. Butler, J. J. Fredberg, and X. Trepat, "Mechanical waves during tissue expansion," *Nature Physics*, vol. 8, pp. 628–634, Aug. 2012.

[58] W. Bialek, A. Cavagna, I. Giardina, T. Mora, E. Silvestri, M. Viale, and A. M. Walczak, "Statistical mechanics for natural flocks of birds," *Proceedings of the National Academy of Sciences*, vol. 109, pp. 4786–4791, Mar. 2012.

[59] P. Guillamat, J. Ignés-Mullol, S. Shankar, M. C. Marchetti, and F. Sagués, "Probing the shear viscosity of an active nematic film," *Physical Review E*, vol. 94, p. 060602, Dec. 2016.

[60] P. C. Martin, O. Parodi, and P. S. Pershan, "Unified Hydrodynamic Theory for Crystals, Liquid Crystals, and Normal Fluids," *Physical Review A*, vol. 6, pp. 2401–2420, Dec. 1972.

[61] D. Forster, T. C. Lubensky, P. C. Martin, J. Swift, and P. S. Pershan, "Hydrodynamics of Liquid Crystals," *Physical Review Letters*, vol. 26, pp. 1016–1019, Apr. 1971.

[62] P. C. Hohenberg and B. I. Halperin, "Theory of dynamic critical phenomena," *Reviews of Modern Physics*, vol. 49, pp. 435–479, July 1977.

[63] L. Onsager, "Reciprocal Relations in Irreversible Processes. I.," *Physical Review*, vol. 37, pp. 405–426, Feb. 1931.

[64] Rayleigh, "Investigation of the Character of the Equilibrium of an Incompressible Heavy Fluid of Variable Density*," *Proceedings of the London Mathematical Society*, vol. s1-14, pp. 170–177, Nov. 1882.

[65] S. De Groot and P. Mazur, *Non-Equilibrium Thermodynamics*. Dove Publications, 1962.

[66] F. Jülicher, S. W. Grill, and G. Salbreux, "Hydrodynamic theory of active matter," *Reports on Progress in Physics*, vol. 81, p. 076601, July 2018.

[67] L. Onsager, "Reciprocal Relations in Irreversible Processes. II.," *Physical Review*, vol. 38, pp. 2265–2279, Dec. 1931.

[68] A. Maitra, P. Srivastava, M. C. Marchetti, J. S. Lintuvuori, S. Ramaswamy, and M. Lenz, "A nonequilibrium force can stabilize 2D active nematics," *Proceedings of the National Academy of Sciences*, vol. 115, pp. 6934–6939, July 2018.

[69] A. I. Teixeira, G. A. Abrams, P. J. Bertics, C. J. Murphy, and P. F. Nealey, "Epithelial contact guidance on well-defined micro- and nanostructured substrates," *Journal of Cell Science*, vol. 116, p. 1881, May 2003.

[70] F. Zhou, L. Yuan, H. Huang, and H. Chen, "Phenomenon of "contact guidance" on the surface with nano-micro-groove-like pattern and cell physiological effects," *Chinese Science Bulletin*, vol. 54, pp. 3200–3205, Sept. 2009.

[71] E. Martínez, E. Engel, J. Planell, and J. Samitier, "Effects of artificial micro- and nano-structured surfaces on cell behaviour," *Annals of Anatomy - Anatomischer Anzeiger*, vol. 191, pp. 126–135, Jan. 2009.

[72] C. L. Gilchrist, D. S. Ruch, D. Little, and F. Guilak, "Micro-scale and meso-scale architectural cues cooperate and compete to direct aligned tissue formation," *Biomaterials*, vol. 35, pp. 10015–10024, Dec. 2014.

[73] R. Zhang, N. Kumar, J. L. Ross, M. L. Gardel, and J. J. de Pablo, "Interplay of structure, elasticity, and dynamics in actin-based nematic materials," *Proceedings of the National Academy of Sciences*, vol. 115, pp. E124–E133, Jan. 2018.

[74] J. F. Joanny, F. Jülicher, K. Kruse, and J. Prost, "Hydrodynamic theory for multicomponent active polar gels," *New Journal of Physics*, vol. 9, pp. 422–422, Nov. 2007.

[75] J. Ranft, J. Prost, F. Jülicher, and J. F. Joanny, "Tissue dynamics with permeation," *The European Physical Journal E*, vol. 35, p. 46, June 2012.

[76] M. Basan, T. Risler, J.-F. Joanny, X. Sastre-Garau, and J. Prost, "Homeostatic competition drives tumor growth and metastasis nucleation," *HFSP Journal*, vol. 3, pp. 265–272, Aug. 2009.

[77] F. Montel, M. Delarue, J. Elgeti, L. Malaquin, M. Basan, T. Risler, B. Cabane, D. Vignjevic, J. Prost, G. Cappello, and J.-F. Joanny, "Stress Clamp Experiments on Multicellular Tumor Spheroids," *Physical Review Letters*, vol. 107, p. 188102, Oct. 2011.

[78] M. Delarue, F. Montel, O. Caen, J. Elgeti, J.-M. Siaugue, D. Vignjevic, J. Prost, J.-F. Joanny, and G. Cappello, "Mechanical Control of Cell flow in Multicellular Spheroids," *Physical Review Letters*, vol. 110, p. 138103, Mar. 2013.

[79] M. Delarue, F. Montel, D. Vignjevic, J. Prost, J.-F. Joanny, and G. Cappello, "Compressive Stress Inhibits Proliferation in Tumor Spheroids through a Volume Limitation," *Biophysical Journal*, vol. 107, pp. 1821–1828, Oct. 2014.

[80] F. Jülicher and J. Prost, "Generic theory of colloidal transport," *The European Physical Journal E*, vol. 29, pp. 27–36, May 2009.

[81] E. Buckingham, "On physically similar systems; illustrations of the use of dimensional equations," *Phys. Rev.*, vol. 4, pp. 345–376, Oct 1914.

[82] L. R. P. de Andrade Lima and A. D. Rey, "Assessing flow alignment of nematic liquid crystals through linear viscoelasticity," *Physical Review E*, vol. 70, p. 011701, July 2004.

[83] C. Blanch-Mercader, P. Guillamat, A. Roux, and K. Kruse, "Integer topological defects of cell monolayers – mechanics and flows," *arXiv:2006.01725 [cond-mat, q-bio]*, June 2020.

[84] C. Blanch-Mercader, P. Guillamat, A. Roux, and K. Kruse, "Quantifying material properties of cell monolayers by analyzing integer topological defects," *arXiv:2006.01575 [cond-mat, q-bio]*, June 2020.

[85] B. Aigouy, R. Farhadifar, D. B. Staple, A. Sagner, J.-C. Röper, F. Jülicher, and S. Eaton, "Cell Flow Reorients the Axis of Planar Polarity in the Wing Epithelium of Drosophila," *Cell*, vol. 142, pp. 773–786, Sept. 2010.

[86] M. Doi and S. Edwards, *The Theory of Polymer Dynamics*. Clarendon Press, 1988.

[87] O. Lehmann, *Flüssigkristalle*. Engelmann, 1904.

[88] Friedel, G., "Les états mésomorphes de la matière," *Ann. Phys.*, vol. 9, no. 18, pp. 273–474, 1922.

[89] M. Kleman, *Points, Lines, and Walls: In Liquid Crystals, Magnetic Systems, and Various Ordered Media*. J Wiley, 1983.

[90] G. Toth, C. Denniston, and J. M. Yeomans, "Hydrodynamics of topological defects in nematic liquid crystals," *Physical Review Letters*, vol. 88, p. 105504, Feb. 2002.

[91] D. Cortese, J. Eggers, and T. B. Liverpool, "Pair creation, motion, and annihilation of topological defects in 2D nematics," *Physical Review E*, vol. 97, p. 022704, Feb. 2018.

[92] A. M. Sonnet and E. G. Virga, "Flow and reorientation in the dynamics of nematic defects," *Liquid Crystals*, vol. 36, pp. 1185–1192, Oct. 2009.

[93] D. Svenšek and S. Žumer, "Hydrodynamics of pair-annihilating disclination lines in nematic liquid crystals," *Physical Review E*, vol. 66, p. 021712, Aug. 2002.

[94] T. Elsdale, "Parallel orientation of fibroblasts in vitro," *Experimental Cell Research*, vol. 51, pp. 439–450, July 1968.

[95] K. Copenhagen, R. Alert, N. S. Wingreen, and J. W. Shaevitz, "Topological defects induce layer formation in $\textit{Myxococcus xanthus}$ colonies," *arXiv:2001.03804 [cond-mat, physics:physics, q-bio]*, Jan. 2020.

[96] A. Livshits, L. Shani-Zerbib, Y. Maroudas-Sacks, E. Braun, and K. Keren, "Structural Inheritance of the Actin Cytoskeletal Organization Determines the Body Axis in Regenerating Hydra," *Cell Reports*, vol. 18, pp. 1410–1421, Feb. 2017.

[97] Y. Maroudas-Sacks, L. Garion, L. Shani-Zerbib, A. Livshits, E. Braun, and K. Keren, "Topological defects in the nematic order of actin fibers as organization centers of Hydra morphogenesis," preprint, Biophysics, Mar. 2020.

[98] L. Metselaar, J. M. Yeomans, and A. Doostmohammadi, "Topology and Morphology of Self-Deforming Active Shells," *Physical Review Letters*, vol. 123, p. 208001, Nov. 2019.

[99] L. Giomi, M. J. Bowick, X. Ma, and M. C. Marchetti, "Defect annihilation and proliferation in active nematics," *Physical Review Letters*, vol. 110, p. 228101, May 2013.

[100] S. Shankar, S. Ramaswamy, M. C. Marchetti, and M. J. Bowick, "Defect Unbinding in Active Nematics," *Physical Review Letters*, vol. 121, p. 108002, Sept. 2018.

[101] T. Sanchez, D. T. N. Chen, S. J. DeCamp, M. Heymann, and Z. Dogic, "Spontaneous motion in hierarchically assembled active matter," *Nature*, vol. 491, pp. 431–434, Nov. 2012.

[102] S. A. Edwards and J. M. Yeomans, "Spontaneous flow states in active nematics: A unified picture," *EPL (Europhysics Letters)*, vol. 85, p. 18008, Jan. 2009.

[103] S. P. Thampi, R. Golestanian, and J. M. Yeomans, "Instabilities and topological defects in active nematics," *EPL (Europhysics Letters)*, vol. 105, p. 18001, Jan. 2014.

[104] S. P. Thampi, R. Golestanian, and J. M. Yeomans, "Vorticity, Defects and Correlations in Active Turbulence," *Philosophical Transactions of the Royal Society A: Mathematical, Physical and Engineering Sciences*, vol. 372, p. 20130366, Nov. 2014.

[105] R. Alert, J.-F. Joanny, and J. Casademunt, "Universal scaling of active nematic turbulence," *Nature Physics*, vol. 16, pp. 682–688, June 2020.

[106] A. Doostmohammadi, J. Ignés-Mullol, J. M. Yeomans, and F. Sagués, "Active nematics," *Nature Communications*, vol. 9, p. 3246, Dec. 2018.

[107] K.-T. Wu, J. B. Hishamunda, D. T. N. Chen, S. J. DeCamp, Y.-W. Chang, A. Fernández-Nieves, S. Fraden, and Z. Dogic, "Transition from turbulent to coherent flows in confined three-dimensional active fluids," *Science*, vol. 355, p. eaal1979, Mar. 2017.

[108] J. M. Kosterlitz and D. J. Thouless, "Ordering, metastability and phase transitions in two-dimensional systems," *Journal of Physics C: Solid State Physics*, vol. 6, pp. 1181–1203, Apr. 1973.

[109] E. Putzig, G. S. Redner, A. Baskaran, and A. Baskaran, "Instabilities, defects, and defect ordering in an overdamped active nematic," *arXiv:1506.03501 [cond-mat]*, June 2015.

[110] L. Pismen, *Vortices in Nonlinear Fields*. Clarendon Press, 1999.

[111] G. Duclos, C. Erlenkämper, J.-F. Joanny, and P. Silberzan, "SI - Topological defects in confined populations of spindle-shaped cells," *Nature Physics*, vol. 13, pp. 58–62, Jan. 2017.

[112] T. B. Saw, W. Xi, B. Ladoux, and C. T. Lim, "Biological Tissues as Active Nematic Liquid Crystals," *Advanced Materials*, vol. 30, p. 1802579, Nov. 2018.

[113] R. Di Leonardo, S. Keen, F. Ianni, J. Leach, M. Padgett, and G. Ruocco, "Hydrodynamic Interactions in Two Dimensions," *Physical Review E*, vol. 78, p. 031406, Sept. 2008.

[114] F. Bowman, *Introduction to Bessel Functions*. Dover Publications Inc., 1958.

[115] H. Helmholtz, "über integrale der hydrodynamischen gleichungen, welcher der wirbelbewegungen entsprechen," *Journal für die reine und angewandte Mathematik*, 1858.

[116] E. J. Hemingway, P. Mishra, M. C. Marchetti, and S. M. Fielding, "Correlation lengths in hydrodynamic models of active nematics," *Soft Matter*, vol. 12, no. 38, pp. 7943–7952, 2016.

[117] S. Shankar, A. Souslov, M. J. Bowick, M. C. Marchetti, and V. Vitelli, "Topological active matter," *arXiv:2010.00364 [cond-mat]*, Oct. 2020.

Appendix A

Ericksen stress

We derive the Ericksen stress corresponding to the variation of the free energy with the volume [35, 66, 74]. The Ericksen stress is a generalization of the thermodynamic pressure for anisotropic system. Consider a volume V that is translated onto a volume $V' = V + \delta V$ by an infinitely small and constant displacement u_α. Consider a free energy density f that depends on the polarization p_α, on gradients of the polarization $\partial_\alpha p_\beta$ and on the mass density ρ. The variation of free energy δF due to the displacement u_α is:

$$\delta F = \int_{V+\delta V} \mathrm{d}^3 r\ f(p_\alpha + \delta p_\alpha, \partial_\alpha p_\beta + \delta\partial_\alpha p_\beta, \rho + \delta\rho) - \int_V \mathrm{d}^3 r\ f(p_\alpha, \partial_\alpha p_\beta, \rho) \tag{A.1}$$

$$= \int_{\delta V} \mathrm{d}^3 r\ f(p_\alpha, \partial_\alpha p_\beta, \rho) + \int_V \mathrm{d}^3 r\ \left\{ \frac{\partial f}{\partial \rho}\delta\rho + \frac{\partial f}{\partial p_\alpha}\delta p_\alpha + \frac{\partial f}{\partial(\partial_\beta p_\alpha)}\delta\partial_\beta p_\alpha \right\} \tag{A.2}$$

$$= \int_{\delta V} \mathrm{d}^3 r\ f(p_\alpha, \partial_\alpha p_\beta, \rho) + \int_V \mathrm{d}^3 r\ \{\mu_c \delta\rho - h_\alpha \delta p_\alpha\} + \int_S \mathrm{d}S_\beta\ \frac{\partial f}{\partial(\partial_\beta p_\alpha)}\delta p_\alpha \tag{A.3}$$

We introduced the chemical potential $\mu_c = \partial f/\partial\rho$ and the molecular field $h_\alpha = -\partial f/\partial p_\alpha + \partial_\beta(\partial f/\partial(\partial_\alpha p_\beta))$. Since there is translation invariance, if we call p'_α the new orientation field after application of the small displacement u_α, $p'_\alpha(r_\alpha + u_\alpha) = p_\alpha(r_\alpha)$. Therefore, the variations $\delta p_\alpha = p'_\alpha(r_\alpha) - p_\alpha(r_\alpha)$ and $\delta\rho = \rho'(r_\alpha) - \rho(\alpha)$ are given by:

$$\delta p_\alpha = -u_\gamma \partial_\gamma p_\alpha \tag{A.4}$$

$$\delta\rho = -u_\gamma \partial_\gamma \rho \tag{A.5}$$

Using $\int_{\delta V} f = \int_S \mathrm{d}S_\beta\ u_\beta f$, eq. (A.3) becomes:

$$\delta F = \int_V \mathrm{d}^3 r\ u_\beta \left(\rho\partial_\beta\mu_c + h_\alpha\partial_\beta p_\alpha\right) + \int_S \mathrm{d}S_\beta\ u_\beta(f - \mu_c\rho) - \int_S \mathrm{d}S_\beta\ \frac{\partial f}{\partial(\partial_\beta p_\alpha)} u_\gamma \partial_\gamma p_\alpha \tag{A.6}$$

We can now identify the Ericksen stress with the surface contribution:

$$\sigma^E_{\beta\alpha} = (f - \mu_c\rho)\delta_{\beta\alpha} - \frac{\partial f}{\partial(\partial_\beta p_\gamma)}\partial_\alpha p_\gamma \tag{A.7}$$

Translation invariance imposes $\delta F = 0$, which gives the Gibbs-Duhem relation eq. (1.17):

$$-\partial_\beta \sigma^E_{\beta\alpha} = \rho \partial_\alpha \mu_c + h_\gamma \partial_\alpha p_\gamma \tag{A.8}$$

The diagonal part of the Ericksen stress given by eq. (A.7) renormalizes the pressure and has no particular hydrodynamic consequence. The non-diagonal part of the Ericksen stress is of second order with respect to derivative of the polarization, and is therefore negligible in several situations where a uniform state is perturbed.

A.1 Ericksen stress in stripes

In the particular geometry of the stripe, since there is a $y-$invariance, the xy-component of the Ericksen stress vanishes and does not play a role in section 2.2.2:

$$\sigma^E_{xy} = -K \partial_x p_\alpha \partial_y p_\alpha = 0 \tag{A.9}$$

A.2 Ericksen stress for $+1/2$ defects

In the case of a topological defect, the Ericksen stress is not negligible because the gradient of orientation is fixed. In force-balance eq. (3.15), there is an additional term coming from the Gibbs-Duhem relation (A.8): $-h_\gamma \partial_\alpha p_\gamma = -h_\perp/(2r)\mathbf{e}_\theta$. When $\gamma \ll \eta$ this term is negligible but outside of this approximation it is relevant. With the Ericksen stress, the equation for the stream function eq. (3.83) is:

$$\Delta \left[\Delta\psi - \frac{\lambda}{r}\partial_r \psi - \psi \right] + \frac{\lambda}{r}\partial_r \left[\Delta\psi - \frac{\partial_r \psi}{r} \right] = -\alpha \frac{\sin\theta}{r^2} \tag{A.10}$$

When the Ericksen stress is taken into account, the force-balance equation (A.10) is a fourth-order differential equation. Because of the $\lambda/r\partial_r[\dots]$ term, we can no longer integrate a Poisson equation and solve a second-order differential equation.

Appendix B

Amplitude equations

I detail in this appendix the derivation of the amplitudes given in eqs. (2.32) and (2.65) from the nonlinear equations eqs. (2.24) and (2.60). If we expand eqs. (2.24) and (2.60) for $\theta = \pi/2 + \delta\theta$, at steady state we obtain an equation of the form

$$\partial_x^2 \delta\theta + q_c^2 \delta\theta - g\delta\theta^3 = 0 \tag{B.1}$$

To look for solutions of eq. (B.1) for lengths close to the critical length, we can make a weakly non-linear perturbation in the small parameter $\varepsilon = (L - L_c)/L_c$ and look for $\delta\theta$ of the form

$$\delta\theta(x) = \varepsilon^{1/2} u_0(x) + \varepsilon u_1(x) + \varepsilon^{3/2} u_2(x) + O(\varepsilon^2), \tag{B.2}$$

with

$$u_0(x) = A_0(\varepsilon^{1/2} x)\cos(qx), \tag{B.3}$$

and u_1, u_2 are functions to describe the higher order terms of the perturbation angle.

$$d_x^2 u_0(x) = \left(-q^2 A_0 - 2q\varepsilon^{1/2} d_x A_0(\varepsilon^{1/2}x) + \varepsilon d_x^2 A_0(\varepsilon^{1/2}x)\right)\cos(qx) \tag{B.4}$$

and

$$u_0^3(x) = \frac{1}{4} A_0^3(3\cos(qx) + \cos(3qx)) \tag{B.5}$$

At order $\varepsilon^{1/2}$, eq. (B.1) is:

$$\partial_x^2 u_0 + q_c^2 u_0 = 0 \tag{B.6}$$

and is verified because of eq. (B.3) and $q = q_c(1 - \varepsilon)$

At order ε:

$$\partial_x^2 u_1 + q_c^2 u_1 = 2q d_x A_0(\varepsilon^{1/2}x)\cos(q_c x) \tag{B.7}$$

To avoid secular terms, we need $d_x A_0 = 0$. Therefore A_0 is a constant.

At order $\varepsilon^{3/2}$:

$$\partial_x^2 u_2 + q_c^2 u_2 = (-2q_c^2 A_0 + \frac{3}{4} g A_0^3)\cos(q_c x) + \dots \tag{B.8}$$

To avoid secular terms, we need

$$A_0 = 2\sqrt{\frac{2}{3g}}q_c \tag{B.9}$$

Equation (B.9) gives eqs. (2.32) and (2.65) after computing the nonlinear coefficient g from equations eqs. (2.24) and (2.60).

Appendix C

Pressure-dependent division rate in stripes

We will make in this appendix a short remark that coupling the division rate to the stress or the pressure should not change the critical length (2.27) in stripes.

Imagine we make a linear coupling between net division rate and pressure:

$$k = -\frac{1}{\kappa}(P - P_h), \tag{C.1}$$

The definition of k through (C.1) implies that there is a homeostatic pressure P_h, such that division and extrusion are balanced at P_h. If $P > P_h$ there is net extrusion and if $P < P_h$ there is net division. When rewriting the constitutive equations with this assumption, we obtain the following set of equations:

$$0 = \eta \partial_x v_y - \frac{\zeta \Delta\mu}{2} \sin 2\theta + \frac{\nu}{2}(h_\parallel \sin 2\theta + h_\perp \cos 2\theta) - \frac{h_\perp}{2} \tag{C.2}$$

$$0 = \frac{h_\parallel}{\gamma} + \nu k \cos^2\theta - \frac{\nu}{2}\partial_x v_y \sin 2\theta, \tag{C.3}$$

$$\partial_t \theta - v_x \partial_x \theta = \frac{h_\perp}{\gamma} - \frac{\nu k}{2} \sin 2\theta - \frac{\partial_x v_y}{2}(\nu \cos 2\theta - 1) \tag{C.4}$$

$$k = -\frac{1}{\kappa}(P - P_h) \tag{C.5}$$

$$\partial_x v_x = k \tag{C.6}$$

We see in (C.3) and (C.4) that the terms that involve the net division rate k are always multiplied by a function of the angle θ. Therefore, to linear order in orientation, a non-uniform pressure that would depend on the angle θ would have no effect on the critical length. All the effects due to the pressure-dependent division rate are non-linear.

Appendix D

Averaging experimental data in stripes

From a theoretical perspective, the hydrodynamic theory introduced in section 1.2 is a theory valid in the limit of a large number of cells. Take for a example the coarse-grained velocity field: it is supposed to represent the average value of the velocity of all cells in a coarse-grained volume. When constructing the hydrodynamic theory, we considered that the fluctuations of these coarse-grained variables were negligible with respect to their average value. Although this is true in a large coarse-graining volume containing a large number of cells, experimentally the coarse-graining volumes made of pixels are of the order of several cells. Therefore, fluctuations are relevant when looking at one stripe. To obtain the average value described by the hydrodynamic theory, a multitude of identical stripes are observed, and then averaged.

In the presence of abrasions, as seen on fig. 2.4, there are two branches that go from $\theta(0) = \pm\pi/2$ to $\theta(0) = 0$, a positive and a negative one. These two branches seem to be equivalent, there is no prevalence for positive or negative values. This leads to a certain problem for averaging: because of the symmetry between the positive and negative branches, one cannot simply average the values of the angle of different stripes of the same width, because half the stripes have positive angles and the other half negative ones. The average is therefore always going to be zero. To have a non-zero average, one needs a way of distinguishing between the two branches. One can think of taking the absolute values of the angle to only have positive values. However, by taking the absolute value fluctuations no longer average out.

We come up with a way, first suggested by Carles Blanch-Mercader, to select the positive branch based on the knowledge of the hydrodynamic theory. From the observation of the direction of shear with respect to the tilt angle in large stripes we can deduce that the cells are extensile, using eq. (2.33). Therefore, we know that on average a negative tilt $-\pi/2 < \theta(0) < 0$ is associated to a negative velocity at the right edge of the stripe $v_y(L/2) < 0$. We can therefore decide to change the sign of the angles associated to a negative velocity at the right edge. Similarly, we change the sign of the velocity if it is associated to a negative tilt. Performing this transformations gives the figures

presented in section 2.6.2, where the comparison between the theory and experiments in stripes is made.

Appendix E

Helmholtz decomposition

The Helmholtz decomposition in eq. (3.108) is not unique, and as a consequence some integration constants in section 3.6 are not determined. The integration constants $A, \tilde{A}$ of the divergence-free and curl-free parts of the velocity are only determined by a single equation (3.118). We can prove that, with the boundary conditions of finite velocity in the far field in the frame of the defect, there is one degree of freedom when defining the velocity by the sum of a curl-free and divergence-free field. Indeed, let us take the decomposition

$$\mathbf{v} = \nabla \times (\psi \mathbf{e_z}) + \nabla \phi \tag{E.1}$$

and ask on what condition this decomposition is unique. Let us write

$$\mathbf{v} = \nabla \times (\psi \mathbf{e_z} + \psi_2 \mathbf{e_z}) + \nabla(\phi + \phi_2), \tag{E.2}$$

For $\mathbf{v}$ to be unchanged, we need

$$\nabla \times (\psi_2 \mathbf{e_z}) = -\nabla \phi_2 \tag{E.3}$$

For $\nabla \cdot \mathbf{v}$ to be unchanged, we need:

$$\Delta \phi_2 = 0 \tag{E.4}$$

Given (E.4), we can always find ψ_2 to satisfy (E.3) because $\nabla \phi_2$ is a divergence-free field.

The conclusion is that any harmonic function that satisfies the boundary conditions can be added to the curl-free part of the velocity ϕ and not change the velocity given the appropriate modification on ψ. Given our boundary condition at infinity that the velocity is along $\mathbf{e_x}$, this leaves functions of the form $\phi_2 = (C\, r + D/r) \cos\theta$. To avoid a divergence of the velocity in 0, $D = 0$. However, $\varphi_2 = C\, r \cos\theta$ is a valid solution. If it were to be added to the solution, it would modify the relation between integration constants that would become:

$$A + a^2 \tilde{A} - C = \sqrt{\frac{\eta}{\xi}} v_0 \tag{E.5}$$

Therefore, we see that a degree of freedom in the expressions of ϕ, ψ remains.

Louis Brézin **18 décembre 2020**

Sujet : Les tissues en tant que matériaux actifs: écoulements spontanés et défauts topologiques dans les nématiques cellulaires actifs

Résumé : Le comportement collectif des cellules dans un tissu est crucial pour des proccessus fondamentaux en biologie comme le développement ou le cancer. Ces dernières décennies, le domaine de la matière active a fournit un cadre théorique à la description des phénomènes collectifs en biologie, à de multiples échelles. Ce travail se porte sur des tissus formés par un grand nombre de cellules allongées qui s'organisent dans une phase nématique, similaire à des cristaux liquides. Le mouvement et l'organisation collective des cellules dans un tissu peuvent être décrits par une théorie hydrodynamique des nématiques actifs. Dans ce cadre, nous étudions l'écoulement spontané de cellules induit par un confinement dans des bandes, avec une déformation du substrat qui favorise une certaine orientation des cellules. De plus, nous nous intéressons aux écoulements cellulaires créés par les défauts topologiques, et leur rôle dans la formation de multi-couches cellulaires.

Mots clés : Tissus biologiques, matière active, hydrodynamique, nématiques, défauts topologiques

Subject : Tissues as active materials: spontaneous flows and topological defects in active cellular nematics

Abstract: The collective behavior of cells in tissues is a key aspect in fundamental biological processes such as development or cancer. In the last decades, the field of active matter has provided a robust framework to describe the collective behavior in biological systems at different scales. This work focuses on tissues made of a large number of elongated cells that organize in a nematic phase, similar to liquid crystals. The collective motion and organization of cells in such tissues can be described using a hydrodynamic theory for active nematics. In this framework, we study the spontaneous motion of cells induced by confinement in stripes, with cues that control the orientation of the cells. Furthermore, we investigate the cellular flows induced by topological defects, and their role in multilayering.

Keywords : Biological tissues, active matter, hydrodynamics, nematics, topological defects